



**AFRL-RZ-WP-TR-2008-2229**

## **HIGH ENERGY DENSITY DIELECTRICS FOR PULSED POWER APPLICATIONS**

**Richard L.C. Wu and Kevin R. Bray**

**K Systems Corporation**

**SEPTEMBER 2008**  
**Final Report**

**THIS IS A SMALL BUSINESS INNOVATION RESEARCH (SBIR) PHASE II REPORT.**

**Approved for public release; distribution unlimited.**

*See additional restrictions described on inside pages*

**STINFO COPY**

**AIR FORCE RESEARCH LABORATORY  
PROPELLSION DIRECTORATE  
WRIGHT-PATTERSON AIR FORCE BASE, OH 45433-7251  
AIR FORCE MATERIEL COMMAND  
UNITED STATES AIR FORCE**

## **NOTICE AND SIGNATURE PAGE**

Using Government drawings, specifications, or other data included in this document for any purpose other than Government procurement does not in any way obligate the U.S. Government. The fact that the Government formulated or supplied the drawings, specifications, or other data does not license the holder or any other person or corporation; or convey any rights or permission to manufacture, use, or sell any patented invention that may relate to them.

This report was cleared for public release by the USAF 88th Air Base Wing (88 ABW) Public Affairs Office (PAO) and is available to the general public, including foreign nationals. Copies may be obtained from the Defense Technical Information Center (DTIC) (<http://www.dtic.mil>).

AFRL-RZ-WP-TR-2008-2229 HAS BEEN REVIEWED AND IS APPROVED FOR PUBLICATION IN ACCORDANCE WITH ASSIGNED DISTRIBUTION STATEMENT.

\*//Signature//

---

JEFFERY T. STRICKER  
Program Manager  
Energy and Power Systems Branch  
Energy/Power/Thermal Division

//Signature//

---

JOSEPH A. WEIMER, Chief  
Energy and Power Systems Branch  
Energy/Power/Thermal Division

//Signature//

---

DEREK M. LINCOLN, Major, USAF  
Deputy Chief  
Energy/Power/Thermal Division  
Propulsion Directorate

This report is published in the interest of scientific and technical information exchange and its publication does not constitute the Government's approval or disapproval of its ideas or findings.

\*Disseminated copies will show “//Signature//” stamped or typed above the signature blocks.

# REPORT DOCUMENTATION PAGE

*Form Approved  
OMB No. 0704-0188*

The public reporting burden for this collection of information is estimated to average 1 hour per response, including the time for reviewing instructions, searching existing data sources, searching existing data sources, gathering and maintaining the data needed, and completing and reviewing the collection of information. Send comments regarding this burden estimate or any other aspect of this collection of information, including suggestions for reducing this burden, to Department of Defense, Washington Headquarters Services, Directorate for Information Operations and Reports (0704-0188), 1215 Jefferson Davis Highway, Suite 1204, Arlington, VA 22202-4302. Respondents should be aware that notwithstanding any other provision of law, no person shall be subject to any penalty for failing to comply with a collection of information if it does not display a currently valid OMB control number. **PLEASE DO NOT RETURN YOUR FORM TO THE ABOVE ADDRESS.**

<b>1. REPORT DATE (DD-MM-YY)</b> September 2008			<b>2. REPORT TYPE</b> Final		<b>3. DATES COVERED (From - To)</b> 17 February 2004 – 31 August 2008	
<b>4. TITLE AND SUBTITLE</b> HIGH ENERGY DENSITY DIELECTRICS FOR PULSED POWER APPLICATIONS			<b>5a. CONTRACT NUMBER</b> FA8650-04-C-2415			
			<b>5b. GRANT NUMBER</b>			
			<b>5c. PROGRAM ELEMENT NUMBER</b> 65502D			
<b>6. AUTHOR(S)</b> Richard L.C. Wu and Kevin R. Bray			<b>5d. PROJECT NUMBER</b> 0605			
			<b>5e. TASK NUMBER</b> PP			
			<b>5f. WORK UNIT NUMBER</b> 0605PP04			
<b>7. PERFORMING ORGANIZATION NAME(S) AND ADDRESS(ES)</b> K Systems Corporation 1522 Marsetta Drive Beavercreek, OH 45432-2733			<b>8. PERFORMING ORGANIZATION REPORT NUMBER</b>			
<b>9. SPONSORING/MONITORING AGENCY NAME(S) AND ADDRESS(ES)</b> Air Force Research Laboratory Propulsion Directorate Wright-Patterson Air Force Base, OH 45433-7251 Air Force Materiel Command United States Air Force			<b>10. SPONSORING/MONITORING AGENCY ACRONYM(S)</b> AFRL/RZPE			
			<b>11. SPONSORING/MONITORING AGENCY REPORT NUMBER(S)</b> AFRL-RZ-WP-TR-2008-2229			
<b>12. DISTRIBUTION/AVAILABILITY STATEMENT</b> Approved for public release; distribution unlimited.						
<b>13. SUPPLEMENTARY NOTES</b> This is a Small Business Innovation Research (SBIR) Phase II Report. Report contains color. PAO Case Number: 88ABW 2009-0803, 02 Mar 2009. K Systems Corporation waives its SBIR data rights to the material in this report (see waiver letter on next page).						
<b>14. ABSTRACT</b> This report was developed under a SBIR contract. Aluminum oxynitride (AlON) capacitors exhibit several promising characteristics for high energy density capacitor applications in extreme environments. Dielectric constants in the range of 9 and dielectric strength in excess of 650 V/ $\mu$ m have been demonstrated in our SBIR Phase II program, resulting in material energy densities greater than 14 J/cc. The dielectric properties remain stable from cryogenic temperatures of -200 °C to temperatures above 400 °C. Stacked capacitor devices have been developed and packaged. The high energy density and wide temperature stability make AlON an attractive candidate for many military, space and commercial applications.						
<b>15. SUBJECT TERMS</b> SBIR Report, high-temperature capacitors, high-energy-density capacitors, aluminum oxynitride, pulsed power capacitors						
<b>16. SECURITY CLASSIFICATION OF:</b> a. REPORT Unclassified			<b>17. LIMITATION OF ABSTRACT:</b> SAR	<b>18. NUMBER OF PAGES</b> 120	<b>19a. NAME OF RESPONSIBLE PERSON</b> (Monitor) Jeffery T. Stricker	
b. ABSTRACT Unclassified			<b>19b. TELEPHONE NUMBER</b> (Include Area Code) (937) 255-7564			



**K SYSTEMS CORPORATION**  
**1522 Marsetta Drive • Beavercreek, Ohio 45432-2733**  
**Phone: (937) 429-5151 • Fax: (937) 429-1122**

November 7, 2008

Ms. Susan Wapelhorst  
AFRL/RZOB, Area B, Bldg. 18, 1950 Fifth St.  
WPAFB, OH 45433-7251

Subject: Final Report for K Systems Corporation Contract No. FA8650-04-C-2415

Dear Ms. Wapelhorst:

Enclosed is an original copy of the final report for K Systems Corporation SBIR Phase II Contract No. FA8650-04-C-2415. Also enclosed is a CD containing the final report. The report contains no SBIR Data Rights, and there is no Export Control Statement.

Should you have any questions, please contact Dr. Richard L.C. Wu (Program Manager of this program).

Thank you very much.

Sincerely,

Richard L.C. Wu, PhD  
Vice President  
K Systems Corporation  
1522 Marsetta Drive  
Beavercreek, OH 45432  
Tel. (937) 429-5151/255-6933  
Fax (937) 429-1122  
e-mail: rlwu@aol.com

## Table of Contents

<u>Section</u>	<u>Page</u>
<b>List of Figures.....</b>	v
<b>List of Tables .....</b>	vii
<b>Foreword.....</b>	viii
<b>Summary.....</b>	x
<b>1. Introduction.....</b>	1
<b>2. Program Objectives .....</b>	3
<b>3. Dual Ion Beam Deposition System .....</b>	4
<b>4. Aluminum Nitride Deposition from N<sub>2</sub>/O<sub>2</sub> .....</b>	8
4.1    Process Optimization.....	8
4.1.1    Taguchi Analysis .....	8
4.1.2    Gas Composition.....	11
4.1.3    Breakdown Strength.....	11
4.2    Chemical Composition .....	14
4.3    Aluminum Nitride Deposition.....	19
4.4    Film Thickness and Surface Characterization.....	19
4.5    Dielectric Properties.....	20
4.5.1    Atmospheric Stability .....	21
4.5.2    Substrate Materials.....	24
<b>5. Aluminum Foil Scanner Characterization .....</b>	28
5.1    Deposition Uniformity .....	28
5.2    Aluminum Foil Scanning .....	34
<b>6. Aluminum Oxynitride Deposition from N<sub>2</sub>O .....</b>	36
6.1    Process Optimization.....	36
6.1.1    Taguchi Analysis .....	36
6.1.2    Aluminum Oxynitride Deposition .....	41
6.1.3    Multilayer Devices.....	46
6.2    Film Thickness and Surface Characterization.....	46
6.3    Dielectric Properties .....	46
6.4    Clearing .....	47
6.5    Electrode Thickness .....	50
6.6    Heavy Edge .....	53
6.7    Electrode Metal .....	53
6.8    Temperature Stability .....	55
6.9    Multilayer Capacitors .....	60
6.9.1    Thermal Properties .....	60
6.9.2    Packaged Devices .....	60
<b>7. Discussion.....</b>	69
<b>8. Conclusions .....</b>	70
<b>9. Deliverables .....</b>	71
<b>10. Technical Publications and Presentations .....</b>	72
10.1    Publications .....	72

## Table of Contents (continued)

<u>Section</u>		<u>Page</u>
10.2	Presentations.....	72
<b>11.</b>	<b>References.....</b>	<b>74</b>
<b>APPENDIX A</b>	.....	<b>76</b>
<b>APPENDIX B</b>	.....	<b>82</b>
<b>APPENDIX C</b>	.....	<b>93</b>
<b>APPENDIX D</b>	.....	<b>100</b>

## List of Figures

<u>Figure</u>	<u>Page</u>
1. Dual Ion Beam Deposition System.....	5
2. Schematic of Dual Ion Beam Deposition System.....	6
3. Schematic of Precision Sample Transfer Manipulator .....	7
4. Breakdown Voltage vs. DC Power .....	9
5. Breakdown Voltage vs. Frequency .....	9
6. Breakdown Voltage vs. Pressure .....	9
7. Dielectric Constant vs. DC Power .....	9
8. Dielectric Constant vs. Frequency .....	9
9. Dielectric Constant vs. Pressure .....	9
10. Dissipation Factor vs. DC Power.....	10
11. Dissipation Factor vs. Frequency.....	10
12. Dissipation Factor vs. Pressure .....	10
13. Capacitance and Dissipation Factor vs. Frequency from N <sub>2</sub> and N <sub>2</sub> :O <sub>2</sub> Plasmas .....	12
14. Breakdown Voltage vs. DC Power at various N <sub>2</sub> :O <sub>2</sub> Ratios.....	13
15. EDS Spectrum of AlN Film.....	15
16. RBS Spectrum of AlN Film.....	16
17. EDS Spectrum of AlON Film.....	17
18. RBS Spectrum of AlON Film .....	18
19. SEM Micrograph of AlN on Si .....	19
20. Optical Micrograph of AlN on Glass.....	20
21. Optical Micrograph of AlN on FPE.....	20
22. Effects of Atmospheric Exposure on the Capacitance.....	22
23. Effect of Atmospheric Exposure on Dissipation Factor .....	23
24. Effects of Substrate on Capacitance and Dissipation Factor .....	25
25. Effects of Substrate on Breakdown Strength .....	26
26. Optical Micrograph of AlON on Stainless Steel Foil .....	27
27. Optical Micrograph of AlON on Titanium Foil.....	27
28. Vertical Deposition Distribution in Source One .....	29
29. Horizontal Deposition Distribution in Source One.....	30
30. Vertical Deposition Distribution in Source Two .....	31
31. Horizontal Deposition Distribution in Source Two .....	32
32. Comparison of Capacitance Values from the Dual Sources in Different Runs .....	33
33. Breakdown Voltage vs. DC Power .....	38
34. Breakdown Voltage vs. Pressure .....	38
35. Breakdown Voltage vs. Gas Ratio .....	38
36. Breakdown Voltage vs. Frequency .....	38
37. Dielectric Constant vs. DC Power .....	38
38. Dielectric Constant vs. Pressure .....	38
39. Dielectric Constant vs. Gas Ratio .....	39
40. Dielectric Constant vs. Frequency .....	39
41. Dissipation Factor vs. DC Power.....	39
42. Dissipation Factor vs. Pressure .....	39

## List of Figures (continued)

<u>Figure</u>	<u>Page</u>
43. Dissipation Factor vs. Frequency.....	39
44. Deposition Rate vs. DC Power .....	39
45. Deposition Rate vs. Pressure.....	40
46. Deposition Rate vs. Gas Ratio .....	40
47. Deposition Rate vs. Frequency .....	40
48. Deposition Rate Comparison for Reactive Gases.....	42
49. Capacitance Comparison for Reactive Gases .....	43
50. Dissipation Factor Comparison for Reactive Gases .....	44
51. Breakdown Strength Comparison for Reactive Gases.....	45
52. Capacitance and Leakage vs. Applied Voltage.....	48
53. Optical Images of Capacitor Surface after Applied Voltage from 0 V to 350 V.....	49
54. Effect of Electrode Thickness on Capacitor Leakage and Clearing .....	51
55. Capacitance vs. Voltage for Different Electrode Thicknesses.....	52
56. Optical Image of ALON Capacitor with Aluminum Electrodes.....	54
57. Optical Image of ALON Capacitor with Titanium Electrodes .....	54
58. Capacitance vs. Frequency at Various Temperatures in Vacuum .....	56
59. Capacitance vs. Frequency at Various Temperatures in Air.....	57
60. Dissipation Factor vs. Frequency at Various Temperatures in Air.....	58
61. Dissipation Factor vs. Frequency at Various Temperatures in Air.....	59
62. Cross-sectional Schematic of Stacked Multilayer Structure.....	62
63. Capacitance vs. Layers for Multilayer Devices .....	63
64. Insulation Resistance vs. Temperature at Various Voltages for a 1 Layer Device.....	64
65. Insulation Resistance vs. Temperature at 100 V for 1 and 2 Layer Devices .....	65
66. Insulation Resistance vs. Temperature at 50 V for 1 and 2 Layer Devices .....	66
67. Arrhenius Plot of Leakage Current Data .....	67
68. Temperature Stability of Packaged Capacitors.....	68

## List of Tables

<u>Table</u>	<u>Page</u>
1. Taguchi Analysis Parameters and Results .....	8
2. Elemental Composition of AlN Film from EDS.....	15
3. Elemental Composition of AlON Film from EDS.....	17
4. Scanner Parameters for AlON Deposition.....	35
5. Taguchi Analysis Parameters and Results for Nitrous Oxide.....	37
A-1. AlN Deposition Conditions .....	76
A-1. AlN Deposition Conditions (continued).....	77
A-1. AlN Deposition Conditions (continued).....	78
A-1. AlN Deposition Conditions (continued).....	79
A-1. AlN Deposition Conditions (continued).....	80
A-1. AlN Deposition Conditions (continued).....	81
B-1. Dielectric Properties of AlN Films .....	82
B-1. Dielectric Properties of AlN Films (continued).....	83
B-1. Dielectric Properties of AlN Films (continued).....	84
B-1. Dielectric Properties of AlN Films (continued).....	85
B-1. Dielectric Properties of AlN Films (continued).....	86
B-1. Dielectric Properties of AlN Films (continued).....	87
B-1. Dielectric Properties of AlN Films (continued).....	88
B-1. Dielectric Properties of AlN Films (continued).....	89
B-1. Dielectric Properties of AlN Films (continued).....	90
B-1. Dielectric Properties of AlN Films (continued).....	91
B-1. Dielectric Properties of AlN Films (continued).....	92
C-1. AlON Deposition Conditions Using N <sub>2</sub> O .....	93
C-2. AlON Deposition Conditions Using N <sub>2</sub> O .....	94
C-2. AlON Deposition Conditions Using N <sub>2</sub> O (continued).....	95
C-2. AlON Deposition Conditions Using N <sub>2</sub> O (continued).....	96
C-2. AlON Deposition Conditions Using N <sub>2</sub> O (continued).....	97
C-2. AlON Deposition Conditions Using N <sub>2</sub> O (continued).....	98
C-2. AlON Deposition Conditions Using N <sub>2</sub> O (continued).....	99
D-1. Dielectric and Electrical Properties .....	100
D-1. Dielectric and Electrical Properties (continued).....	101
D-1. Dielectric and Electrical Properties (continued).....	102
D-1. Dielectric and Electrical Properties (continued).....	103
D-1. Dielectric and Electrical Properties (continued).....	104
D-1. Dielectric and Electrical Properties (continued).....	105
D-1. Dielectric and Electrical Properties (continued).....	106

## **Foreword**

This research and development work entitled “High Energy Density Dielectrics for Pulsed Power Capacitors” was funded by the AF/OSD SBIR Phase II Program under K Systems Corporation Contract No. FA8650-04-C-2415 with the Energy and Power Systems Branch, Energy, Power, and Thermal Division, Propulsion Directorate, Air Force Research Laboratory, Wright-Patterson Air Force Base, OH.

The original program objectives for the aluminum nitride research included:

- (1) Optimize key manufacturing process steps: AlN films, AlN-coated aluminum oils/metallized polymer films. Processes will be optimized to achieve maximum adhesion of AlN, highest AlN dielectric strength and good thermal stability.
- (2) Design and construct prototype AlN deposition system using dual magnetron reactive sputtering technique for simultaneous deposition of AlN films on both sides of capacitor grade aluminum foils/metallized polymer films.
- (3) Design and construct prototype high energy density AlN capacitors by rolling under controlled environmental conditions.
- (4) Characterize and test AlN capacitors under various environmental conditions: develop understanding of the mechanisms of failure. Demonstrate capacitor capabilities with respect to equivalent series resistance (ESR), dissipation factor (DF), Frequency response, and temperature characteristics. The Military Standard Test Methods for Electronic and Electrical Component Parts (MIL-STD-202F) will be performed and, in particular they will include tests for humidity, thermal shock and high voltage conditions.

Aluminum nitride films were deposited on multiple substrates, including thin metal foils and polymers compatible with rolled capacitor technologies. Simple parallel plate capacitor structures were utilized to optimize the dielectric properties. At the conclusion of the original contract, an enhancement and extension were authorized to address unanticipated complications and overcome technical obstacles.

The objectives for the enhancement include:

- (1) Increase the deposition rate of aluminum oxynitride dielectrics deposited from pulsed magnetron reactive sputtering.
- (2) Modify the web-handling system to produce lengths of AlON on foil.
- (3) Construct multilayer capacitor structures for high volume efficiency utilizing the scanner in the web-handling system.
- (4) Improve the AlON capacitor energy density using the multilayer stacked construction.

- (5) Improve the efficiency of the operation by depositing both dielectric and metal electrode in one process.
- (6) Investigate the thickness and materials of the metal electrode for self-clearing and high temperature applications.
- (7) Demonstrate prototype packaged multilayer AlON capacitors.

Aluminum nitride films were deposited on multiple substrates, including thin metal foils and polymers compatible with rolled capacitor technologies. Stacked multilayer capacitor structures have been developed using in-situ processing.

As a result of the work done during this program, seven manuscripts have been submitted and published, and eleven presentations were given at professional conferences.

We would like to thank Ms. Sandra Fries-Carr and Mr. Joseph Weimer, Air Force Research Laboratory (AFRL), Propulsion Directorate, Energy and Power Systems Branch, Wright-Patterson Air Force Base, Ohio, for their interest and support of this program.

Dr. Richard L.C. Wu, Chief Scientist, was the Principle Investigator, and Dr. Kevin R. Bray, Senior Process Engineer, conducted the research and film characterization.

The period of performance was from February 17, 2004 to August 31, 2008.

## **Summary**

Aluminum oxynitride (AlON) capacitors exhibit several promising characteristics for high energy density capacitor applications in extreme environments. Dielectric constants in the range of 9 and dielectric strength in excess of 650 V/ $\mu$ m have been demonstrated in our SBIR Phase II program, resulting in material energy densities greater than 14 J/cc. The dielectric properties remain stable from cryogenic temperatures of -200 °C to temperatures above 400 °C. Stacked capacitor devices have been developed and packaged. The high energy density and wide temperature stability make AlON an attractive candidate for many military, space and commercial applications.

## 1. Introduction

Capacitors are key components in all forms of electronic devices. Military systems utilize millions of capacitors and consider them key components due to their susceptibility for failure. Future needs for weapons systems and aircraft performance require the development of compact, high energy density capacitors for pulsed power and extreme environment applications. Compact, high performance capacitors are the enabling technology for the More Electronic Aircraft (MEA), Directed Energy Weapons (DEW), Directed Energy Attack Aircraft (DE ATAC), Unmanned Combat Aerial Vehicles (UCAV), High Power Microwave (HPW), Electric Propulsion Power Conditioning, Space Based Laser (SBL), and Space Plane Power Management and Distribution (PMAD). Available state-of-the-art (SOTA) dielectric materials include polymer films such as polypropylene (PP), polyester (PET) and polyvinylidene fluoride (PVdF) [1]. Polymer film capacitors dominate current pulsed power and AC applications. Polymers are used for most AC applications because of their non-polar nature and low dielectric losses. Key drawbacks to polymer films include their low operating temperature, typically  $\sim 100$  °C [1], and their large volume-to-weight ratio, which compromises energy storage density.

Most polymers also have a dielectric constant ( $k$ ) in the range of 2 – 4, although  $k$  for PVdF is from 10 – 12 [1]. These low  $k$  values make it difficult to obtain the high energy density required for future military applications. Polymer breakdown voltage is typically in the range of 550 V/ $\mu$ m [1]. Energy density ( $u_v$ ) depends linearly on dielectric constant ( $k$ ) and on the square of the dielectric breakdown strength ( $E_B$ ) of a capacitor as shown in Equation 1,

$$u_v = \frac{1}{2} k \epsilon_0 E_B^2 \quad (1)$$

where  $\epsilon_0$  is the permittivity of free space. Increasing the breakdown voltage increases the energy density more rapidly than increasing the dielectric constant. Energy densities between 3 and 10 J/cc are typical for current SOTA polymer dielectric materials. Improved dielectric materials for capacitors are needed to meet the military's future power applications. Materials with a higher dielectric constant, greater dielectric breakdown strength and superior thermal stability are needed to improve capacitor performance to meet emerging needs.

Crystalline aluminum nitride (AlN) is a semiconductor with one of the largest known bandgaps (6.2 eV) [2,3] with dielectric strength between 400 and 550 V/ $\mu$ m [4] and thermal conductivity of 320 W/mK [3]. Amorphous AlN retains many of the crystalline properties and the insulating properties and high resistivity in conjunction with the high breakdown strength make amorphous AlN a desirable material for high density power applications. Thin AlN films have been deposited using a wide range of processes including MOCVD [5,6], RF and DC magnetron sputtering [4,7,8,9,10], and pulsed laser deposition [3,10]. Film structures from amorphous to epitaxial crystals have been obtained by varying deposition parameters and substrates [11].

Pulsed DC sputter deposition produces faster deposition rates than other deposition methods and also results in less substrate heating and thermal stressing of the films [9]. The aluminum target does not experience the same target poisoning that occurs during  $\text{Al}_2\text{O}_3$  sputtering, making the AlN process easier to control and reproduce [8]. Aluminum oxynitride (AlON) also exhibits a stable magnetron sputtering deposition process. Thin amorphous  $\text{Al}_2\text{O}_3$  films have shown

breakdown strength  $\sim$ 500 V/ $\mu$ m [12]. Oxynitride films improve upon this parameter. In this work, the material and dielectric properties of DC sputtered amorphous AlN and AlON are further investigated.

Aluminum nitride and aluminum oxynitride dielectrics were successfully developed in our initial SBIR phase II program. Aluminum oxynitride (AlON) capacitors exhibit several promising characteristics for high energy density capacitor applications in extreme environments. Dielectric constants in the range of 9 and dielectric strength in excess of 600 V/ $\mu$ m have been measured, resulting in material energy densities greater than 14 J/cc. The dielectric properties remain stable from cryogenic temperatures of -200 °C to temperatures above 400 °C. The high energy density and wide temperature stability make AlON an attractive candidate for many military, space and commercial applications. In the initial phase of this program, films are grown using pulsed DC reactive magnetron sputtering processing with a N<sub>2</sub>/O<sub>2</sub> reactive gas mixture. One key barrier to producing commercially viable AlON capacitors is the relatively low deposition rate of less than 1 Å/s. We investigated altering the gas composition to increase the deposition rate by replacing the N<sub>2</sub>/O<sub>2</sub> gas mixture with different constituents. Both the oxygen and nitrogen species are needed to produce high quality films. The addition of oxygen to the nitrogen plasma improved the dielectric properties, but decreased the deposition rate.

Low deposition rates, problems with the aluminum foil scanner and new power conditioning applications that take advantage of the wide temperature properties necessitate additional experimentation to overcome these challenges. Improvements in the deposition rate and an increase in the volumetric efficiency of the AlON capacitors are needed to enhance the feasibility of AlON devices. Therefore, an enhancement program was implemented to investigate techniques to increase the sputter deposition rate through the addition of an inert gas to the reactive mixture. It also explored the influence of a different reactive gas mixture on the growth rate. Nitrous oxide (N<sub>2</sub>O) is commonly used in the semiconductor industry to deposit nitrogen doped oxide films. Thus, nitrous oxide and nitrogen were used as the sputtering gas.

In addition, a multilayer capacitor stack structure was deposited on wafers and other substrates using an in-situ process and was evaluated for increased volumetric efficiency for power conditioning applications. Several packaged AlON capacitors have been manufactured and tested at high temperatures.

## **2. Program Objectives**

The original program objectives for the aluminum nitride research include:

- (1) Optimize key manufacturing process steps: AlN films, AlN-coated aluminum oils/metallized polymer films. Processes will be optimized to achieve maximum adhesion of AlN, highest AlN dielectric strength and good thermal stability.
- (2) Design and construct prototype AlN deposition system using dual magnetron reactive sputtering technique for simultaneous deposition of AlN films on both sides of capacitor grade aluminum foils/metallized polymer films.
- (3) Design and construct prototype high energy density AlN capacitors by rolling under controlled environmental conditions.
- (4) Characterize and test AlN capacitors under various environmental conditions: develop understanding of the mechanisms of failure. Demonstrate capacitor capabilities with respect to equivalent series resistance (ESR), dissipation factor (DF), Frequency response, and temperature characteristics. The Military Standard Test Methods for Electronic and Electrical Component Parts (MIL-STD-202F) will be performed and, in particular they will include tests for humidity, thermal shock and high voltage conditions.

The objectives for the enhancement include:

- (1) Increase the deposition rate of aluminum oxynitride dielectrics deposited from pulsed magnetron reactive sputtering.
- (2) Modify the web-handling system to produce lengths of AlON on foil.
- (3) Construct multilayer capacitor structures for high volume efficiency utilizing the scanner in the web-handling system.
- (4) Improve the AlON capacitor energy density using the multilayer stacked construction.
- (5) Improve the efficiency of the operation by depositing both dielectric and metal electrode in one process.
- (6) Investigate the thickness and materials of the metal electrode for self-clearing and high temperature applications.
- (7) Demonstrate prototype packaged multilayer AlON capacitors.

### **3. Dual Ion Beam Deposition System**

The unique Dual Ion Beam Source deposition system has been modified for aluminum nitride pulsed magnetron reactive sputtering deposition. The ion beam sources were replaced with 4" diameter magnetron sputtering guns with  $\frac{1}{4}$ " thick 99.999% pure Al targets. The RF power supplies were replaced with pulsed DC power supplies with a range up to 5 kW power and pulse frequencies up to 350 kHz. Research grade Ar, N<sub>2</sub>, O<sub>2</sub>, and N<sub>2</sub>O gases are available for sputtering. The aluminum foil scanner plate used for DLC deposition is also being utilized for AlN film growth. The scanner is equipped with substrate cooling/heating capabilities ranging from 5 °C to 40 °C. A class 100 clean room enclosure houses the entire deposition system. Figure 1 shows the deposition systems in the clean room facilities.

For individual small substrates, a copper plate was designed for substrate mounting. The temperature is monitored via a thermocouple attached to the backside of the mounting plate. A schematic of the deposition system is shown in Figure 2. The Dual Ion Beam Source deposition system was further modified for use in this enhancement. The scanner apparatus was replaced with a precision sample transfer manipulator, shown in Figure 3. The manipulator allowed the use of both sputter sources in the chamber, one for dedicated conductive metal electrode deposition and the other for insulating dielectric layers. Our dual sputter source deposition system and scanner provides us the ability to deposit multilayer capacitor stacks in-situ without outside process steps such as etching. The sputter deposition allows the deposition of both conductive metal electrode films and insulating dielectric layers in the same apparatus without breaking vacuum. This in-situ processing will improve the interfaces between the layers and reduce damage and defects from exposure to air and additional processing steps. Insulating substrates are needed for multilayer stacks. Initial experiments utilized glass plates and subsequently oxidized silicon wafers with 1  $\mu\text{m}$  SiO<sub>2</sub> were used as substrate material.

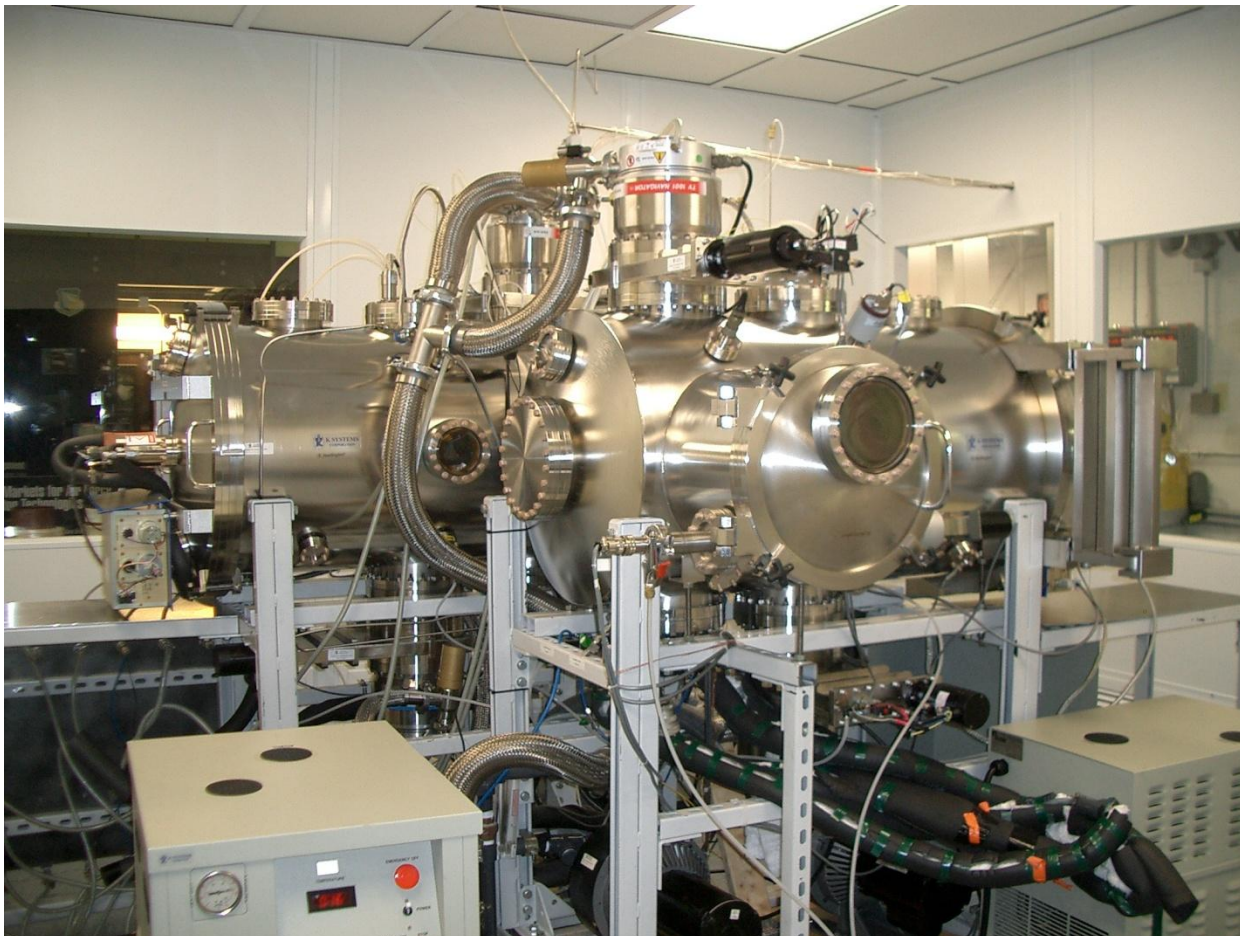


Figure 1. Dual Ion Beam Deposition System

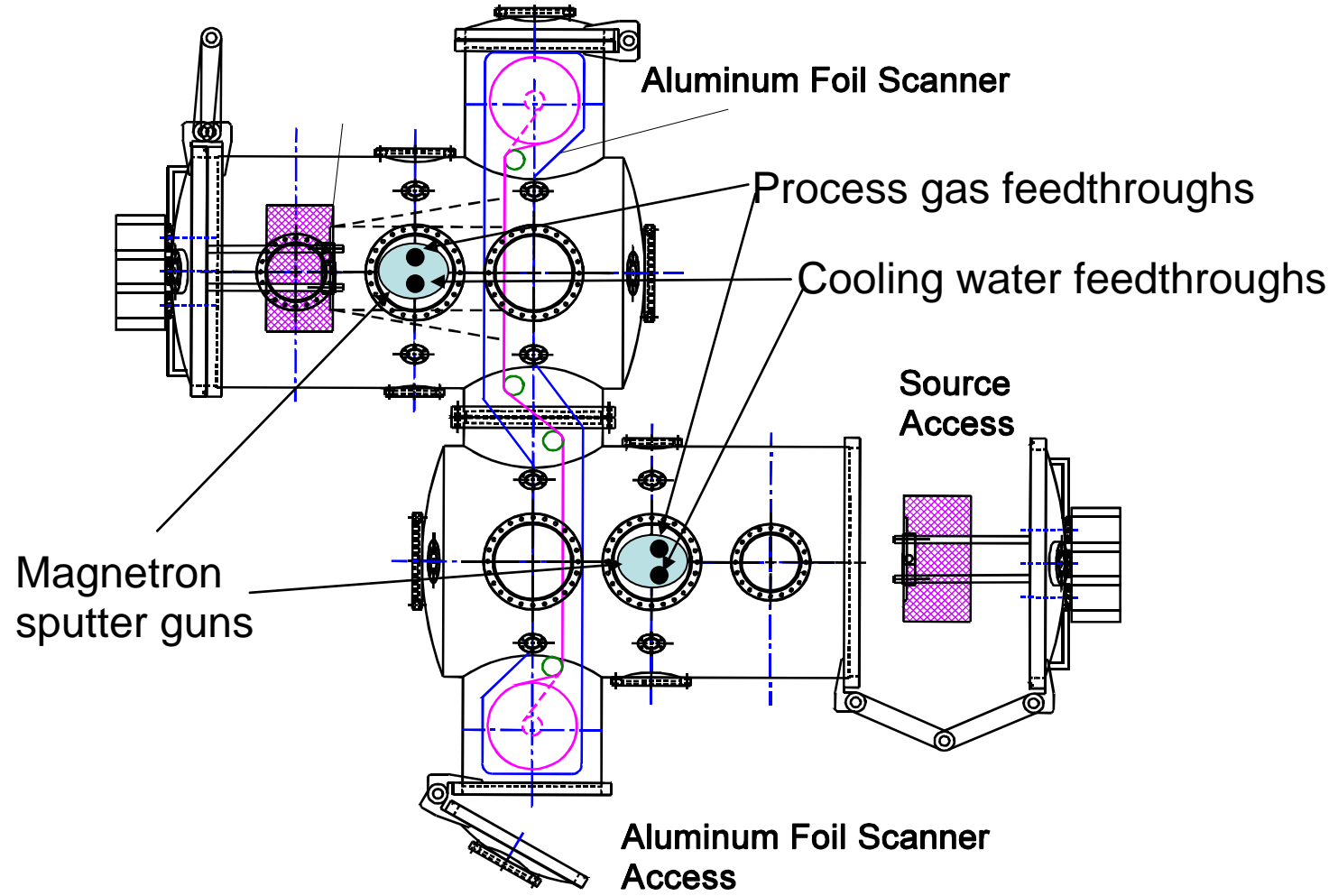


Figure 2. Schematic of Dual Ion Beam Deposition System

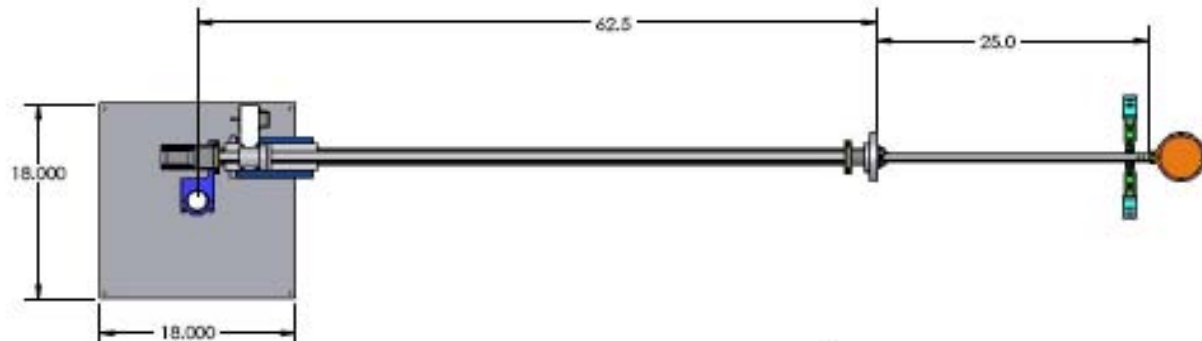


Figure 3. Schematic of Precision Sample Transfer Manipulator

## 4. Aluminum Nitride Deposition from N<sub>2</sub>/O<sub>2</sub>

### 4.1 Process Optimization

The process parameters for AlN deposition were optimized to maximize dielectric performance. The effects of DC power, gas mixture, pulse frequency, target-to-substrate spacing, and process pressure were examined. A statistical process optimization procedure was employed to identify key input parameters.

Genichi Taguchi used orthogonal tables in experiments designed to improve quality control. The purpose of orthogonal design is to study the relationship between process parameters (input parameters) and their corresponding output functions by selecting certain representative combinations of input parameter level settings. By following the orthogonal table, a maximum amount of information can be obtained using the least number of experiments.

#### 4.1.1 Taguchi Analysis

A set of process optimization experiments was performed. Table 1 lists the input parameters examined and the resulting properties. DC power, pulse frequency and process pressure were varied in the analysis. The one factor plots from the analysis are shown in Figure 4 – 12. The most significant effects were observed in relation to the breakdown strength. Both the DC power and frequency influenced this parameter. No significant effects were observed for the dielectric constant and the dissipation factor.

Table 1. Taguchi Analysis Parameters and Results

Sample	Run	Power (W)	Frequency (kHz)	Pressure (mTorr)	k	HV (V/micron)	DF	Rate (Å/s)
AlN060	1	1000	50	10	7.12	445	0.0241	1.36
AlN055	2	1000	150	12.5	8.30	402	0.0317	1.50
AlN057	3	1000	250	15	7.48	527	0.0363	1.67
AlN054	4	1500	50	15	10.36	513	0.0543	2.45
AlN061	5	1500	150	10	10.17	393	0.0313	2.35
AlN052	6	1500	250	12.5	8.43	270	0.0217	2.73
AlN058	7	2000	50	12.5	8.05	349	0.0178	3.01
AlN056	8	2000	150	15	6.93	424	0.0139	2.34
AlN053	9	2000	250	10	9.77	200	0.0159	3.51

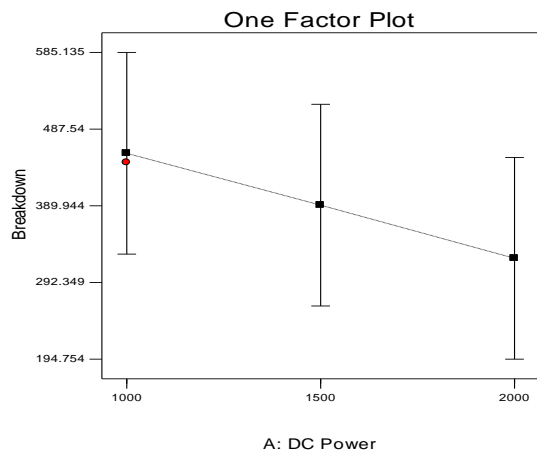


Figure 4. Breakdown Voltage vs. DC Power

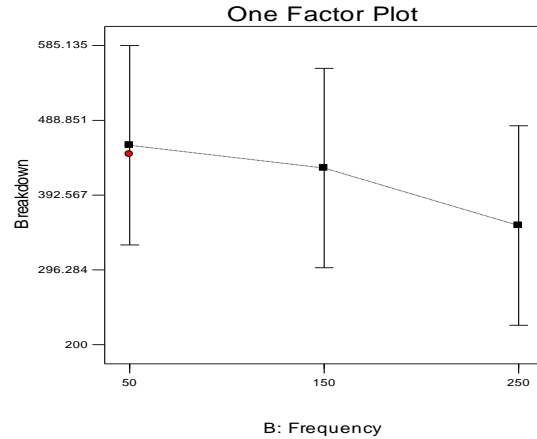


Figure 5. Breakdown Voltage vs. Frequency

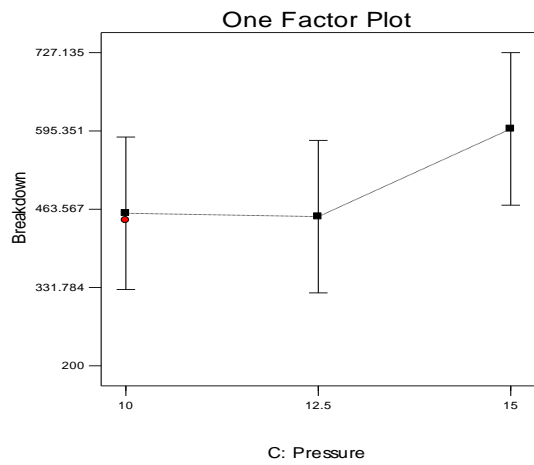


Figure 6. Breakdown Voltage vs. Pressure

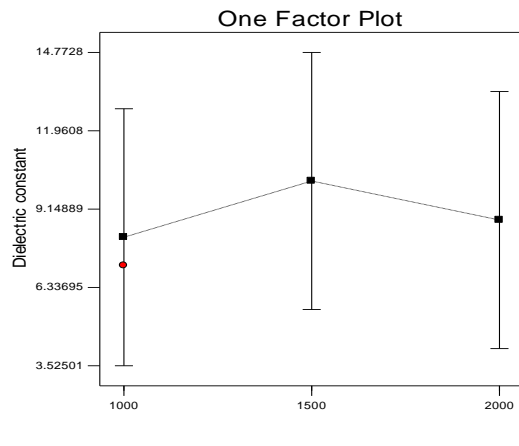


Figure 7. Dielectric Constant vs. DC Power

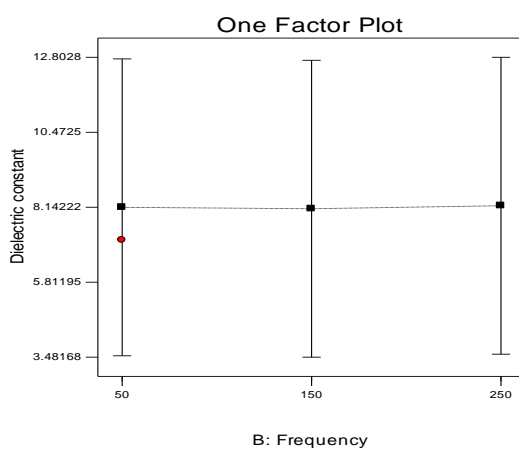


Figure 8. Dielectric Constant vs. Frequency

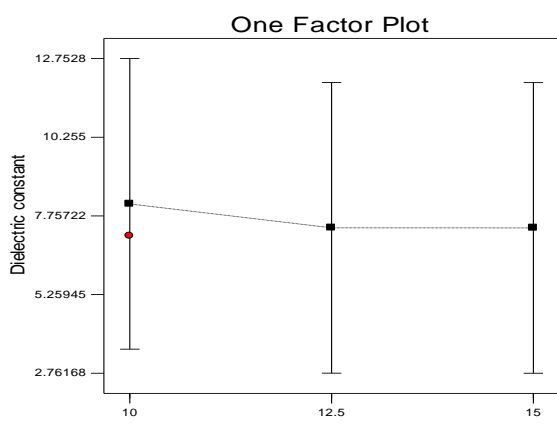


Figure 9. Dielectric Constant vs. Pressure

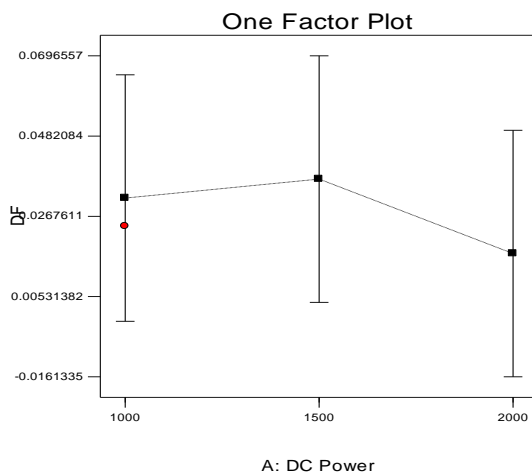


Figure 10. Dissipation Factor vs. DC Power

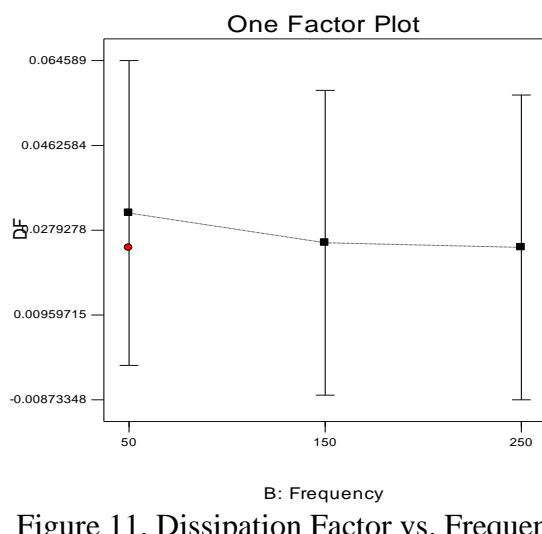


Figure 11. Dissipation Factor vs. Frequency

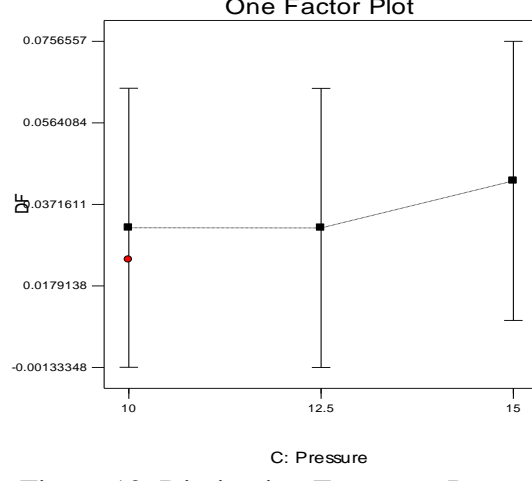


Figure 12. Dissipation Factor vs. Pressure

#### 4.1.2 Gas Composition

Initial aluminum nitride films were deposited from pure nitrogen plasma. The capacitance and dissipation factor exhibited significant frequency dependence and additional studies were undertaken to examine the effects of process gas composition. Figure 13 shows the capacitance and dissipation factor plotted vs. frequency for films deposited from pure nitrogen plasma and an N<sub>2</sub>:O<sub>2</sub> mixture. The aluminum nitride deposition was optimized to stabilize the capacitance and dissipation factor with respect to frequency. The addition of oxygen improves the frequency stability of the capacitance. It also lowers the dissipation factor by an order of magnitude. The addition of oxygen also had the adverse effect of decreasing the deposition rate. Argon was also mixed in the system to increase the sputtering rate. This raised the deposition rate, but the film quality was degraded and argon was removed from the process.

#### 4.1.3 Breakdown Strength

Dielectric breakdown strength is one of the most critical film properties for high power density devices. Examination of deposition parameters including DC power, deposition pressure and pulse frequency determined that DC power was the most significant process input into film breakdown. Figure 14 plots breakdown strength vs. DC Power for different N<sub>2</sub>:O<sub>2</sub> gas ratios. The breakdown strength increases with increasing power initially, achieves a maximum and then decreases at higher powers. The optimal DC power to achieve the maximum breakdown can be shifted by altering the N<sub>2</sub>:O<sub>2</sub> ratio. Maximum breakdown strength of ~600 V/ $\mu$ m has been measured. This is consistent with increasingly energetic particles sputtered from the target with increasing power. As more energetic material reaches the substrate, it is capable of diffusing and adhering to the optimal location. As the power increases beyond the optimal setting, the particles arrive at the surface too rapidly, and there is not sufficient time for diffusion before the subsequent layer deposits. Increased power during film growth also results in a higher aluminum fraction in the deposited film. Increased DC power has also been shown to increase micro voids in the dielectric. The higher metal content or the increased void concentration creates defect sites that breakdown under lower applied voltage.

## Capacitance and Dissipation Factor vs. Frequency

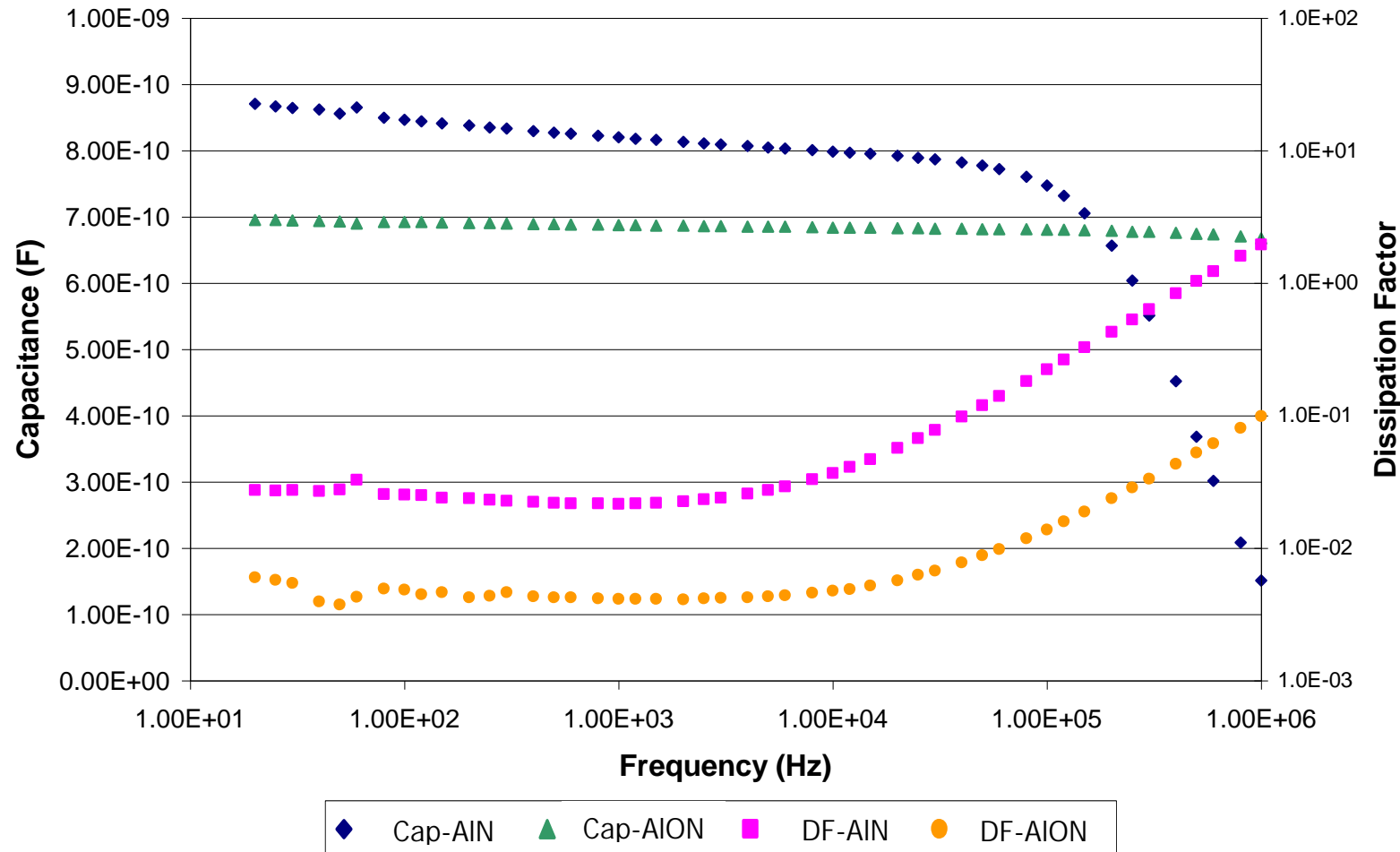


Figure 13. Capacitance and Dissipation Factor vs. Frequency from  $N_2$  and  $N_2:O_2$  Plasmas

## Breakdown Voltage vs. DC Power

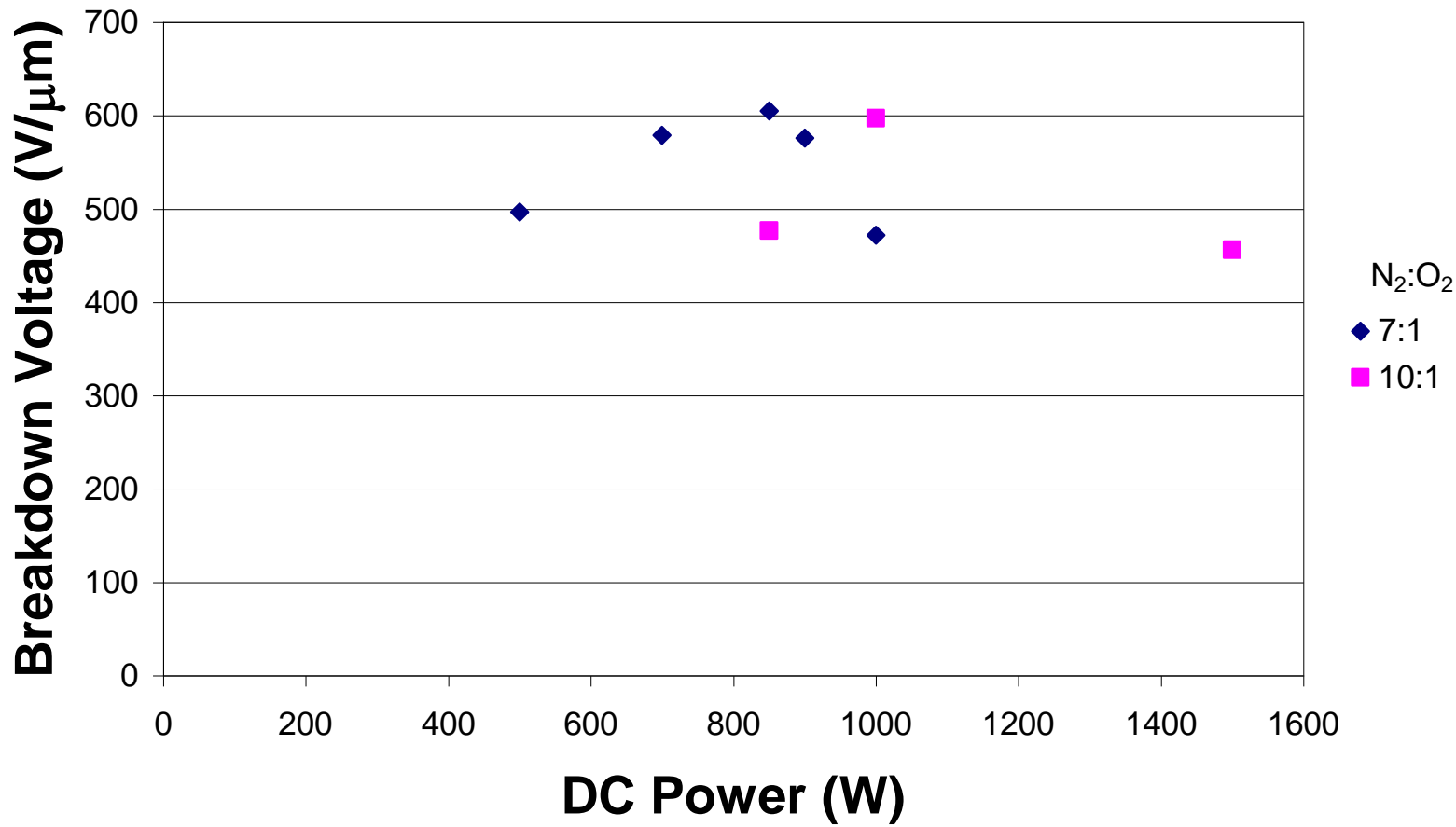


Figure 14. Breakdown Voltage vs. DC Power at various N<sub>2</sub>:O<sub>2</sub> Ratios

## 4.2 Chemical Composition

Energy Dispersive X-ray Spectroscopy (EDS) and Rutherford Backscattering Spectroscopy (RBS) were used to evaluate the chemical composition of our AlN and AlON films and to identify impurities and contaminants. Figure 15 shows the EDS spectrum of AlN096, deposited from pure nitrogen plasma. Table 2 lists the elemental composition of the film. Although no oxygen was introduced into the process, residual gas in the deposition chamber was incorporated in the film. The high concentration of carbon observed in our previous report was eliminated by thoroughly flushing the gas lines. The Al:N ratio is ~1:1, with a slight excess of Al. RBS analysis of the same sample reports the same results as shown in Fig. 16, the RBS composition vs. depth profile. Al, O and N are observed, with a uniform distribution throughout the film.

The results change dramatically when oxygen is intentionally added to the process. Figure 17 is the EDS spectrum for AlN112, deposited with a 10:1 ratio of N:O. The oxygen completely replaces the nitrogen in the film and an AlO compound is formed. Although evaluation of the spectrum does not indicate any nitrogen in the film, closer inspection indicates a shoulder on the oxygen peak from a small amount of nitrogen. The RBS spectrum in Fig. 18 confirms both of these results. The sample is primarily AlO, with an Al:O ratio of ~1:2, and ~7% N present. The standard heats of formation for crystalline AlN and  $\text{Al}_2\text{O}_3$  are -318 kJ/mol and -1675.7 kJ/mol respectively. The formation of aluminum oxide is ~5X more thermodynamically favorable than aluminum nitride. Although reactive sputtering does not operate at thermodynamic equilibrium, the heats of formation indicate any excess oxygen will displace nitrogen in the films.

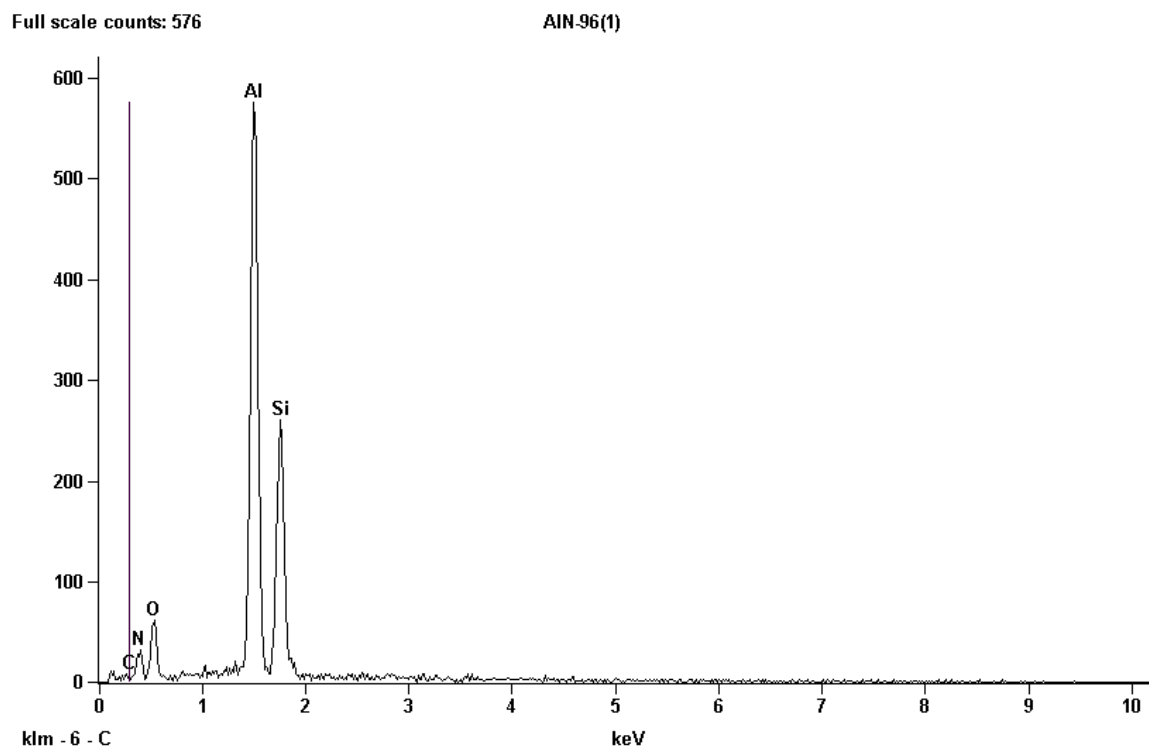


Figure 15. EDS Spectrum of AlN Film

Table 2. Elemental Composition of AlN Film from EDS

SAMPLE NO.	ATOM CONCENTRATION %			
	C	N	O	Al
AlN096	0.00	35.73	23.54	40.73

# Charles Evans & Associates

Figure \_\_\_\_\_

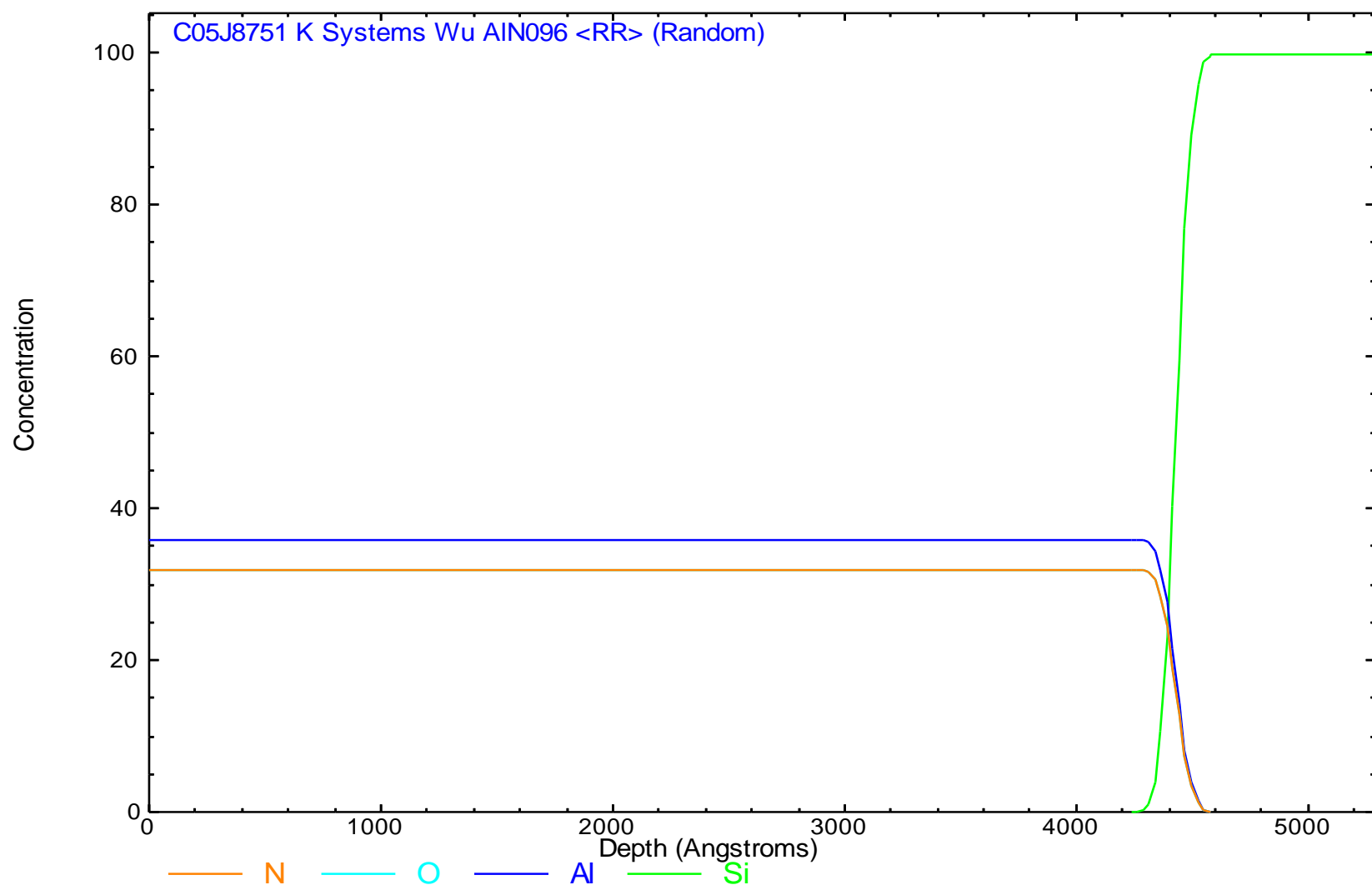


Figure 16. RBS Spectrum of AlN Film

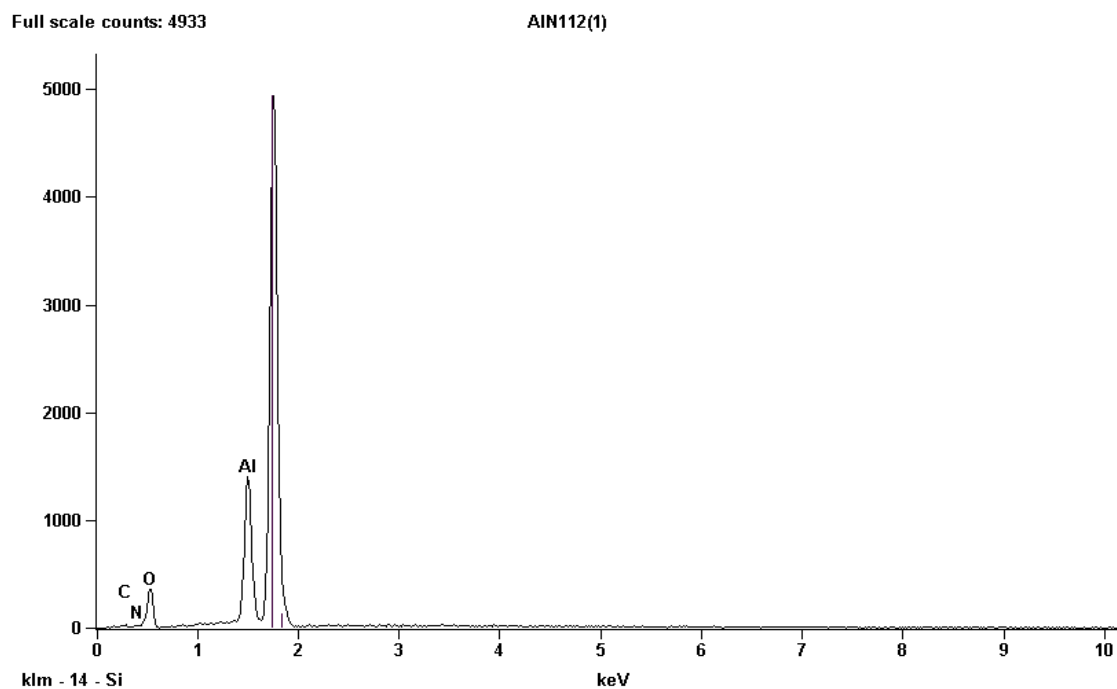


Figure 17. EDS Spectrum of AlON Film

Table 3. Elemental Composition of AlON Film from EDS

SAMPLE NO.	ATOM CONCENTRATION %			
	C	N	O	Al
AlN12	18.90	0.00	56.06	25.04

# Charles Evans & Associates

Figure \_\_\_\_\_

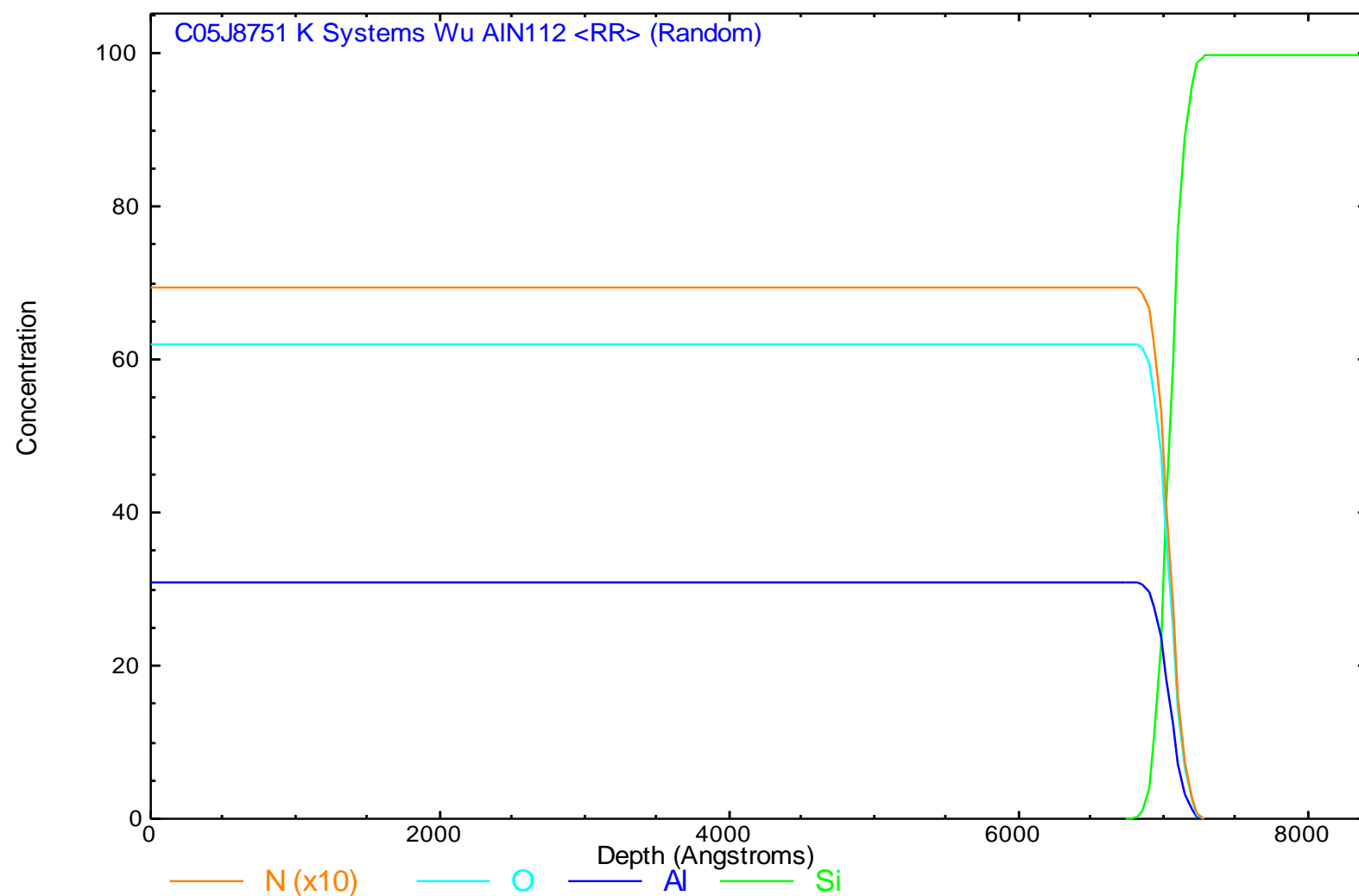


Figure 18. RBS Spectrum of AlON Film

### 4.3 Aluminum Nitride Deposition

Aluminum nitride deposition runs were conducted on numerous substrates and utilizing a wide variety of process settings. DC power ranged from 500 W to 2000 W, with pressures between 5 mTorr and 20 mTorr. Films were deposited on metallized silicon wafers, metallized glass, aluminum foil, and metallized polymers. Nitrogen plasma with argon and oxygen dilution was also examined. The target-to-substrate distance was varied from 3" to 6". Active substrate cooling was also investigated. Deposition times were adjusted to achieve 5000-Å-films. Appendix A summarizes the deposition conditions for each experimental run from the initial aluminum nitride investigation.

### 4.4 Film Thickness and Surface Characterization

A Dektak 3ST surface profilometer was utilized to measure the film thickness across the deposited films. A portion of each Si or glass substrate was masked with a thin strip of stainless steel foil or high temperature tape to create a thickness step. Multiple step height measurements across the entire sample were averaged to obtain the reported film thickness.

An Olympus optical microscope with integrated digital camera and a Scanning Electron Microscope (SEM) were employed to image the surface structure of the AlN films deposited on a variety of substrates. Optical surface images at magnifications from 100X to 1000X were obtained. Figure 19 shows a typical SEM image of an AlN film on silicon. The surface is smooth and amorphous. Figures 20 and 21 are optical images of films deposited on glass and FPE polymer. Some small surface defects were observable, but large pinholes were not present in the majority of the samples. Good adhesion was observed on all of the substrates investigated without any surface pretreatments.

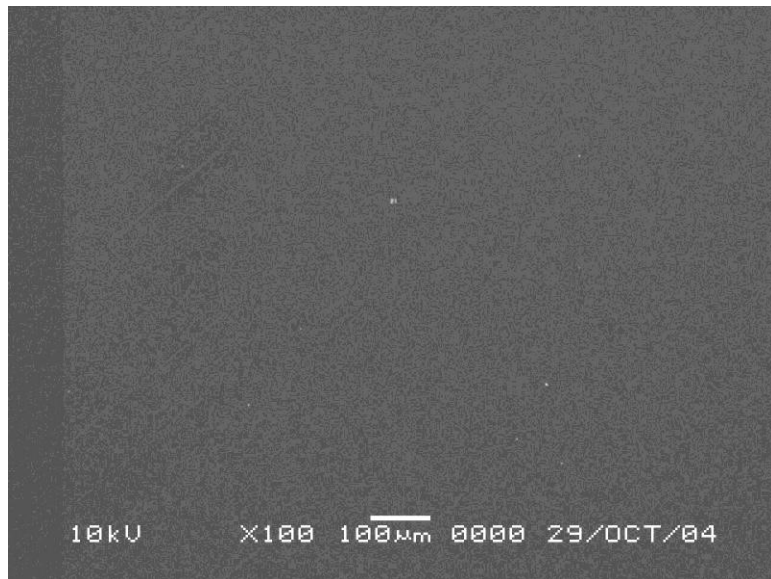


Figure 19. SEM Micrograph of AlN on Si

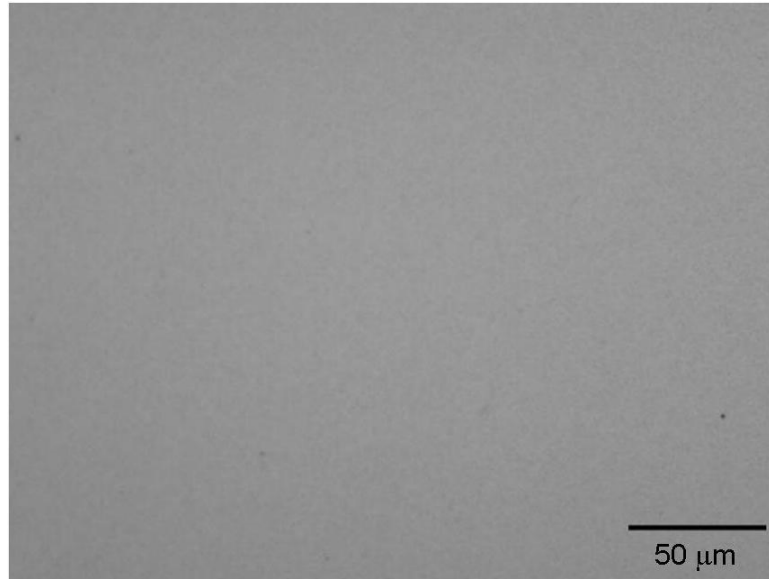


Figure 20. Optical Micrograph of AlN on Glass

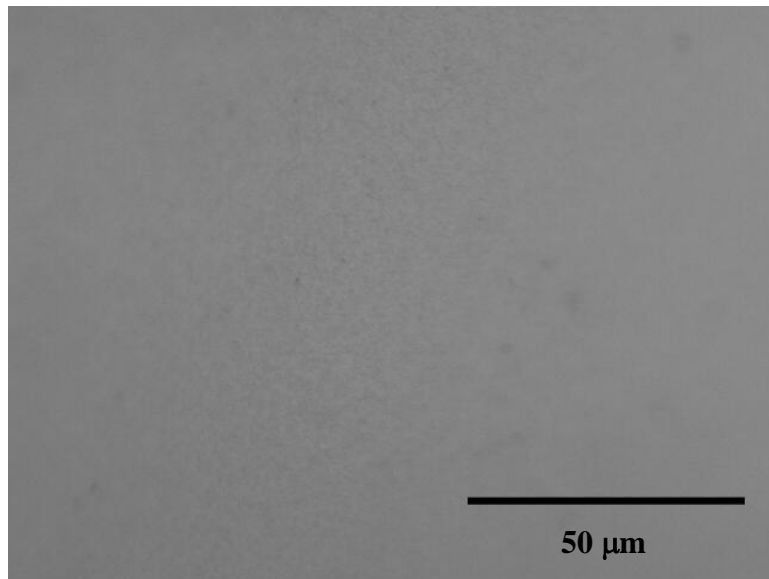


Figure 21. Optical Micrograph of AlN on FPE

#### 4.5 Dielectric Properties

Extensive dielectric properties of AlN films have been characterized at K Systems facilities in the AFRL/RZPE Capacitor Research Center, WPAFB, OH. The characterizations include: (1) spot check, (2) frequency characterization, (3) insulation resistance and (4) dielectric breakdown. Values of the dielectric constant and dissipation factor are obtained from the spot checks and frequency analysis. The resistance is calculated from the AC frequency measurements and the DC IR measurements. Breakdown voltage was determined by applying a voltage stepped in

regular increments to a capacitor for a set time duration and measuring the resulting current until complete breakdown occurs. Steps of 5 V and 10 V were applied for 3 or 5 seconds in typical tests. The average dielectric constant at 1 kHz is ~9, with a dissipation factor of ~ 0.005 and a breakdown voltage of ~600 V/ $\mu$ m. Appendix B summarized the dielectric results. “Film” refers to the film thickness measured by profilometry or estimated from the deposition rate. “HV” is the actual breakdown voltage. Blank cells in the table could not be measured.

#### 4.5.1 Atmospheric Stability

The stability of the capacitance and dissipation factor with respect to atmospheric exposure was also measured as a function of frequency. Figures 22 and 23 plot capacitance and dissipation factor vs. frequency for AlN112, deposited in January, 2005. The film was originally measured directly after deposition. It was then allowed to sit on the desktop open to the laboratory atmosphere for six months. The second trace on the plots is the frequency response after this six month exposure. The capacitance remains constant with frequency for both measurements. There is approximately a 6% change in the capacitance value, reflecting a small change in the dielectric constant. The dissipation factor is equivalent below ~5 kHz, and then there is a minor change with the aged film showing a slightly lower value at higher frequencies.

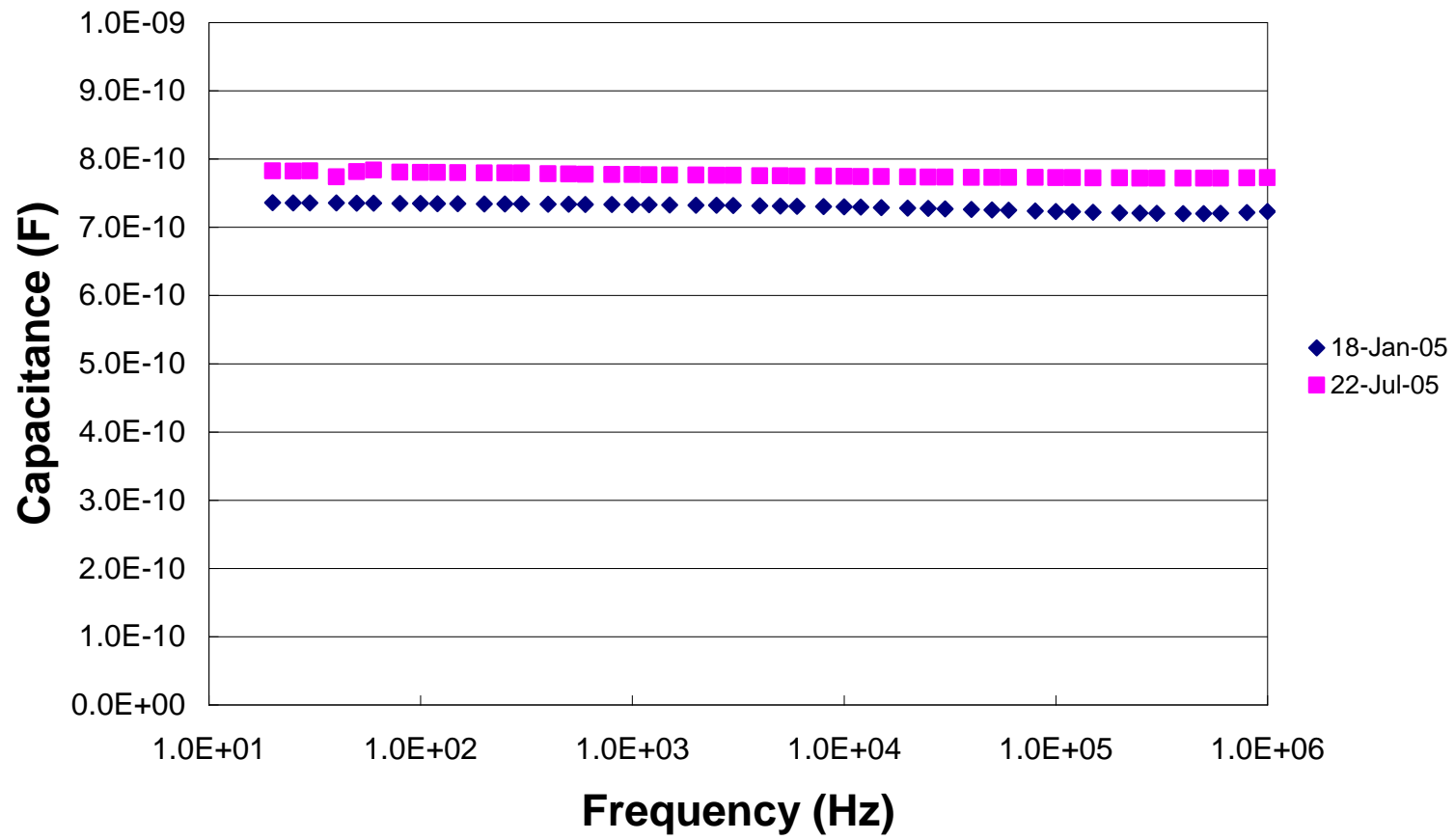


Figure 22. Effects of Atmospheric Exposure on the Capacitance

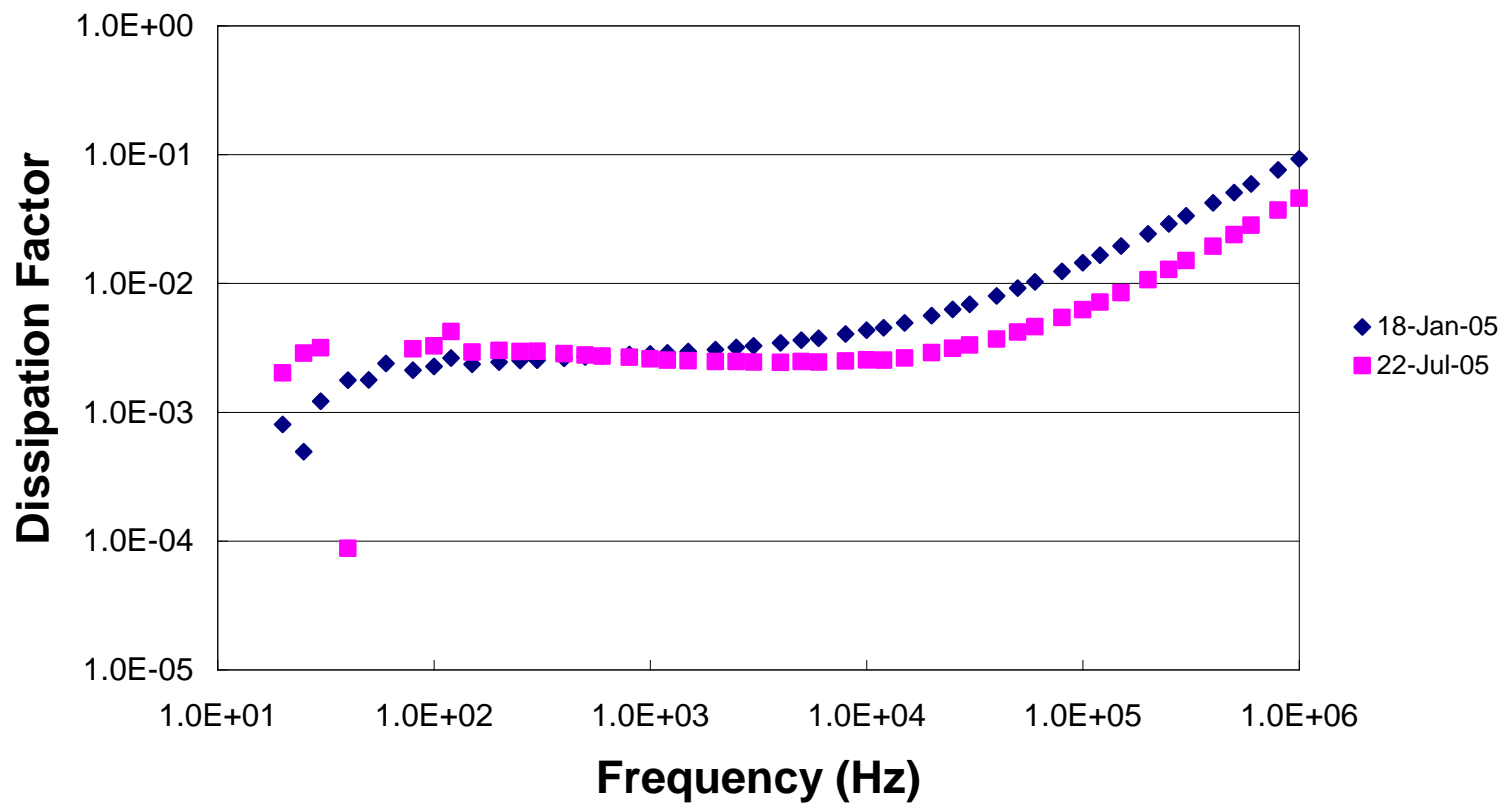


Figure 23. Effect of Atmospheric Exposure on Dissipation Factor

#### 4.5.2 Substrate Materials

Aluminum oxynitride films have been deposited on a variety of substrates including both rigid materials such as glass and silicon and flexible substrates such as polymers and thin metal foils. The ability to deposit AlON films on flexible substrates is important for constructing rolled capacitor devices. Polymer films along with aluminum, stainless steel and titanium metal foil substrates were investigated. Initial polymer testing utilized Mylar, a polyester film. Previous work on DLC capacitors had utilized Mylar as a substrate. But the AlON sputter deposition involves a higher energy deposition than the DLC process. The Mylar material was consistently burned and warped during deposition. We then turned our attention to a high temperature polymer, fluorine polyester (FPE). Results with this material were much more successful. We were able to deposit 5000 Å AlON films on 5-μm-thick FPE substrates. The high temperature properties of FPE were able to withstand the intense plasma beam. Dielectric constants of ~9 and DF ~0.005 were observed at 1 kHz on all substrates. Figure 24 shows the capacitance and dissipation factor for films grown on a variety of substrates. The capacitance remains independent of the substrate material for all the materials examined. Below 5 kHz, the dissipation factor behaves similarly for each substrate. The metallized glass and metal foil substrates continue to exhibit comparable behavior to 1 MHz. The sample on FPE begins to deviate from the other materials around 5 kHz.

The initial substrate smoothness also has a considerable influence on the breakdown strength. Figure 25 plots the leakage current vs. applied field for 5000-Å-thick films deposited on thin stainless steel and titanium foils under identical deposition conditions. The film on the stainless steel foil shows over 200 V/μm increase in the breakdown field strength compared to the film on the titanium. Examination of the film surfaces using optical microscopy, shown in Figures 26 and 27, helps explain these dramatic differences. The stainless steel foil is much smoother than the titanium. The initial roughness of the titanium results in local areas where the AlON is thinner than estimated, resulting in preferential breakdown sites at lower fields. Films grown on other smooth substrates, including silicon, glass, and FPE, exhibit dielectric strengths of ~600 V/μm.

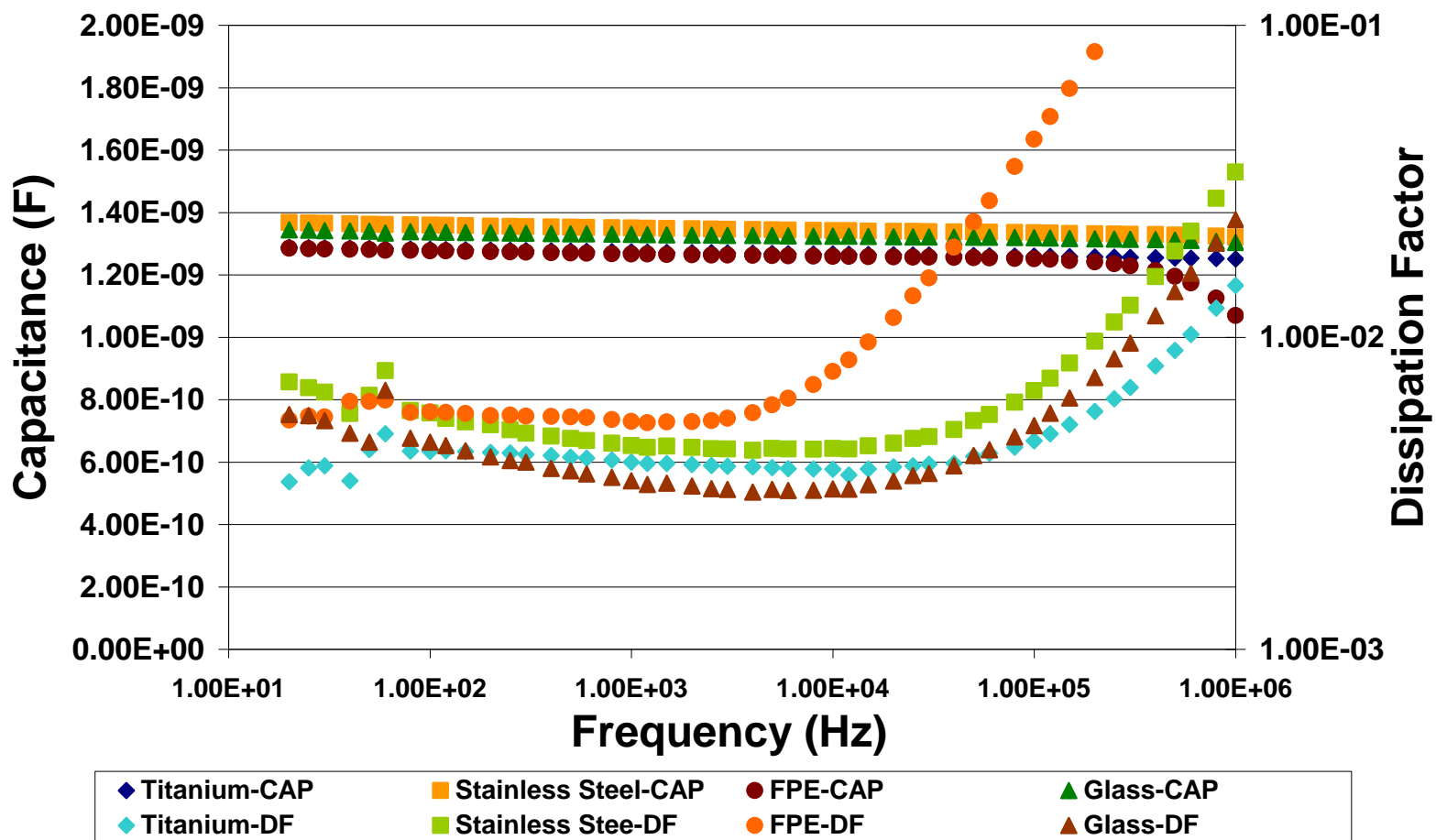


Figure 24. Effects of Substrate on Capacitance and Dissipation Factor

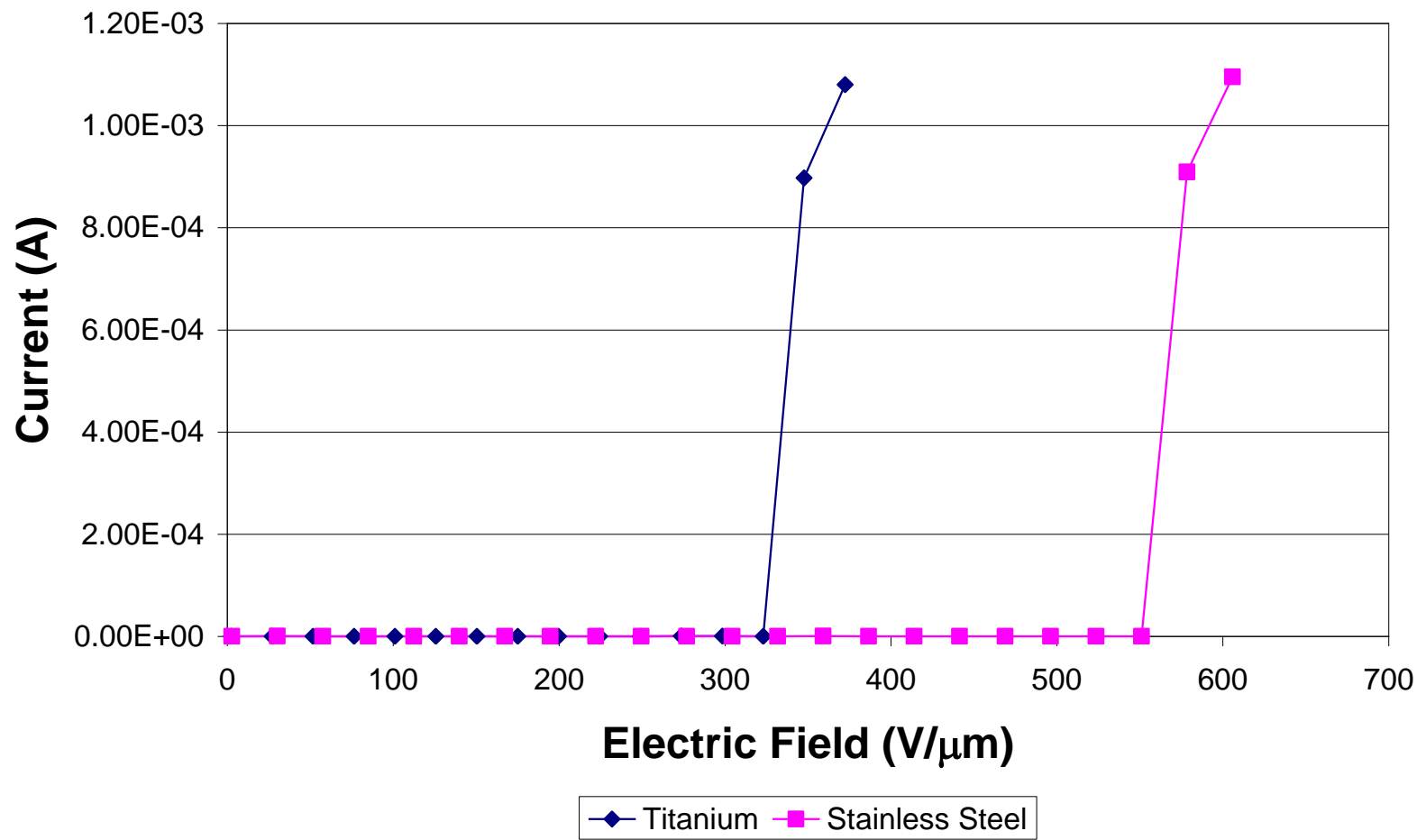


Figure 25. Effects of Substrate on Breakdown Strength



Figure 26. Optical Micrograph of AlON on Stainless Steel Foil

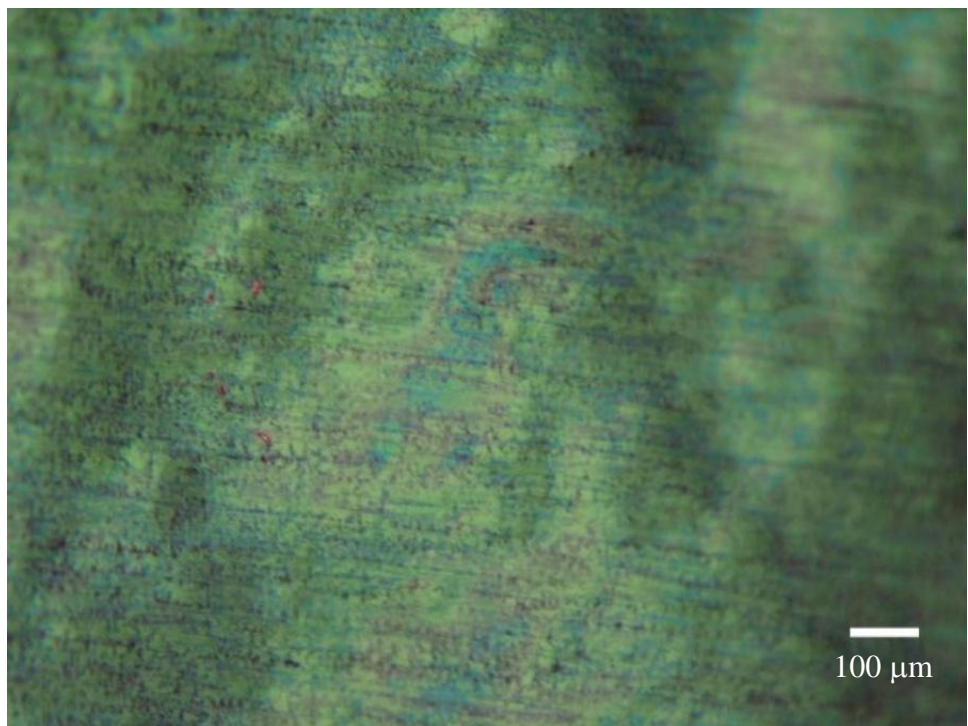


Figure 27. Optical Micrograph of AlON on Titanium Foil

## **5. Aluminum Foil Scanner Characterization**

### **5.1 Deposition Uniformity**

The dual ion beam deposition system is equipped with a scanner system for depositing dielectric films directly onto spooling aluminum foil or polymer films. The film thickness distribution was examined across the exposed scanner deposition area. Figures 28 and 29 show the vertical and horizontal thickness distribution in Source One while Figures 30 and 31 show the same information in Source Two. The vertical distribution is approximately constant for greater than two inches in both chambers, and then slowly begins to decrease. The horizontal growth profiles in both chambers are very similar. The data fit reasonably with a second order polynomial. The equations for the data fits shown in Figures 29 and 31 are very similar, indicating good reproducibility between the two chambers. The thickness distribution equations were utilized to calculate the average deposition rate across the scanner area. The scan speed necessary to coat 5000 Å uniformly across a moving foil was determined from the average deposition rate.

Figure 32 plots the capacitance vs. frequency for samples deposited in both Source One and Source Two in different deposition runs. The data is reproducible and falls within  $\pm 10\%$  deviation. This suggests the film quality is similar in both deposition chambers.

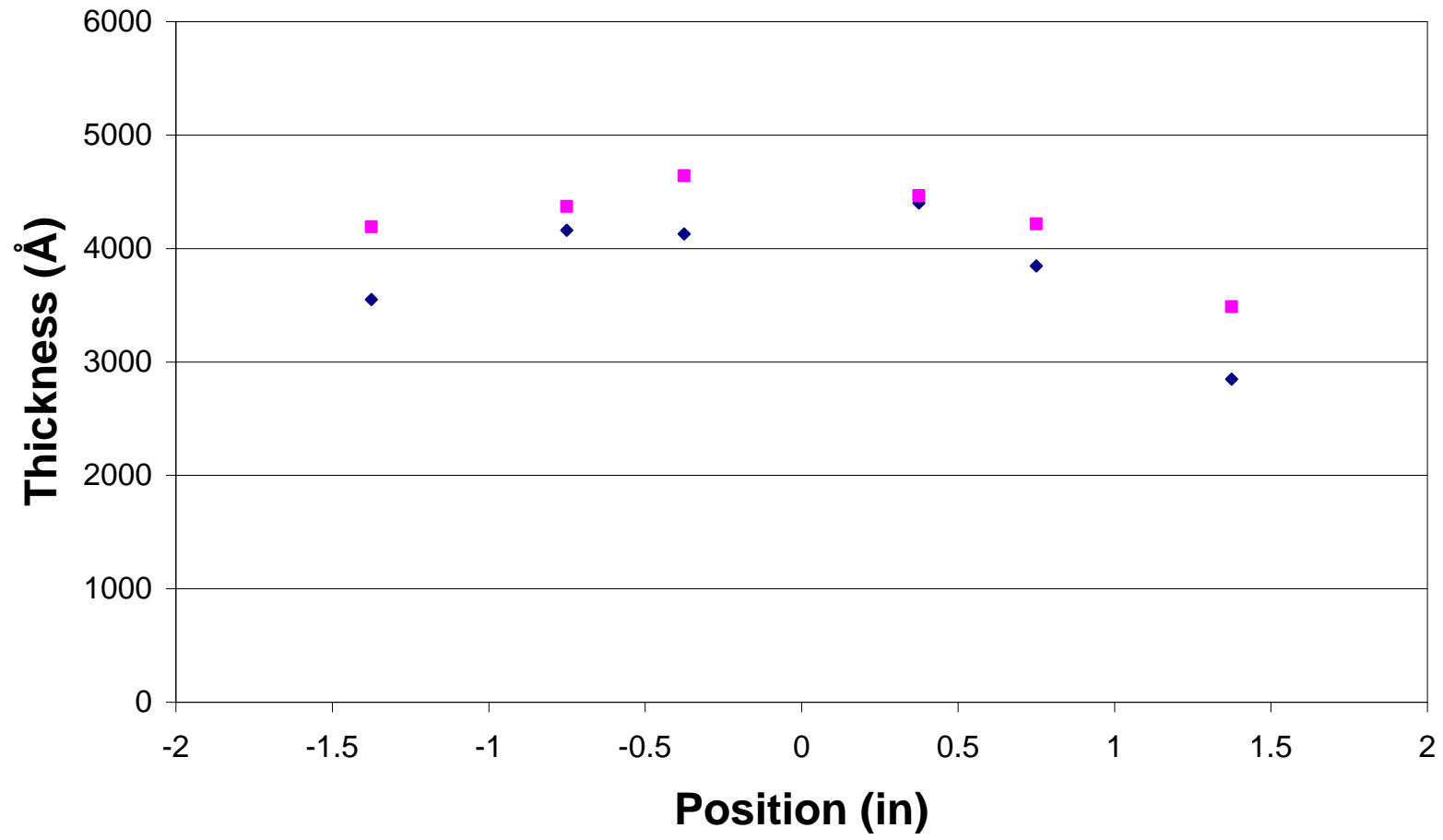


Figure 28. Vertical Deposition Distribution in Source One

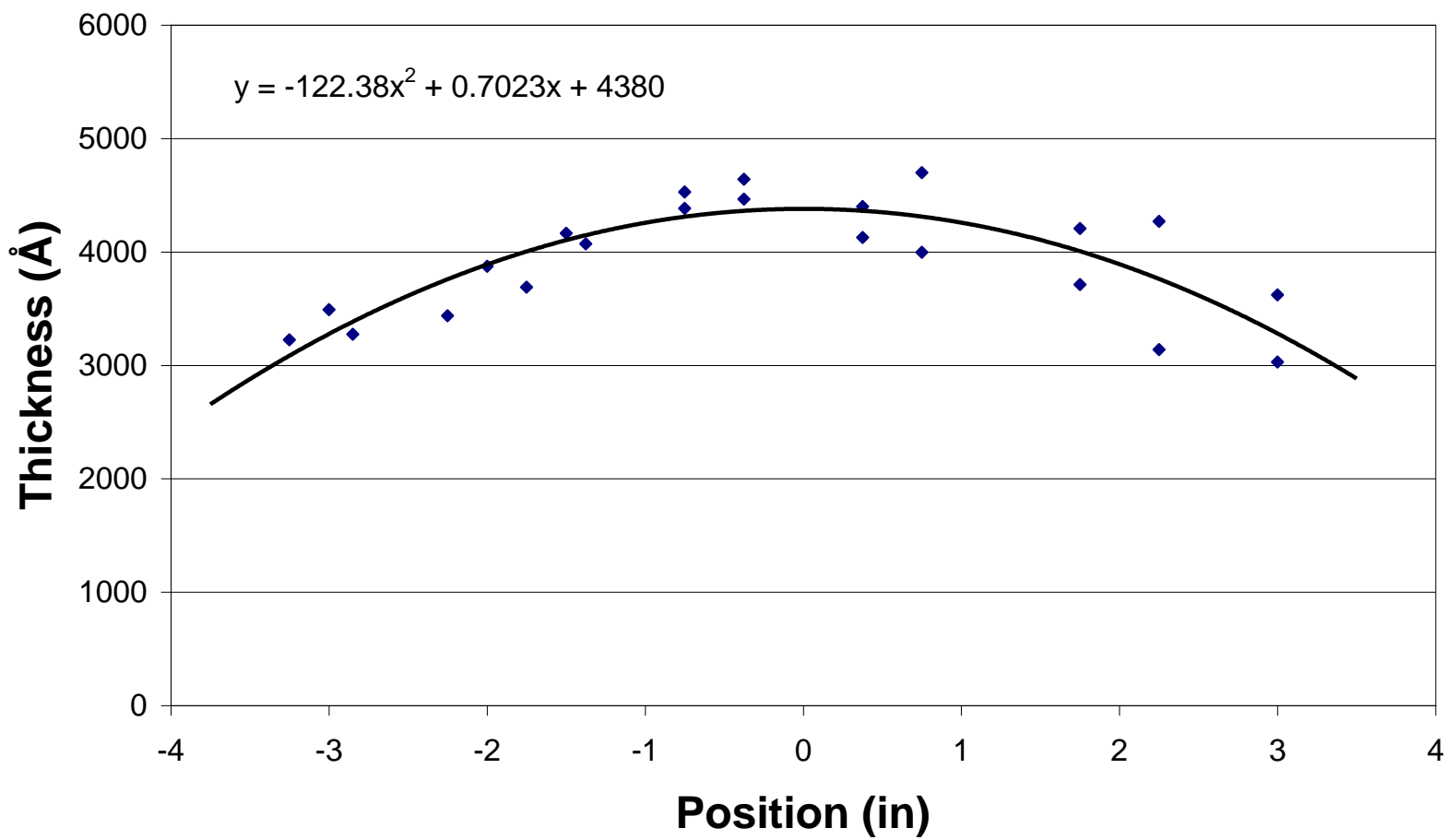


Figure 29. Horizontal Deposition Distribution in Source One

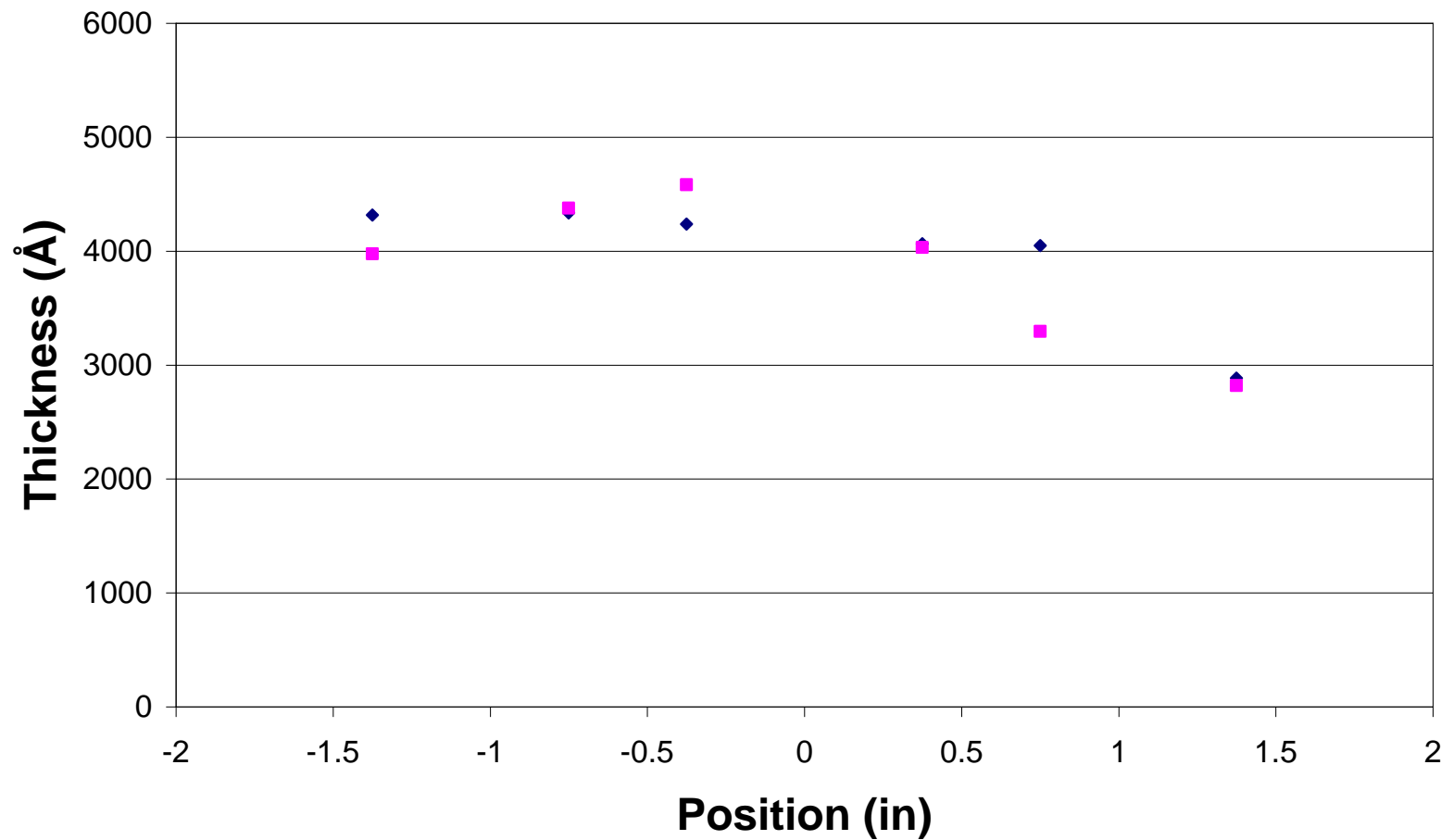


Figure 30. Vertical Deposition Distribution in Source Two

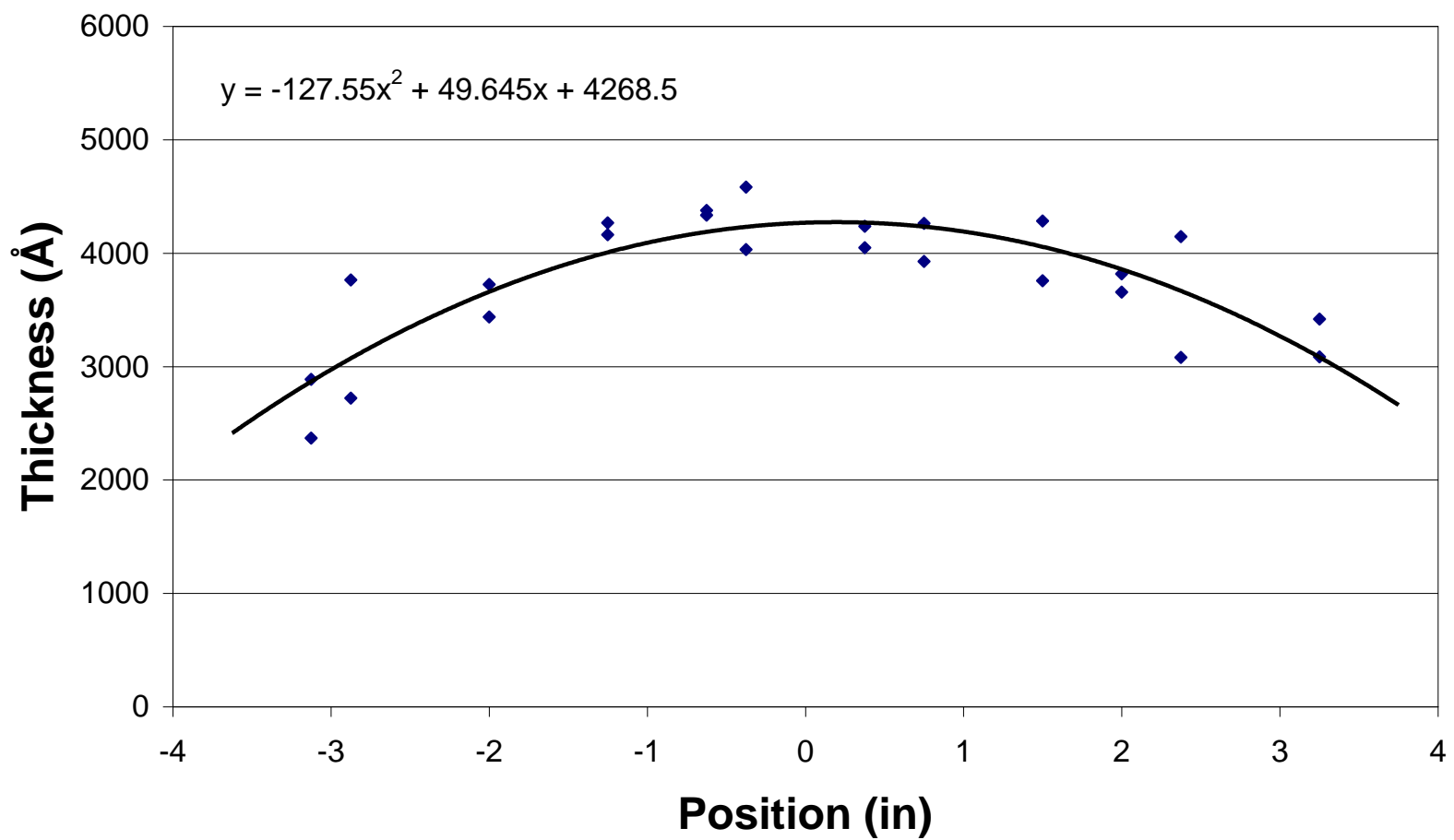


Figure 31. Horizontal Deposition Distribution in Source Two

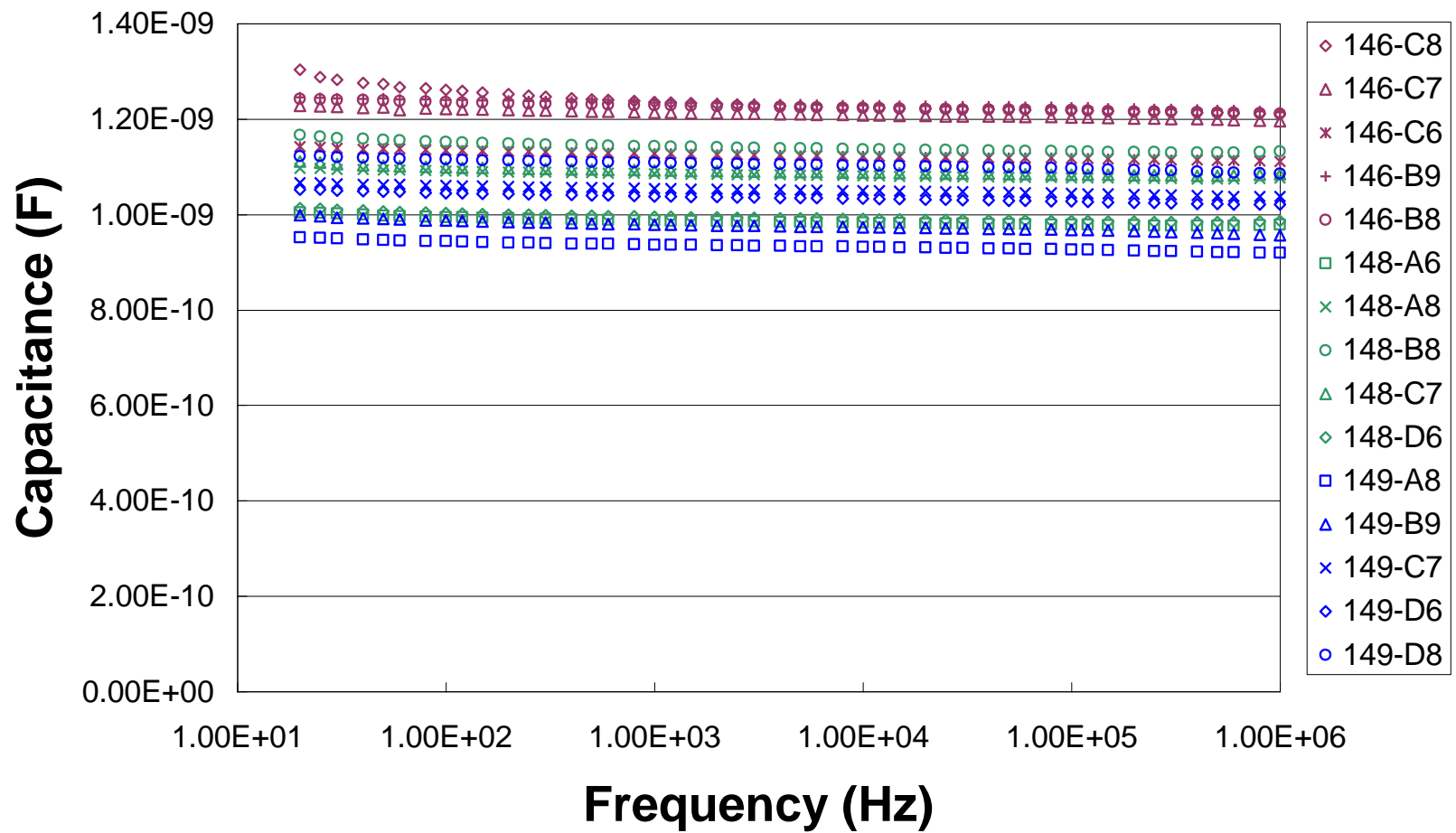


Figure 32. Comparison of Capacitance Values from the Dual Sources in Different Runs

## 5.2 Aluminum Foil Scanning

Operation of the Aluminum Foil Scanner was investigated with various DC power levels, scanner speeds and film tensions. Both single and double-sided deposition onto aluminum foil was examined. Table 4 summarizes the deposition conditions and scanner settings studied. Several observations can be drawn from analyzing the data. First, the foil broke in all depositions with the tension set higher than 1 lb. Lowering the tension introduces other problems into the system as the foil does not remain rigid and would sag away from the back plate, creating thickness variations across the foil. Even with  $T = 1.0$  lb, the foil still broke when the DC power was greater than 500W. Actively cooling the foil during deposition does not improve the ability of the scanner to operate. Cooled foils broke under similar conditions as uncooled material. The scanning speed did not appear to influence the ability of the foil to withstand the plasma and films were successfully deposited on scanning foil with speeds from 0.5 in/min to 4.0 in/min. Lengths up to 18 inches were coated, using up to 70 deposition passes. Once stable process conditions are obtained, the scanner is capable of producing longer lengths of material. The scanner apparatus needs to be redesigned to prevent the foil from sagging to support deposition under the optimal process conditions.

Table 4. Scanner Parameters for AlON Deposition

<u>DC power (W)</u>	<u>Scan Speed (in/min)</u>	<u>Tension (lb)</u>	<u>DepPress (mTorr)</u>	<u># of Scans</u>	<u>Gas ambient N<sub>2</sub>:O<sub>2</sub>:Ar</u>	<u>Sides</u>	<u>Frequency (kHz)</u>	<u>Distance (inch)</u>	<u>Broke ?</u>	<u>Length (in)</u>	<u>Cooled ?</u>
850	0.14	4.0	11.5	1	7:1:0	2	50	5	Y	0.5	N
850	1.40	4.0	11.5	1	7:1:0	2	50	5	Y	2.6	N
850	1.4	2.0	11.5	1	7:1:0	2	50	5	Y	17.0	N
850	2.8	2.0	11.5	2	7:1:0	2	50	5	Y	-0.0	N
850	2.8	2.0	11.5	2	7:1:0	2	50	5	Y	-4.5	N
850	2.8	2.0	11.5	2	7:1:0	2	50	5	Y	-2.0	N
850	1.4	2.0	11.5	1	7:1:0	1	50	5	Y	11.4	N
850	2.8	2.0	11.5	2	7:1:0	1	50	5	Y	-1.0	N
850	2.8	2.0	11.5	2	7:1:0	1	50	5	Y	-12.1	N
850	3.5	2.0	11.5	2	7:1:0	1	50	5	Y	-4.0	N
850	3.5	2.0	11.5	3	7:1:0	1	50	5	Y	16.6	N
850	3.5	2.0	11.5	3	7:1:0	1	50	5	Y	3.9	N
850	3.5	2.0	11.5	4	7:1:0	1	50	5	Y	-3.0	N
850	3.5	2.0	11.5	4	7:1:0	1	50	5	Y	-9.3	Y
850	3.5	1.0	11.5	5	7:1:0	1	50	5	Y	11.1	N
500	3.5	1.0	11.5	45	7:1:0	1	50	5	N	6.0	N
600	1.0	1.0	11.5	3	7:1:0	1	50	5	Y	6.1	N
500	2.0	1.0	11.5	32	7:1:0	1	50	5	N	12.0	N
500	0.5	1.0	11.5	16	7:1:0	1	50	5	N	12.0	N
500	0.5	2.0	11.5	3	7:1:0	1	50	5	Y	6.7	N
500	4.0	1.0	11.5	70	7:1:0	1	50	5	N	18.0	N
500	4.0	1.0	11.5	15	7:1:0	2	50	5	Y	76.0	N
500	4.0	2.0	11.5	11	7:1:0	1	50	5	Y	23.0	N
600	4.0	1.0	11.5	4	7:1:0	1	50	5	Y	-8.2	N

## 6. Aluminum Oxynitride Deposition from N<sub>2</sub>O

### 6.1 Process Optimization

The process parameters for AlON deposition were further optimized to maximize dielectric performance and improve deposition rate. Nitrous oxide (N<sub>2</sub>O) is commonly used in the semiconductor industry to deposit nitrogen doped oxide films. Reactive sputtering with N<sub>2</sub>O has been used to introduce nitrogen into metal oxide films [13,14]. The double bonded nitrogen in N<sub>2</sub>O has a bond strength of ~ 450 kJ/mol compared to the triple bond strength of ~950 kJ/mol in N<sub>2</sub>. It is also easier to break the nitrogen-oxygen bond in N<sub>2</sub>O than the oxygen-oxygen bond in O<sub>2</sub> [15]. The weaker bond strengths in N<sub>2</sub>O result in a more reactive gas mixture with both oxygen and nitrogen present. The more reactive nitrogen species may increase the nitrogen content in the films, increasing the deposition rate and the dielectric strength. The effects of DC power, gas mixture, pulse frequency, target-to-substrate spacing, and process pressure were examined. A statistical process optimization procedure was employed to identify key input parameters.

#### 6.1.1 Taguchi Analysis

Genichi Taguchi used orthogonal tables in experiments designed to improve quality control. The purpose of orthogonal design is to study the relationship between process parameters (input parameters) and their corresponding output functions by selecting certain representative combinations of input parameter level settings. By following the orthogonal table, a maximum amount of information can be obtained using the least number of experiments.

Nitrous oxide was as an alternative reactive gas to improve the deposition rate. Table 5 lists the input parameters examined and the resulting properties. DC power, pulse frequency, reactive gas ratio and process pressure were varied in the analysis. The one factor plots from the analysis are shown in Figure 33 – 47. The most significant effects were observed in relation to the breakdown strength and deposition rate. DC power is the most significant influence for both these parameters. Higher power improves both properties. Dissipation factor also improved at higher power. The frequency also effected the dissipation. Lower frequency lowered the dissipation factor. Although lower frequency slightly lowered the breakdown voltage, the 50 kHz setting was selected as the optimal setting due to the better dissipation and only modest decrease in breakdown. No significant effects were observed for the dielectric constant.

Table 5. Taguchi Analysis Parameters and Results for Nitrous Oxide

SAMPLE	RUN	POWER (W)	PRESSURE (mTorr)	GAS RATIO (N <sub>2</sub> :N <sub>2</sub> O)	FREQUENCY (kHz)	K	DF	BD (V/ $\mu$ m)	RATE ( $\text{\AA}/\text{sec}$ )
AIN270	1	500	10	9	50	9.23	0.0121	114	1.30
AIN271	2	1000	5	9	150	8.45	0.0077	398	1.00
AIN279	3	1000	15	1	50				0.91
AIN280	4	1000	10	0	250	8.75	0.0134	349	0.76
AIN274	5	1500	15	9	250	7.73	0.0073	419	1.16
AIN275	6	500	15	0	150	9.85	0.0091	66	0.33
AIN281	7	500	5	1	250	9.31	0.0115	459	0.26
AIN282	8	1500	5	0	50	7.27	0.0032	622	1.67
AIN278	9	1500	10	1	150	7.12	0.0038	403	2.41

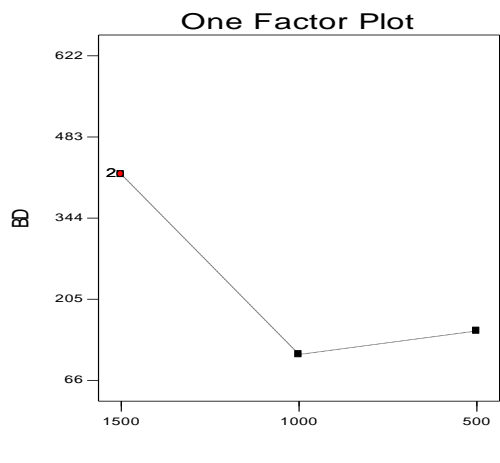


Figure 33. Breakdown Voltage vs. DC Power

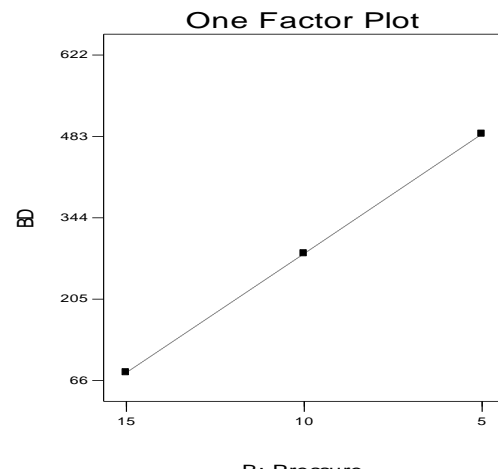


Figure 34. Breakdown Voltage vs. Pressure

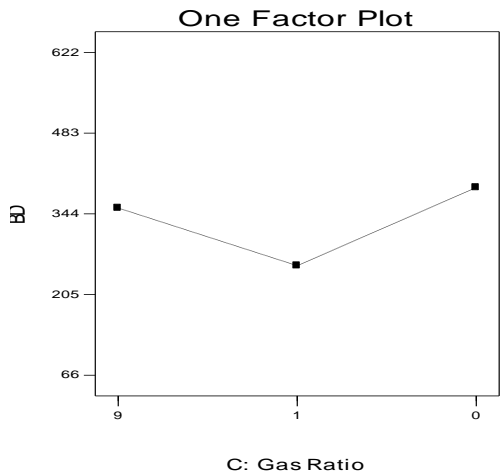


Figure 35. Breakdown Voltage vs. Gas Ratio

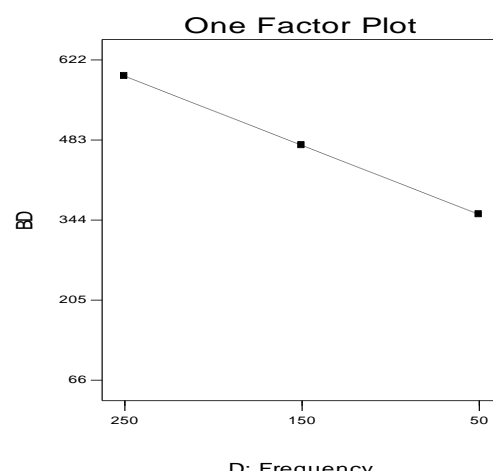


Figure 36. Breakdown Voltage vs. Frequency

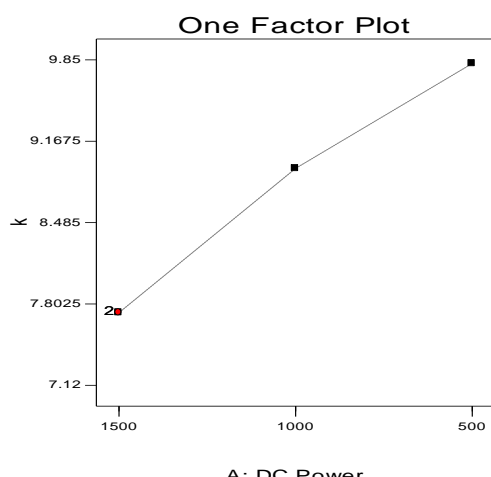


Figure 37. Dielectric Constant vs. DC Power

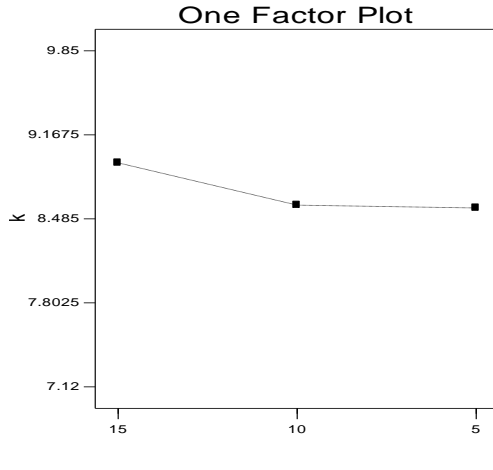


Figure 38. Dielectric Constant vs. Pressure

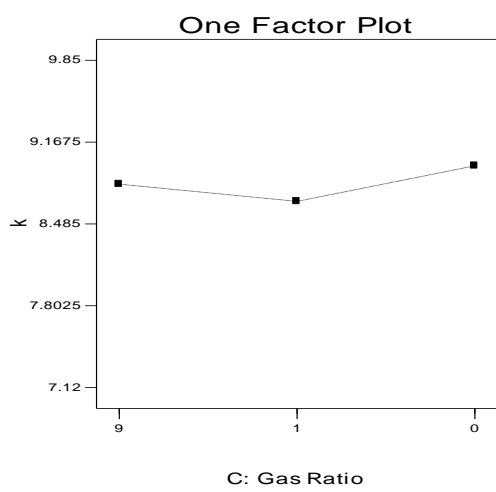


Figure 39. Dielectric Constant vs. Gas Ratio

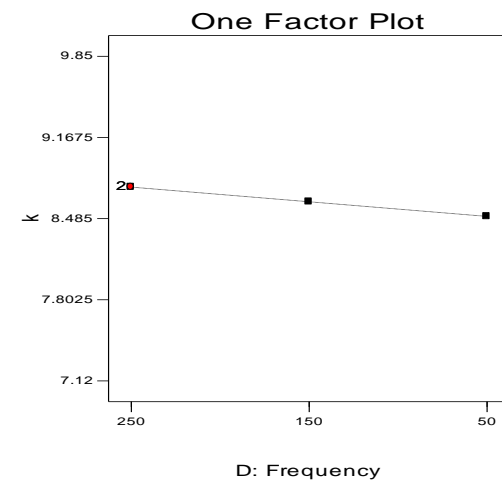


Figure 40. Dielectric Constant vs. Frequency

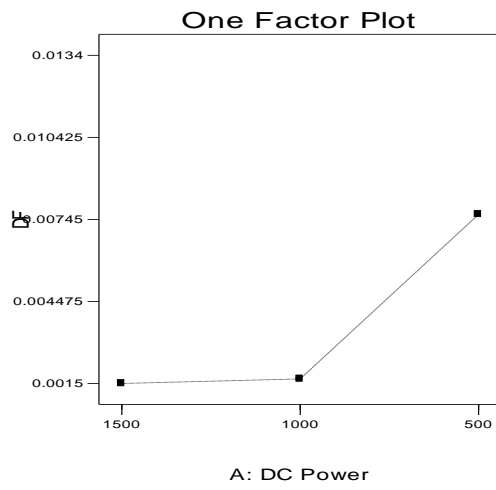


Figure 41. Dissipation Factor vs. DC Power

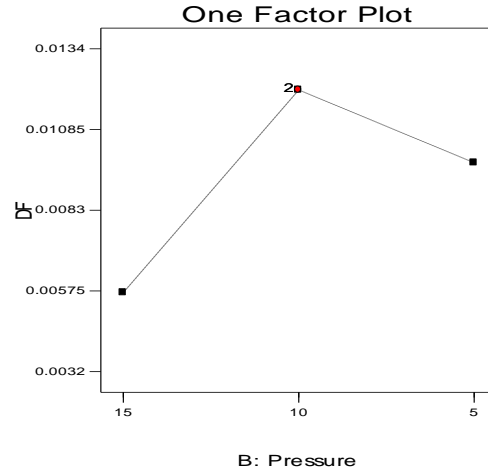


Figure 42. Dissipation Factor vs. Pressure

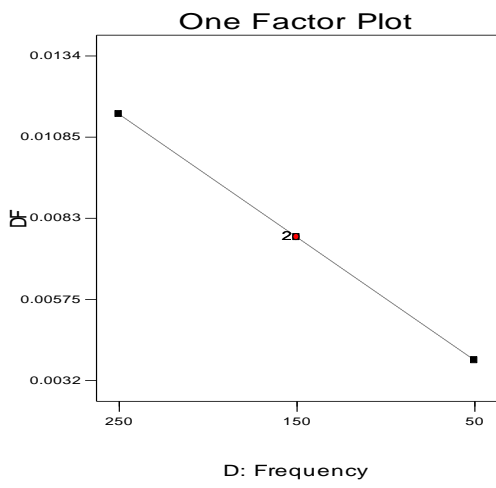


Figure 43. Dissipation Factor vs. Frequency

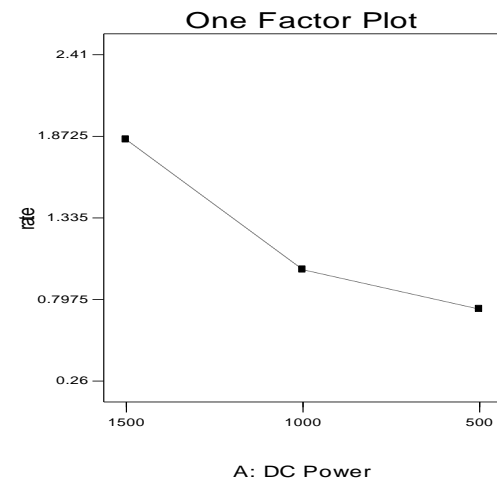


Figure 44. Deposition Rate vs. DC Power

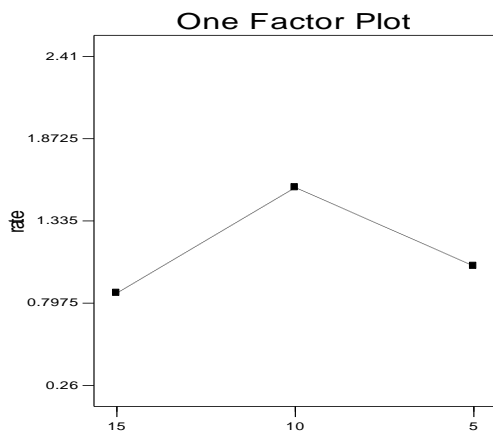


Figure 45. Deposition Rate vs. Pressure

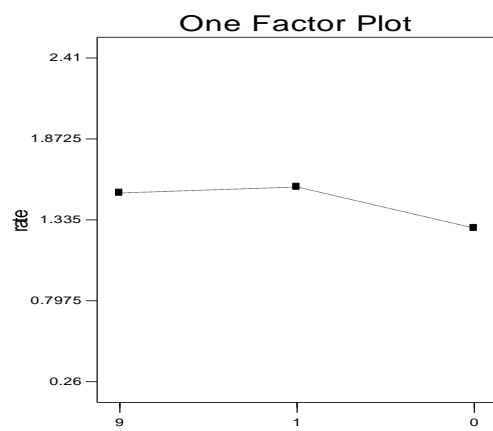


Figure 46. Deposition Rate vs. Gas Ratio

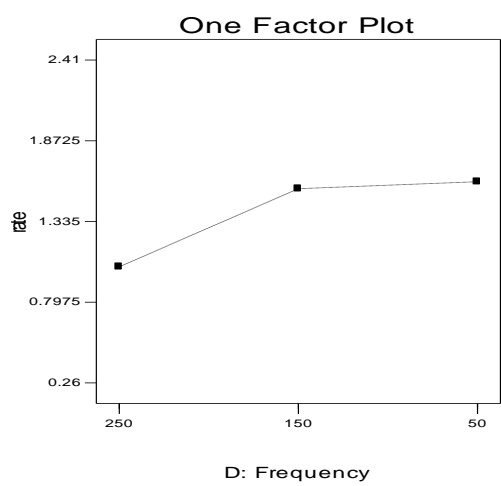


Figure 47. Deposition Rate vs. Frequency

### 6.1.2 Aluminum Oxynitride Deposition

Nitrous oxide ( $\text{N}_2\text{O}$ ) is a more reactive species than nitrogen ( $\text{N}_2$ ) and oxygen ( $\text{O}_2$ ) due to its weaker bonding energy.  $\text{N}_2\text{O}$  was utilized as the source for both the oxygen and nitrogen species in the oxynitride material. This modification in the deposition chemistry increased the deposition rate by a factor of two under conditions producing optimal dielectric properties. The dielectric properties of the films remained the same when grown from  $\text{N}_2\text{O}$  or  $\text{N}_2/\text{O}_2$ . Figure 48 compares the deposition rate from deposition in  $\text{N}_2\text{O}$  and  $\text{N}_2/\text{O}_2$ . Figures 49, 50, and 51 compare the capacitance, dissipation factor, and breakdown strength of  $\text{N}_2\text{O}$  and  $\text{N}_2/\text{O}_2$  films. These dielectric properties are comparable between the two gas mixtures. The differences in the capacitance in Figure 49 are due to difference in the film thickness resulting from the higher deposition rate with  $\text{N}_2\text{O}$ . The dielectric constant is similar for both films. The increased rate with steady dielectric properties prompted a transition to  $\text{N}_2\text{O}$  chemistry for further deposition.

Aluminum nitride deposition runs were conducted on numerous substrates and utilizing a wide variety of process settings. DC power ranged from 500 W to 2000 W, with pressures between 5 mTorr and 20 mTorr. Films were deposited on metallized silicon wafers, metallized glass, aluminum foil, and silicon dioxide. Nitrous oxide plasma with nitrogen dilution was also examined. The target-to-substrate distance was initially set at 5 inches. Deposition times were adjusted to achieve 5000 Å films. Appendix C summarizes the deposition conditions for each experimental run.

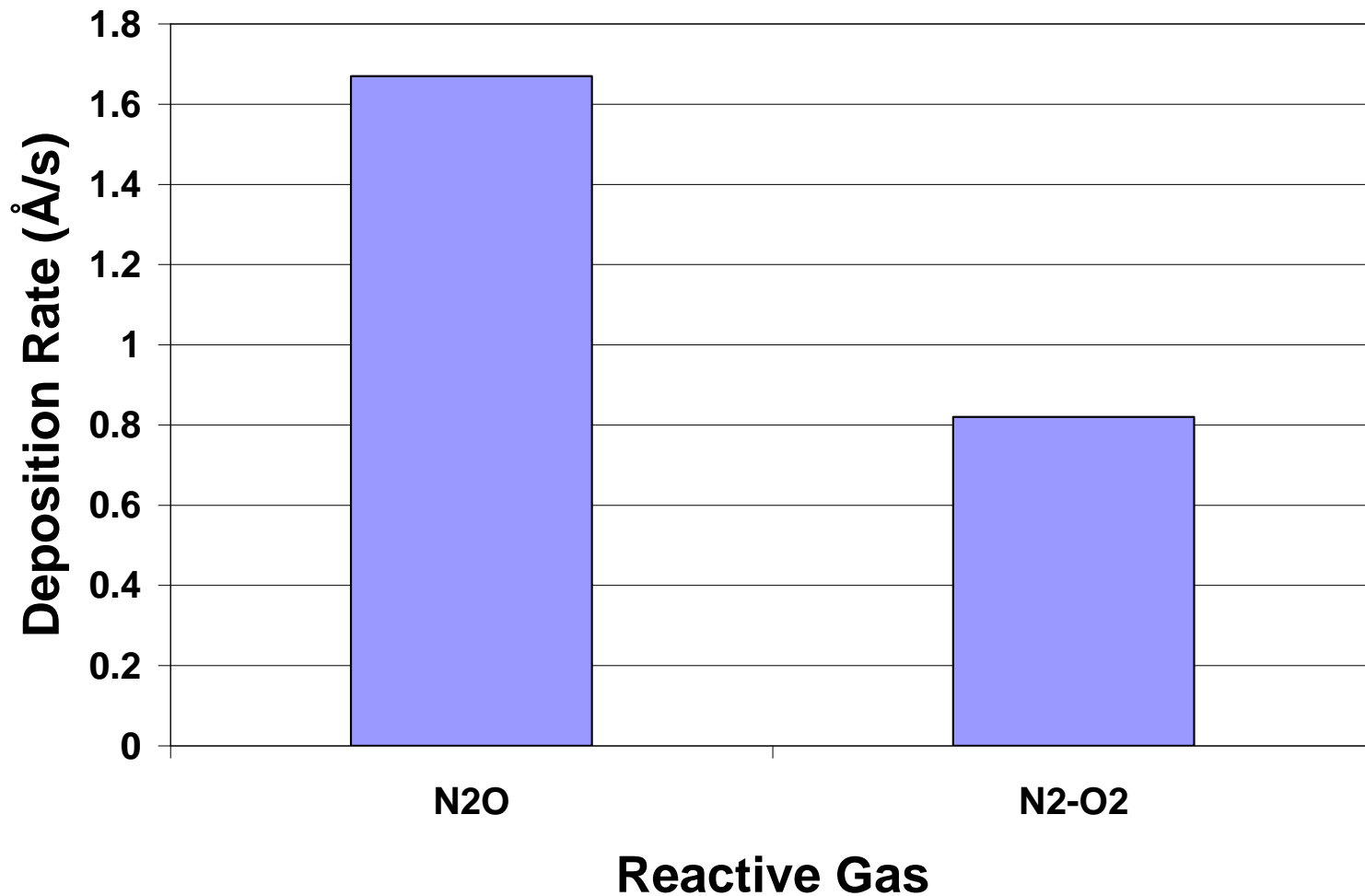


Figure 48. Deposition Rate Comparison for Reactive Gases

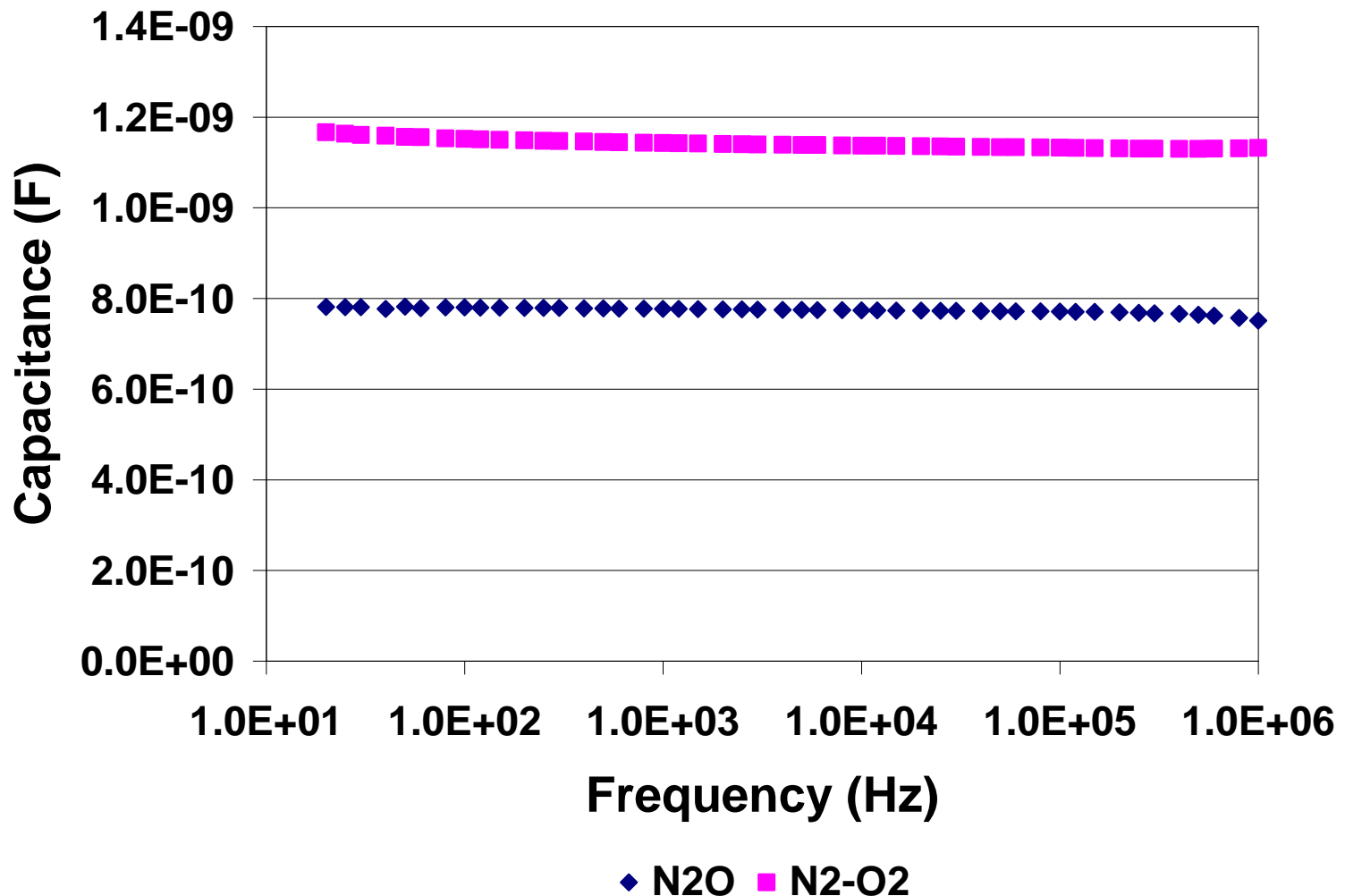


Figure 49. Capacitance Comparison for Reactive Gases

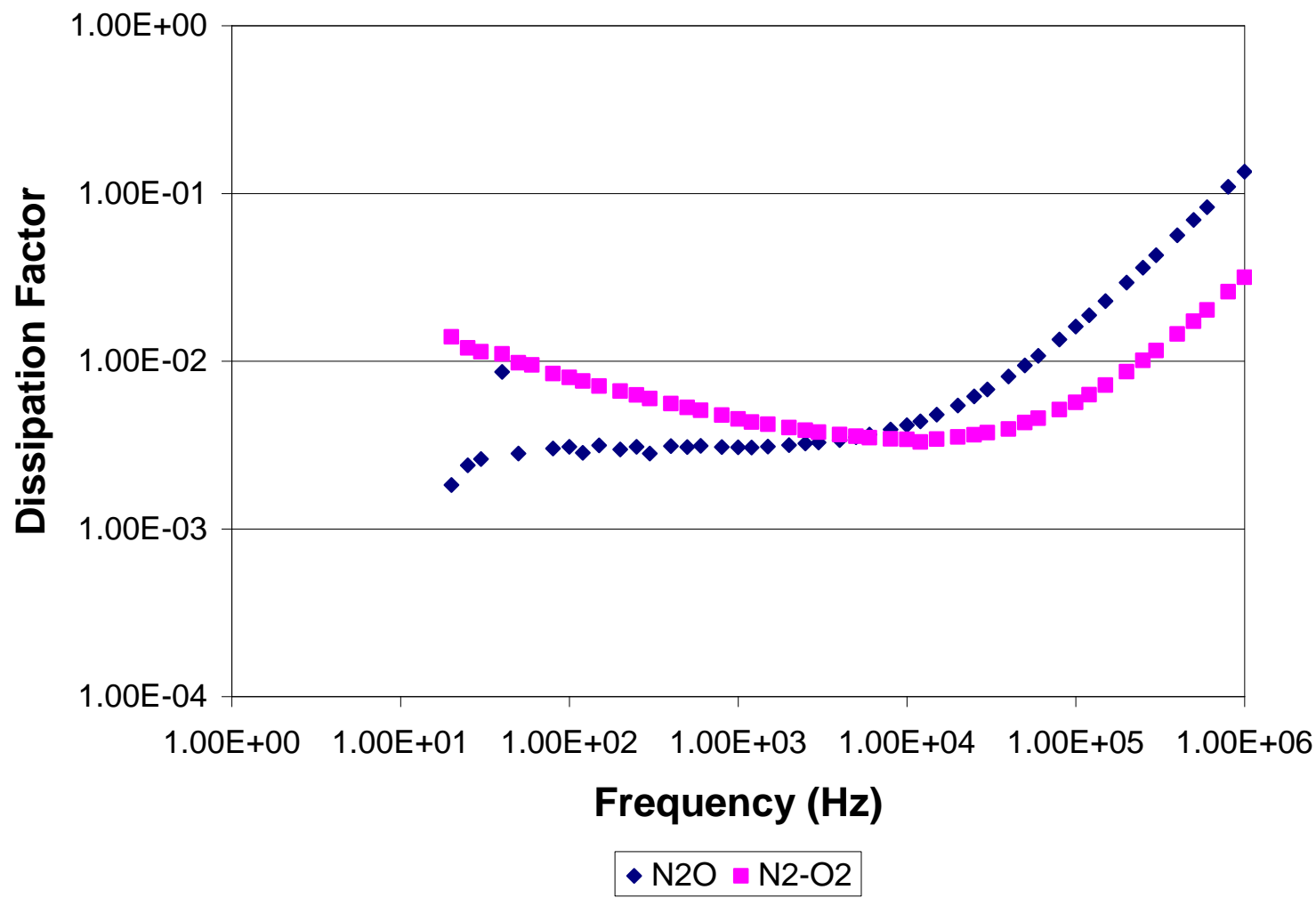


Figure 50. Dissipation Factor Comparison for Reactive Gases

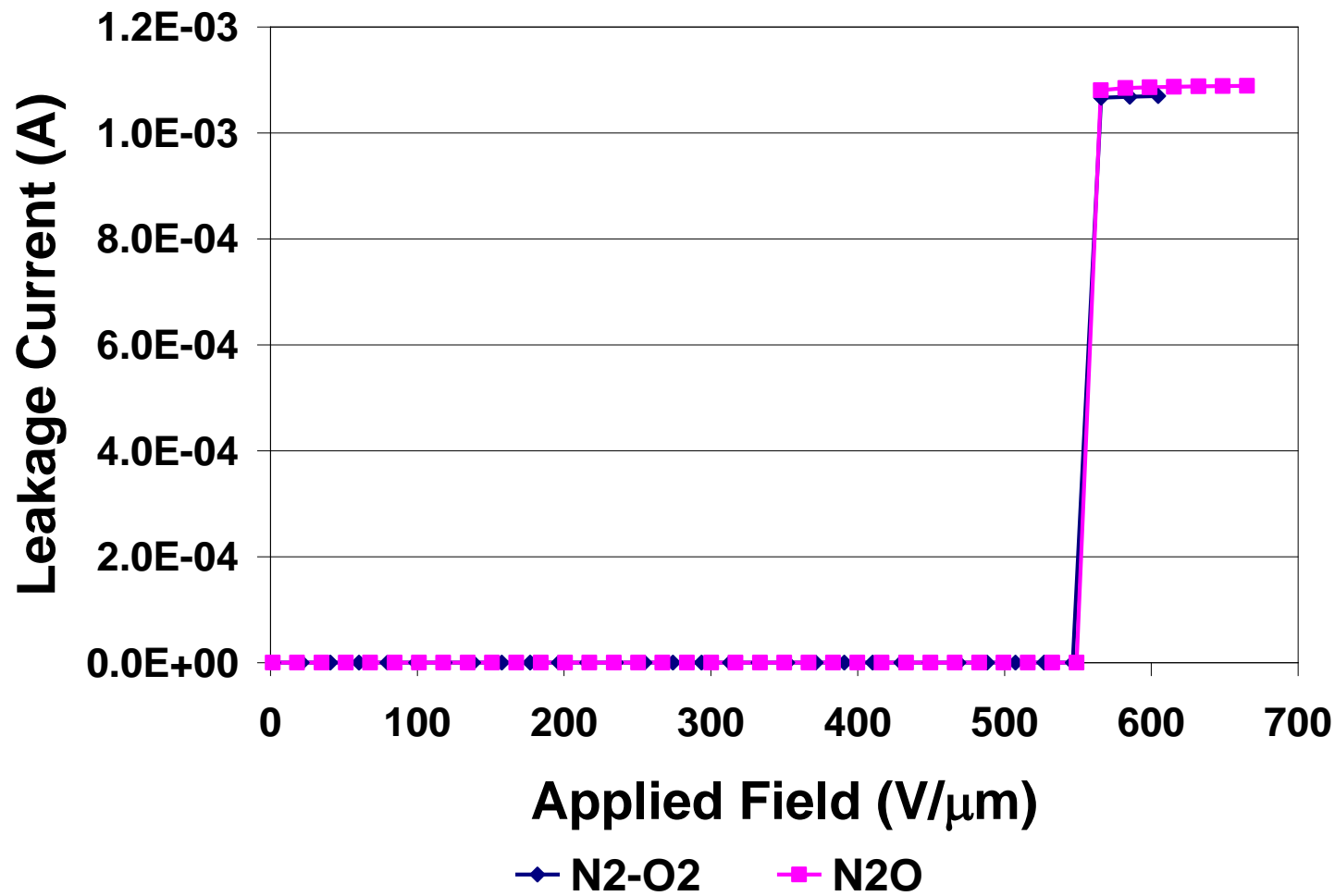


Figure 51. Breakdown Strength Comparison for Reactive Gases

### 6.1.3 Multilayer Devices

Nitrous oxide ( $\text{N}_2\text{O}$ ) reactive gas at 5 mTorr chamber pressure and 1500 W DC power provided the optimal dielectric properties. The aluminum foil scanner was modified to mask areas for multilayer capacitor deposition. Openings were created in the foil and the scanner positioned the openings over stationary substrates. Alternating metal, dielectric and metal layers were deposited in the same chamber. Targets were cleaned with Ar plasma for 30 - 45 minutes between dielectric and metal depositions. Devices with up to eight dielectric layers were constructed. Layer alignment was a critical issue with this deposition design. The foil mask was not under stress during the deposition. This allowed the foil to sag and created an undesirable offset between the layers. In extreme cases, the offset was sufficiently large that the layers did not overlap and there was no capacitance. We replaced the scanner with a precision transfer arm to repeatably position substrates in the requisite position behind stationary masks. The precision placement allowed capacitors with up to ten layers to be successfully deposited.

For the in-situ stacked layer processing, shadow masks were placed in the chamber. To reduce the edge distortion around the masks, the sputter sources were moved closer to the substrates. The shadow mask configuration for capacitor deposition allows some film spread beyond the edge of the mask. Often this spread can be so wide the entire electrode is coated by the dielectric and no contact can be made. The influence of the source-to-substrate separation on the dielectric spreading was examined with the distance varying from 1.75 to 4 inches. The best resolution was achieved at 4 inches, so that distance was maintained for the subsequent deposition runs. This resulted in an increase in the deposition rate from  $\sim 1.5 \text{ \AA/s}$  to  $\sim 2.5 \text{ \AA/s}$ . We examined different size masks to limit the influence of the dielectric spread on device performance. The capacitor active area was also reduced. This created larger electrode contacts that could be successfully connected for device testing, although it also had the deleterious effect of reducing the device capacitance.

## 6.2 Film Thickness and Surface Characterization

A Dektak 3ST surface profilometer was utilized to measure the film thickness across the deposited films. A portion of each Si or glass substrate was masked with a thin strip of stainless steel foil or high temperature tape to create a thickness step. Multiple step height measurements across the entire sample were averaged to obtain the reported film thickness. Some small surface defects were observable, but large pinholes were not present in the majority of the samples. Good adhesion was observed on all of the substrates investigated without any surface pretreatments.

## 6.3 Dielectric Properties

Extensive dielectric properties of AlN films have been characterized at K Systems facilities in the AFRL/RZPE Capacitor Research Center, WPAFB, OH. The characterizations include: (1) spot check, (2) frequency characterization, (3) insulation resistance and (4) dielectric breakdown. Values of the dielectric constant and dissipation factor are obtained from the spot checks and

frequency analysis. The resistance is calculated from the AC frequency measurements and the DC IR measurements. Breakdown voltage was determined by applying a voltage stepped in regular increments to a capacitor for a set time duration and measuring the resulting current until complete breakdown occurs. Steps of 5 V and 10 V were applied for 3 or 5 seconds in typical tests. A complete list of results is tabulated in Table B-1 in Appendix B. “Film” refers to the film thickness measured by profilometry or estimated from the deposition rate. “HV” is the actual breakdown voltage or the highest measured voltage before loss of capacitance. Blank cells in the table could not be measured.

#### 6.4 Clearing

Thin aluminum electrodes of 100 Å or less were deposited to form capacitor structures. The thin metal allows the capacitor to clear to increase the breakdown voltage. Figure 52 plots the leakage current through the capacitor and the capacitance vs. the applied voltage for two single layer devices. The leakage increases relatively smoothly until there are some sharp spikes around 350 V and 450 V. The capacitance remains constant with voltage until 350 V and 450 V respectively. A significant drop in capacitance is observed at these voltages which correspond with the spikes in the leakage current.

Figure 53 shows optical images of the capacitor surface after applied voltages from 0 V to 350 V. Images (a) – (f) depict the surface from as deposited to 250 V. No effects from the voltage are visible. One major clearing site is visible in Figure 53(g) at 300 V, but it does not affect the overall capacitance of the device as seen in Figure 52. As the voltage is ramped further, another clearing event is observed (not shown) immediately adjacent to the previous site and most apparently resulting from damage during the previous clearing and not inherent defects in the material. The breakdown test continued from 350 V and the capacitor lost contact almost immediately. Figure 53(h) displays the capacitor after the final 350 V biasing. Two different types of features are visible, the large clearing damage in Fig. 53(g) with an adjacent clearing and thin intertwined defects that propagate from the edge of the underlying bottom electrode. These smaller clearing defects spread across the whole edge of the electrode almost simultaneously, in contrast to the larger clearings which occur as individual identifiable events. This suggests that the large clearings (Fig. 53(g)) are caused by a defect or pinhole in the dielectric which resulted in self-healing of the capacitor with no significant loss of capacitance. The smaller, more rapid clearing concentrated on the edge of the electrode results from the enhanced electric field effect in the device. This rapid clearing isolates the electrode from the contacts, resulting in an open circuit. The loss of the capacitor transpires at  $\sim 650$  V/ $\mu$ m, but the dielectric has still not physically broken down under this voltage.

Thinner metal electrodes were also examined. A 50-Å-aluminum electrode did not provide sufficient continuity for the capacitor to hold charge. High temperature titanium was also evaluated. The sputtering process did not produce a uniform metal film and a different approach may be needed for commercial metallization.

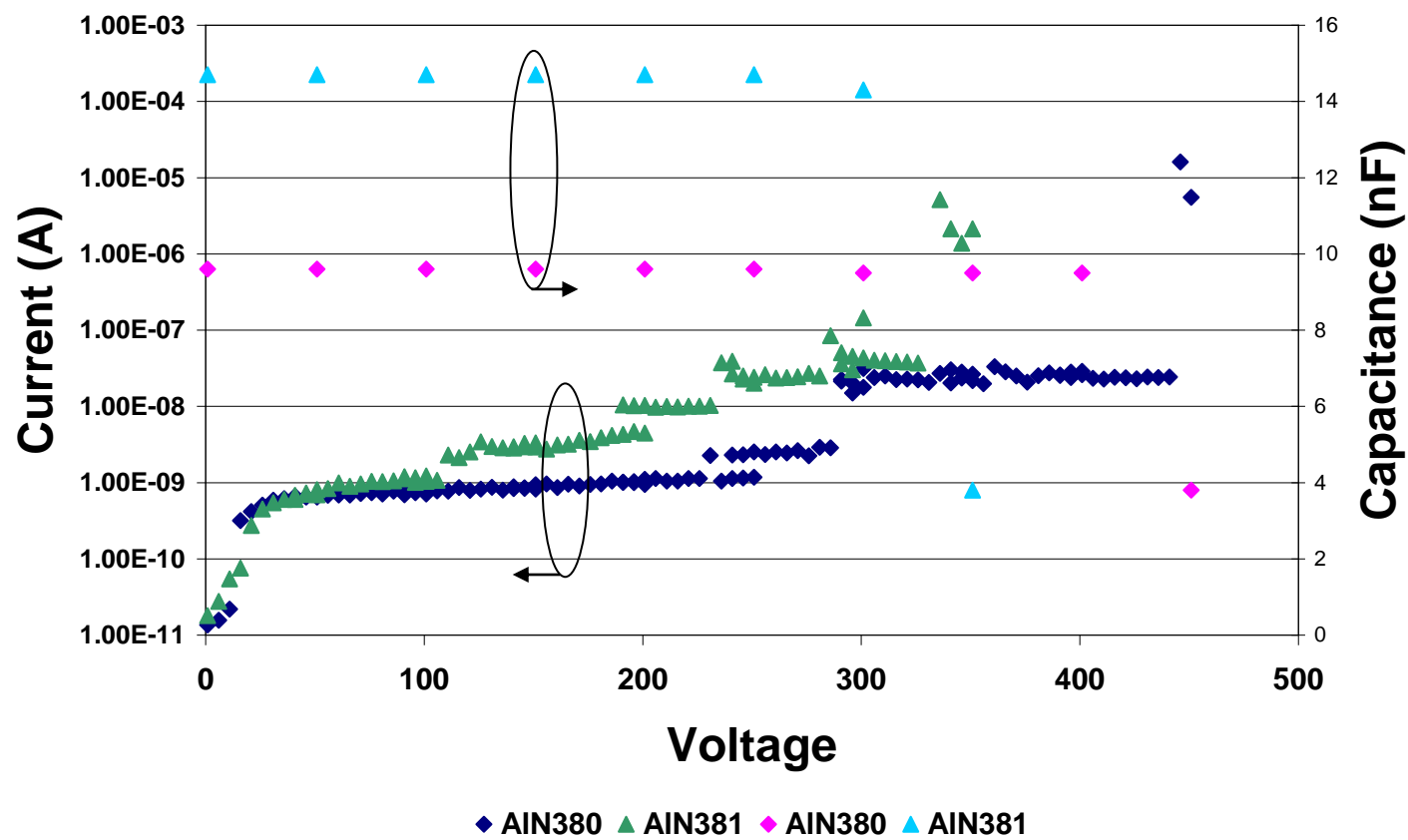


Figure 52. Capacitance and Leakage vs. Applied Voltage



Figure 53. Optical Images of Capacitor Surface after Applied Voltage from 0 V to 350 V

## 6.5 Electrode Thickness

The effects of the electrode thickness on device performance and clearing are an important consideration. Comparisons of breakdown tests for capacitors with 100 Å, 200 Å and 300 Å aluminum electrodes are shown in Figure 54. The clearing, discernable by the increased leakage current, originates at lower voltages for the thicker electrodes. The thicker electrodes also display higher leakage than the thinner electrodes, indicative of more powerful clearing events. Figure 55 plots the capacitance vs. voltage for the same capacitors in Fig. 54. Due to the more energetic clearing, the 300-Å-electrode device begins losing significant capacitance between 200 V and 250 V. The 200-Å-electrode device first declines about 10 % of the capacitance around 200 V. This corresponds with the high energy clearing seen at around 180 V, but the capacitance remains stable after those events until above 250 V. The 100-Å-electrode capacitor maintains its value to above 300 V. As with the 200-Å-capacitor, there is about 10 % loss in capacitance due to isolated clearing around 280 V prior to the primary clearing events.

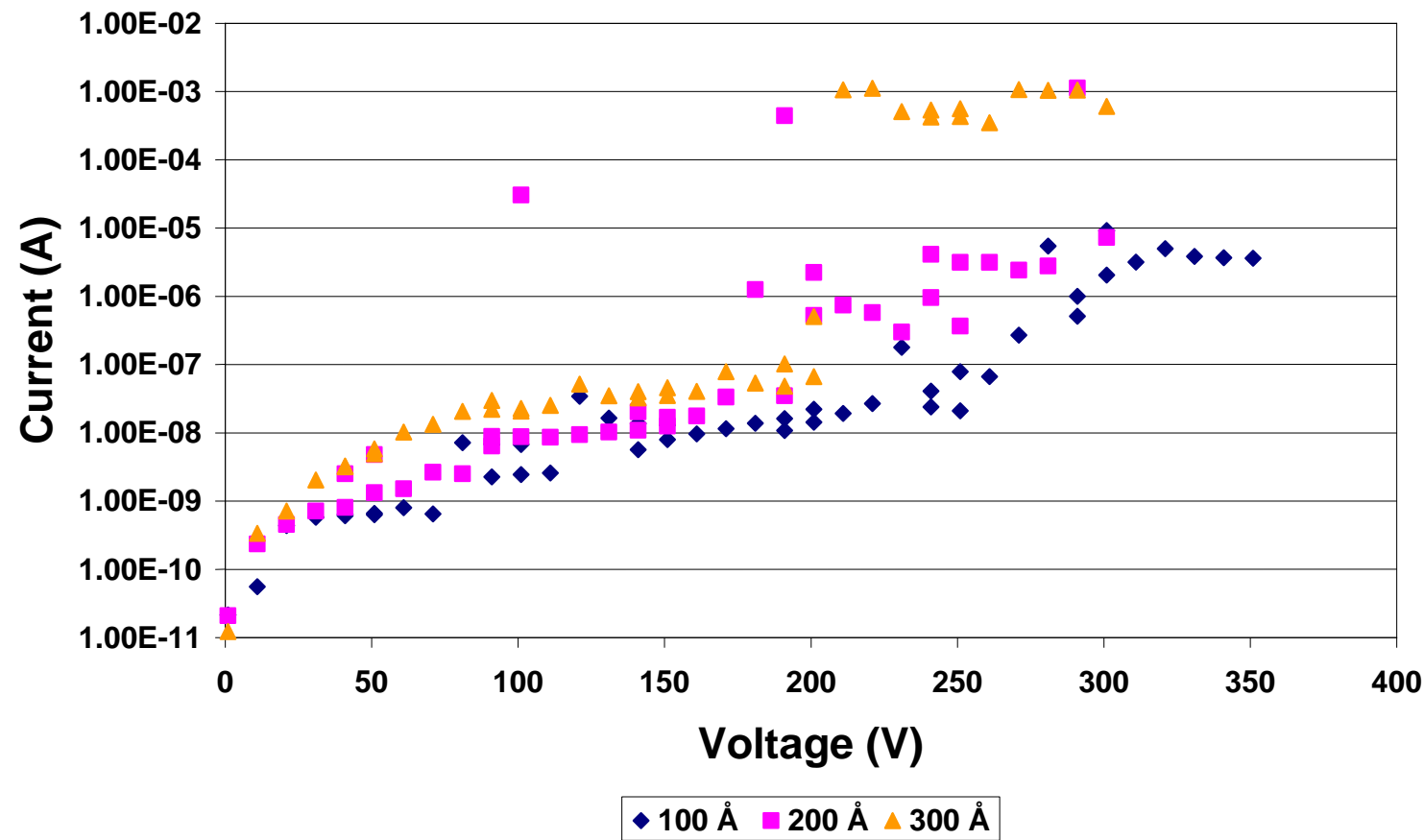


Figure 54. Effect of Electrode Thickness on Capacitor Leakage and Clearing

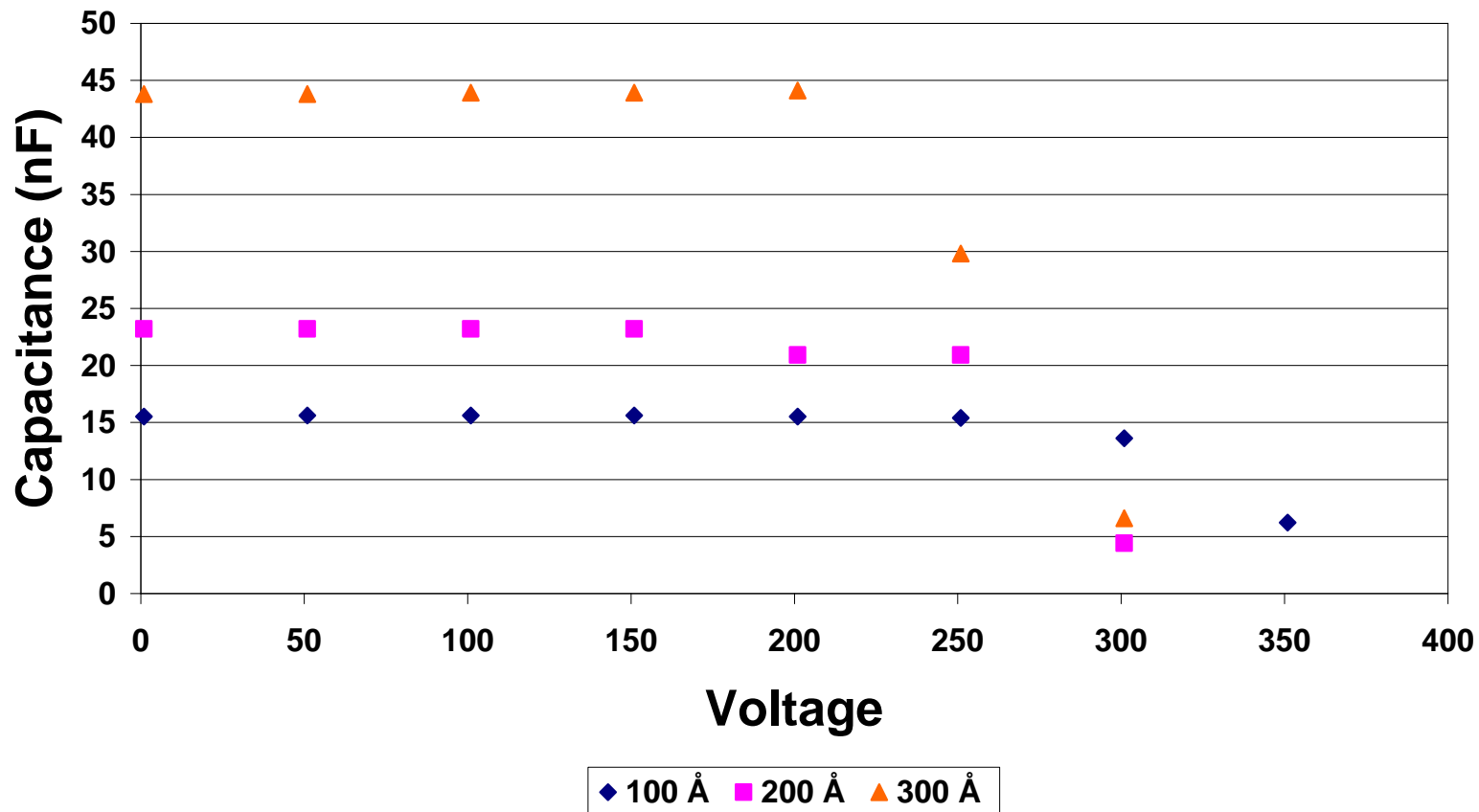


Figure 55. Capacitance vs. Voltage for Different Electrode Thicknesses

## 6.6 Heavy Edge

Heavy edge contacts have also been examined to reduce the effects of sharp edges on the loss of the electrode contact during breakdown testing. Initial assessment of the heavy edge capacitors revealed extremely good properties. Closer examination disclosed that the large area of the heavy edge pads was creating a pathway through the silicon dioxide substrate and not though the AlON. All heavy edge results on  $\text{SiO}_2$  are suspect. Heavy edge tests on glass substrates did not show any significant improvement over standard designs. ANSYS modeling has been done to study the effects of the electrode edge. Results show a strong electric field enhancement at the edge of the electrode. Putting a heavy edge to reduce the step over the dielectric edge does not reduce the field enhancement. The field effect of the edge and not the physical step of the electrode is responsible for the loss of the electrode during clearing events. A heavy edge will improve the contact for packaging and improve high current carrying capabilities.

## 6.7 Electrode Metal

Aluminum and titanium were evaluated as AlON capacitor electrodes. Electrodes were deposited using magnetron sputtering with shadow masks to produce the desired pattern. Aluminum has been the standard metal in capacitor evaluations. It has remained stable up to 400 °C and produced dissipation factors as low as 0.003. A minimum thickness of ~75 Å has been reached with aluminum. Thinner layers are not conductive when deposited in our apparatus or the electrodes are not visible to make contact. Figure 56 shows an optical image of an AlON capacitor with aluminum electrodes. The metallization is uniform and smooth.

Titanium is a high temperature metal which is desirable for capacitor application above the operating temperature of aluminum. It is more difficult to sputter titanium than aluminum. Figure 57 is an optical micrograph of a capacitor with titanium electrodes. The ~50-Å-thick metal has not completely coalesced. 100-Å-thick electrodes also exhibited the same island behavior. For optimal capacitor performance the electrode thickness needs to remain in the 100-Å-regime. Although thick contacts for heavy edge structures showed coalesced films, these metals are too thick to be used for the active capacitor contacts. Titanium may still be a potential electrode material for high temperature capacitors, but more experimentation with the deposition parameters or even a different deposition process may be needed.

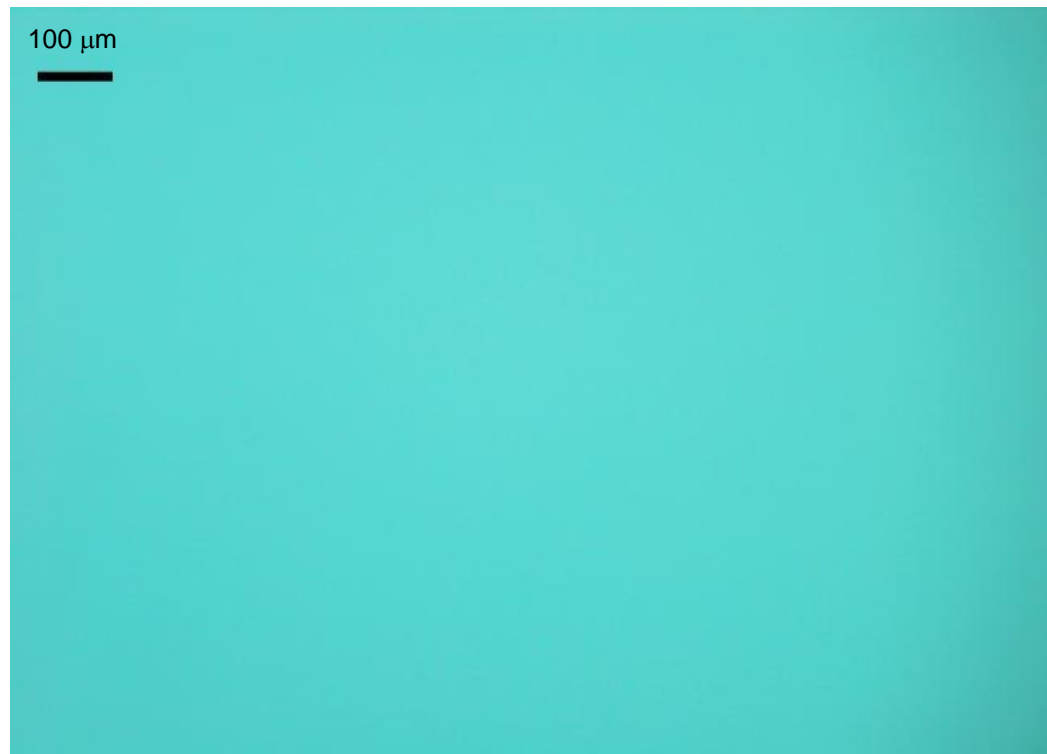


Figure 56. Optical Image of AlON Capacitor with Aluminum Electrodes



Figure 57. Optical Image of AlON Capacitor with Titanium Electrodes

## 6.8 Temperature Stability

Dielectric thermal stability is a critical issue for capacitor performance in extreme conditions. Figure 58 plots the capacitance vs. frequency for AlON capacitors under both elevated and cryogenic temperature exposure. The capacitance remains constant with frequency and is stable with increasing temperature to 300 °C. As the temperature is increased above 300 °C, the capacitance increases at low frequencies, while above 5 kHz no temperature effects are observed up to 400 °C. The capacitance also remains stable under cryogenic conditions, with no variations observed down to -200 °C. Two different capacitors with different capacitances were tested for the high temperature and cryogenic evaluation. When capacitors are heated in ambient air, Figure 59, the capacitance at low frequency begins to increase around 250 °C but still remains constant at high frequencies. At 1 kHz, a dielectric constant of ~9 is achieved.

The dissipation factor was also evaluated under the same temperature conditions. Stronger temperature dependence was observed. At room temperature, the dissipation factor is ~0.003 at 1 kHz. Under vacuum conditions, shown in Figure 60, significant increases in DF begin above 200 °C while in air, Figure 61, increases are observed around 150 °C. Again, the temperature primary influences the properties below 5 kHz. No change in the dissipation factor is observed under cryogenic conditions. The difference between film performance in vacuum and in ambient air at elevated temperatures may be related to the atmospheric boundary layer present on the surface. Interactions with particulates in the atmospheric boundary layer over the top electrode may begin to alter the electric field as the temperature increases. The boundary layer is more pronounced in atmospheric air compared to vacuum environment and the temperatures effects are seen at lower temperatures. The temperature effects on both capacitance and dissipation factor are reversible. The original values for both the capacitance and dissipation factor are reacquired after returning the material back to room temperature and are stable after multiple temperature cycles. The high and low temperature values are also repeatably obtained on each temperature cycle. This indicates the observed capacitance and dissipation shifts are not caused by a chemical reaction, but by reversible interactions between the atmosphere and the surface.

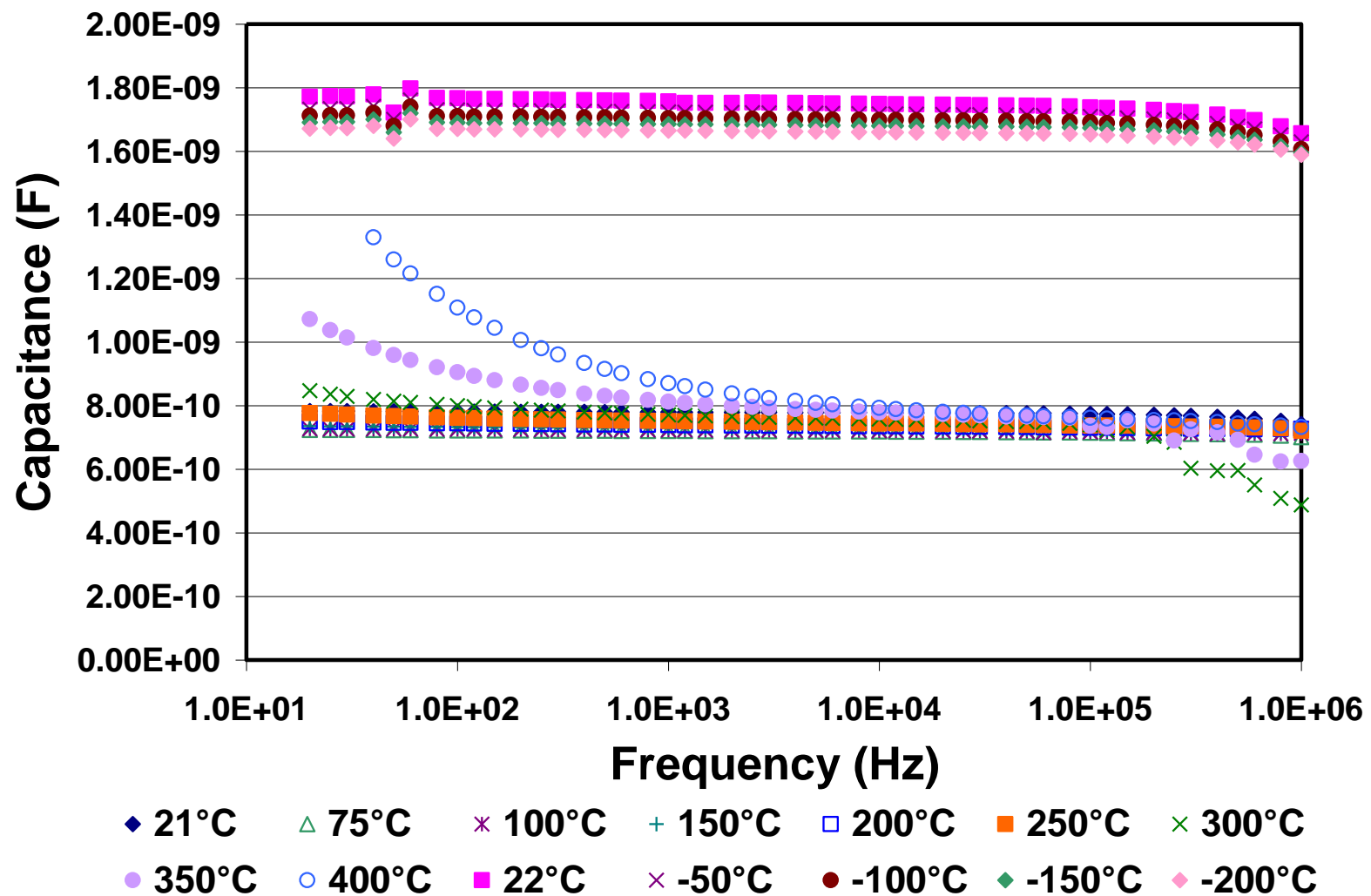


Figure 58. Capacitance vs. Frequency at Various Temperatures in Vacuum

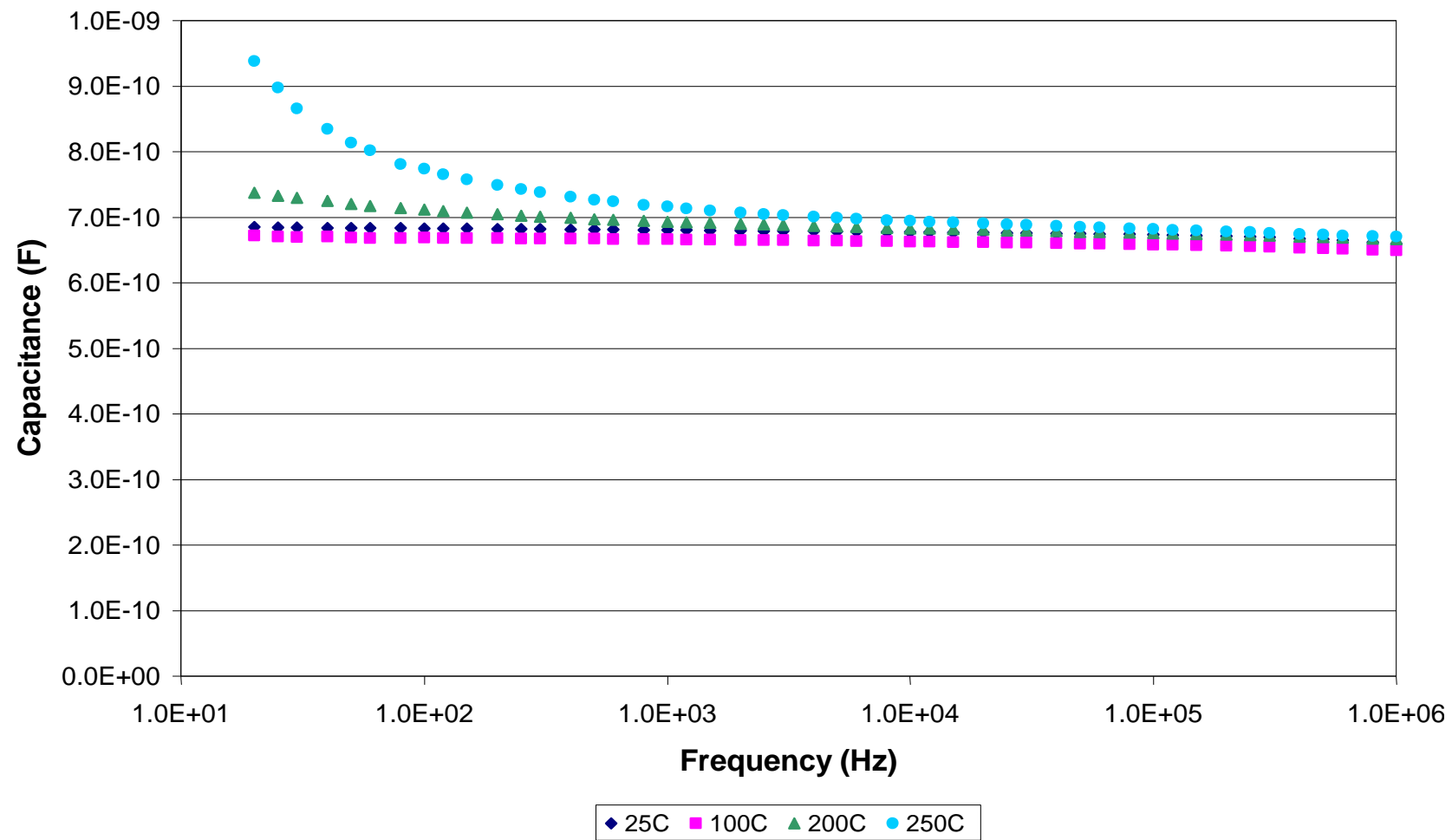


Figure 59. Capacitance vs. Frequency at Various Temperatures in Air

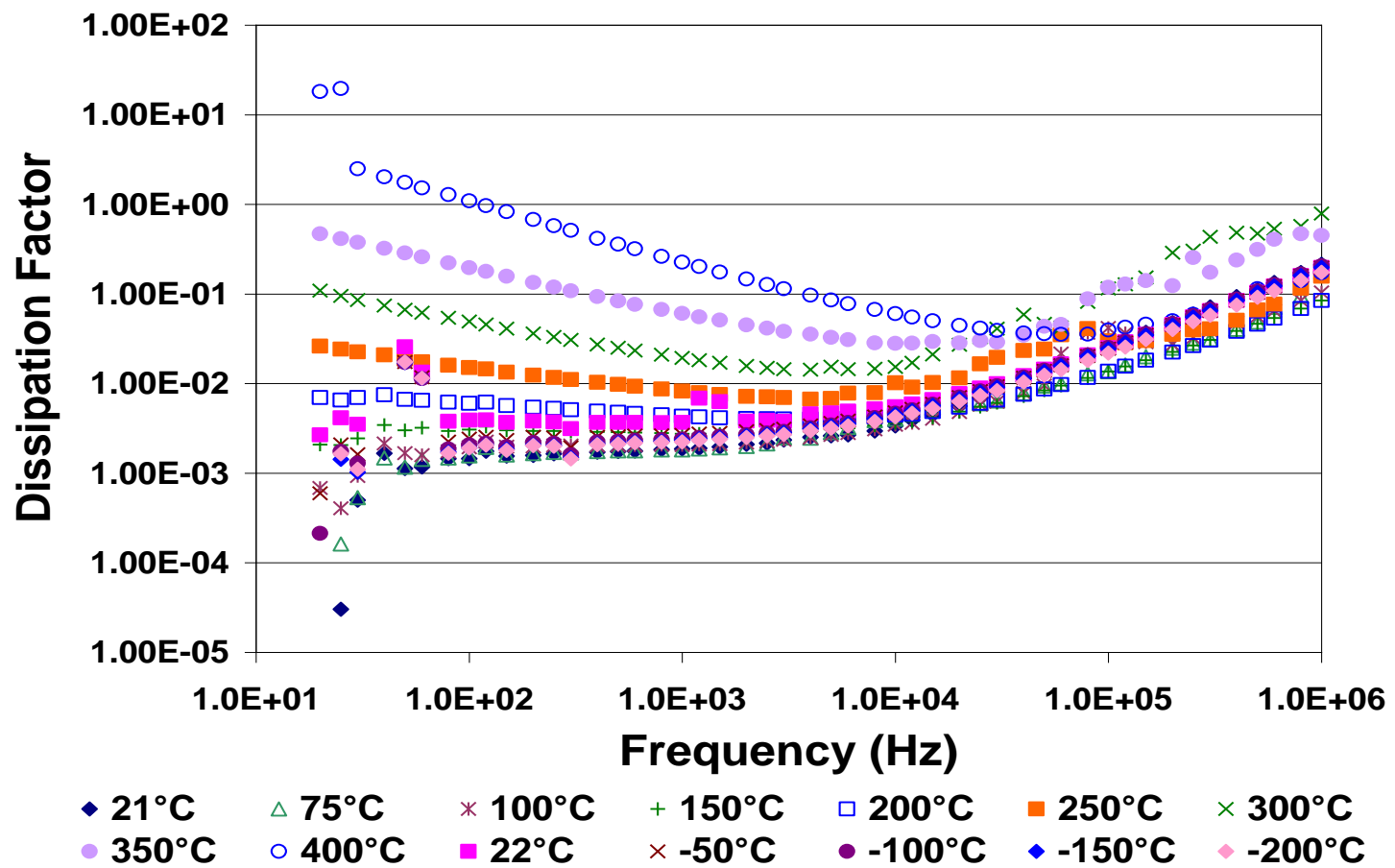


Figure 60. Dissipation Factor vs. Frequency at Various Temperatures in Air

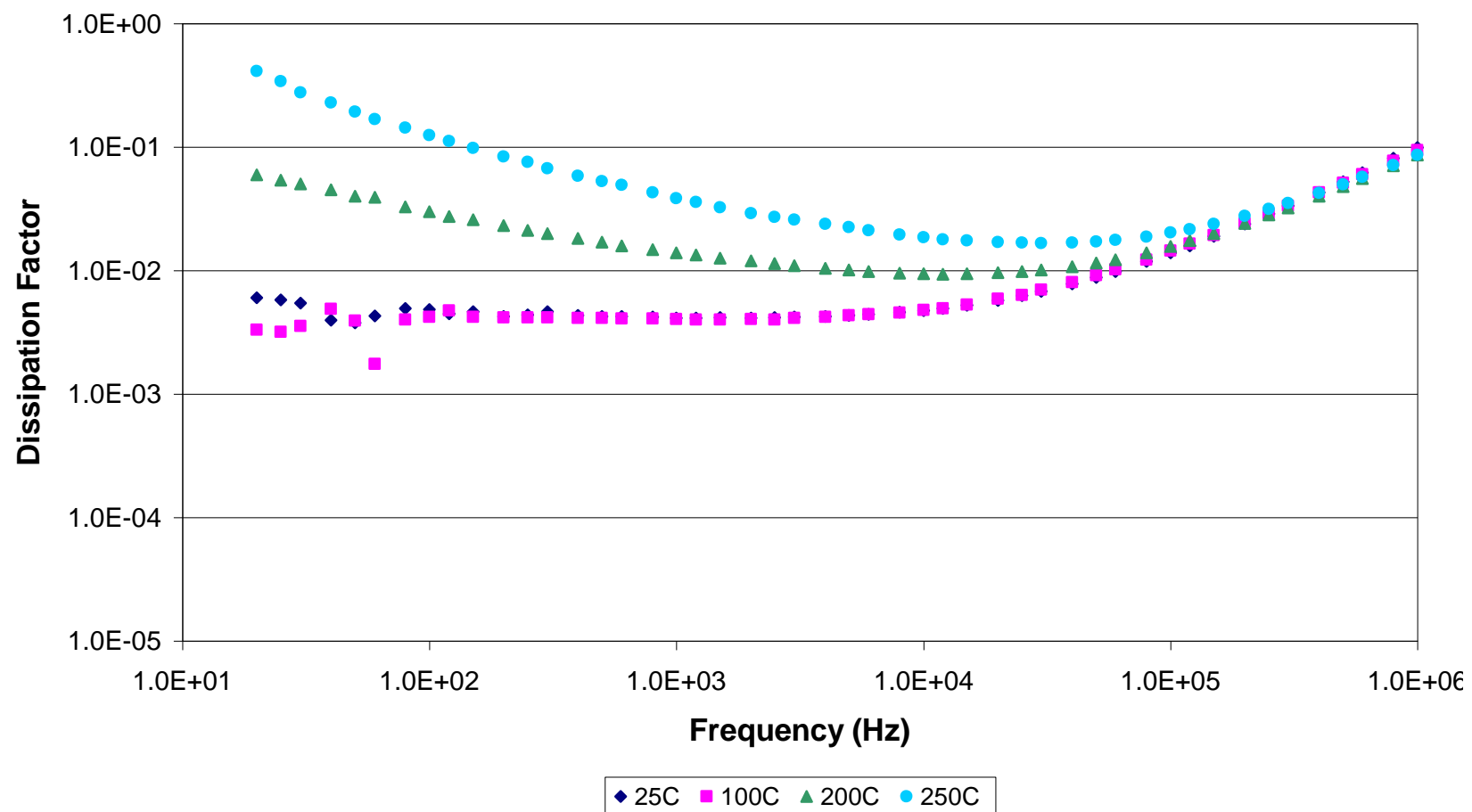


Figure 61. Dissipation Factor vs. Frequency at Various Temperatures in Air

## 6.9 Multilayer Capacitors

Multilayer capacitors with one to ten dielectric layers have been fabricated using in-situ processing. Figure 62 is a cross-sectional schematic of a three layer structure. The capacitance at 1 kHz is plotted vs. layers in Figure 63. A precision transfer arm to position substrates for metal and dielectric deposition allowed repeatable sample processing. Attempts at measuring hard breakdown strength of the multilayer structures were not very successful. Clearing events removed the electrodes and created an open circuit. Breakdown values were taken from the loss of capacitance observed from the clearing. Initial results do indicate AlON is suitable for stacked capacitor designs

### 6.9.1 Thermal Properties

Temperature testing was conducted to observe insulation resistance under applied voltage. Figure 64 plot IR data for 25 °C to 300 °C for one layer devices at 50 V, 100 V and 200 V. The devices maintain a reproducible trend under each voltage applied. Comparisons of one and two layer devices at 100 V and 50 V are shown in Figures 65 and 66. At low temperature, there is some variation between the one and two layer device at 100 V, but at 50 V and at high temperatures, they behave similarly. Figure 67 is an Arrhenius plot of the leakage current data. Two distinct regions are discernible. At low temperature (<125 °C), the leakage remains constant with increasing temperature, while at higher temperature, a thermally activated component, with an activation energy of 0.7 eV, is observed. Annealing the samples in air or vacuum before measurements did not influence the performance.

### 6.9.2 Packaged Devices

Majelac Technologies, PA, packaged two, five and ten layer capacitors. We tested the capacitance and the insulation resistance at 100 V for these packaged devices from room temperature to 250 °C. Figure 68 shows the change in capacitance with temperature. The capacitance of the five layer device varies less than 3 % up to 200 °C. The two layer sample is slightly less stable and varies almost 10 % over the same range. There is significant clearing in the ten layer capacitor which reduced the capacitance ~70 % initially, but after these events, the capacitance remained stable to 180 °C. Each capacitor tested lost capacitance above 200 °C. This may be an artifact of the conductive epoxy that was used to connect the electrodes to the package leads. Testing of the dielectric material shows the capacitance is stable to 400 °C. Some oxidation of the aluminum bond pads may occur due to oxygen in the epoxy material. Gold bonds pads were deposited to investigate this theory. The same epoxy bonding systems was examined with gold bond pads on the capacitors. The capacitors maintained continuity in the measurement up to 250 °C. This reinforces the initial testing which shows AlON is stable to 400 °C.

The insulation resistance (IR) was also measured. The IR for two and five layer device remained above 1000 MΩ at 100 V and 200 °C. The ten layer capacitor exhibited much lower IR, near 1 MΩ at the same conditions. The lower resistance with the increased layers may result from difficulties in closely masking the wafer during deposition. A gap is maintained between the

substrate and the mask to allow the substrate to move. But this gap also decreases the precision of the layer alignment. Improved process equipment should improve the alignment and increase the resistance of higher layer devices. Aluminum oxynitride appears an excellent potential for high temperature high capacitance devices, but processing and packaging challenges still exist to produce commercially viable AlON capacitors.



Figure 62. Cross-sectional Schematic of Stacked Multilayer Structure

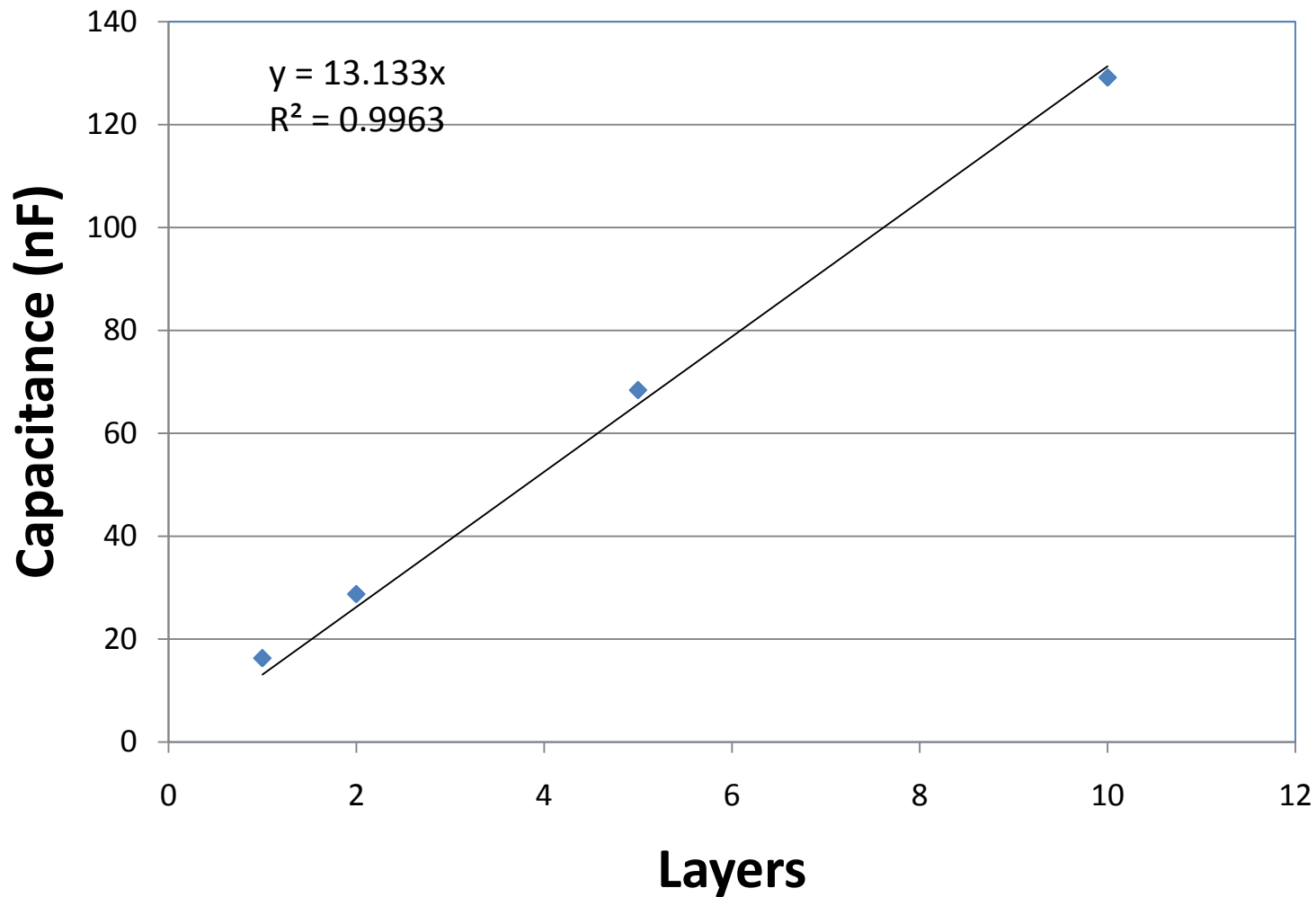


Figure 63. Capacitance vs. Layers for Multilayer Devices

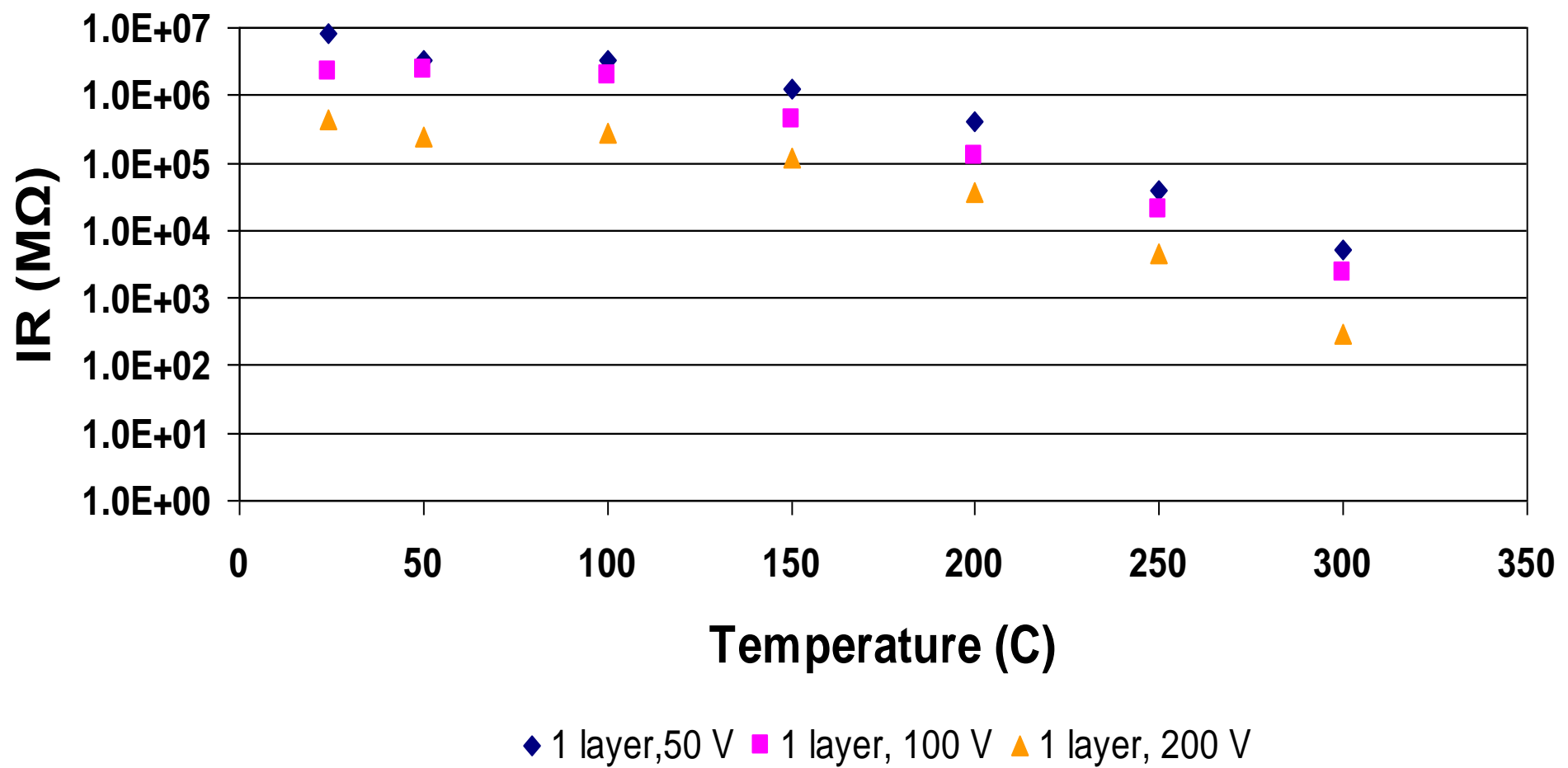


Figure 64. Insulation Resistance vs. Temperature at Various Voltages for a 1 Layer Device

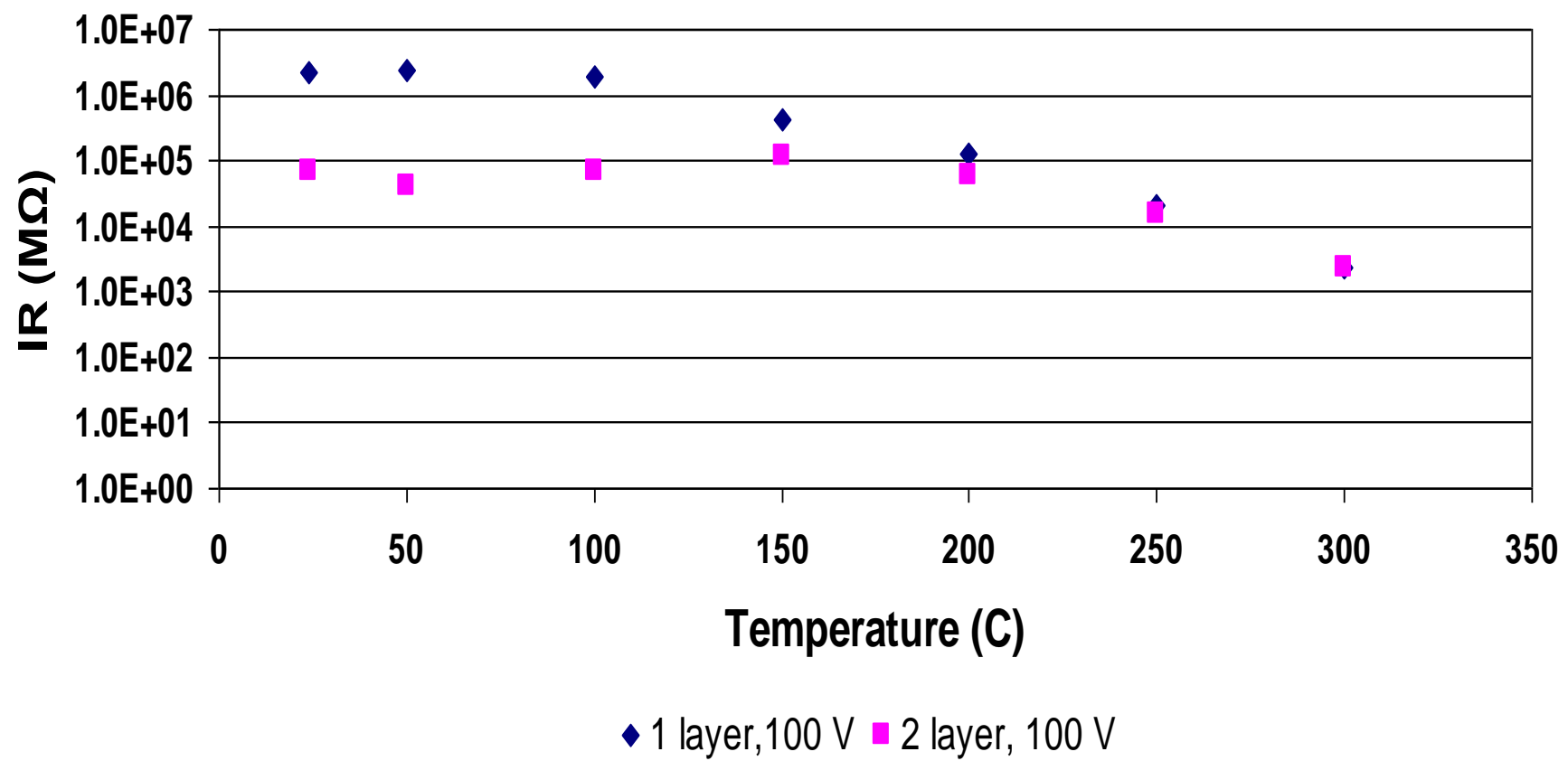


Figure 65. Insulation Resistance vs. Temperature at 100 V for 1 and 2 Layer Devices

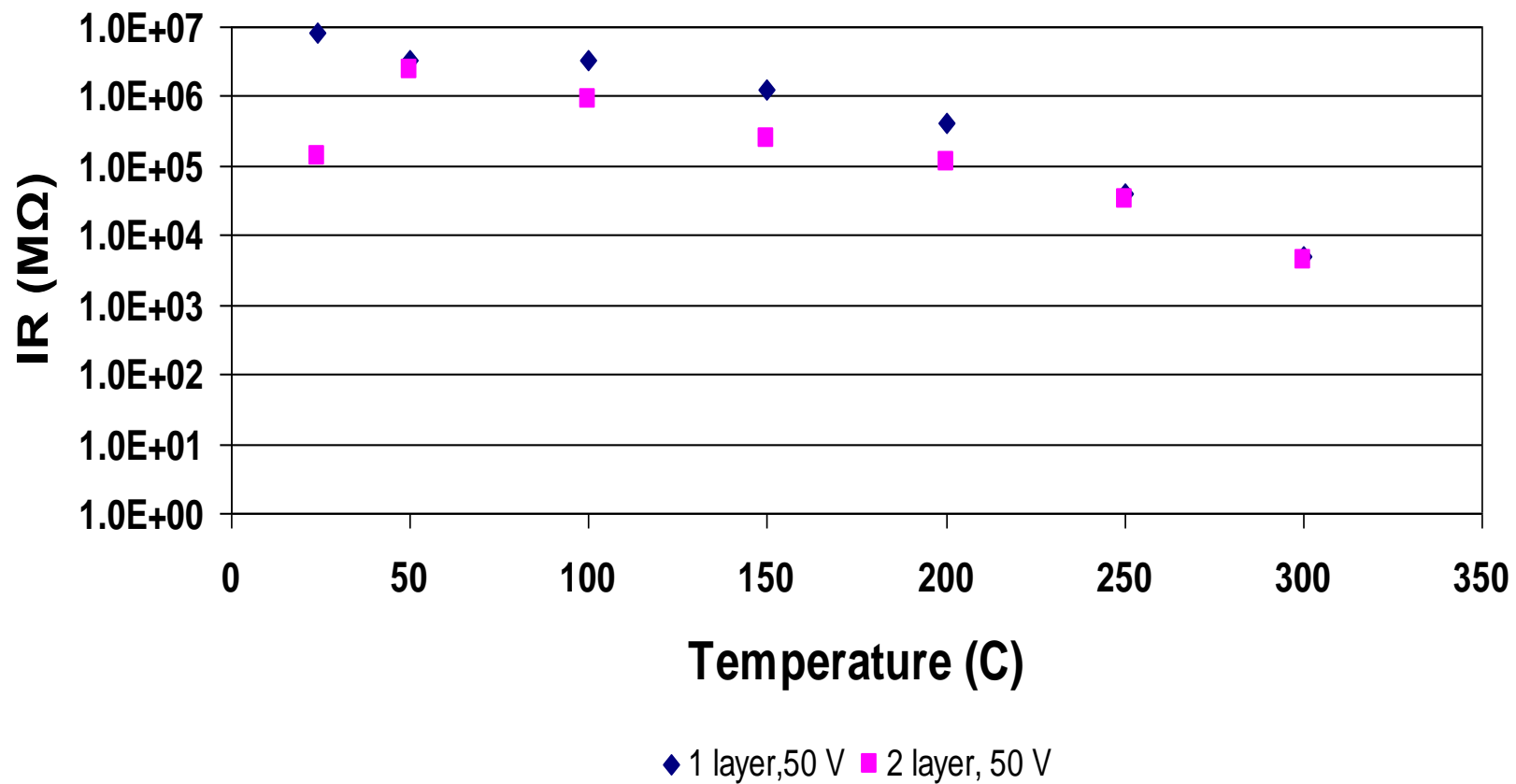


Figure 66. Insulation Resistance vs. Temperature at 50 V for 1 and 2 Layer Devices

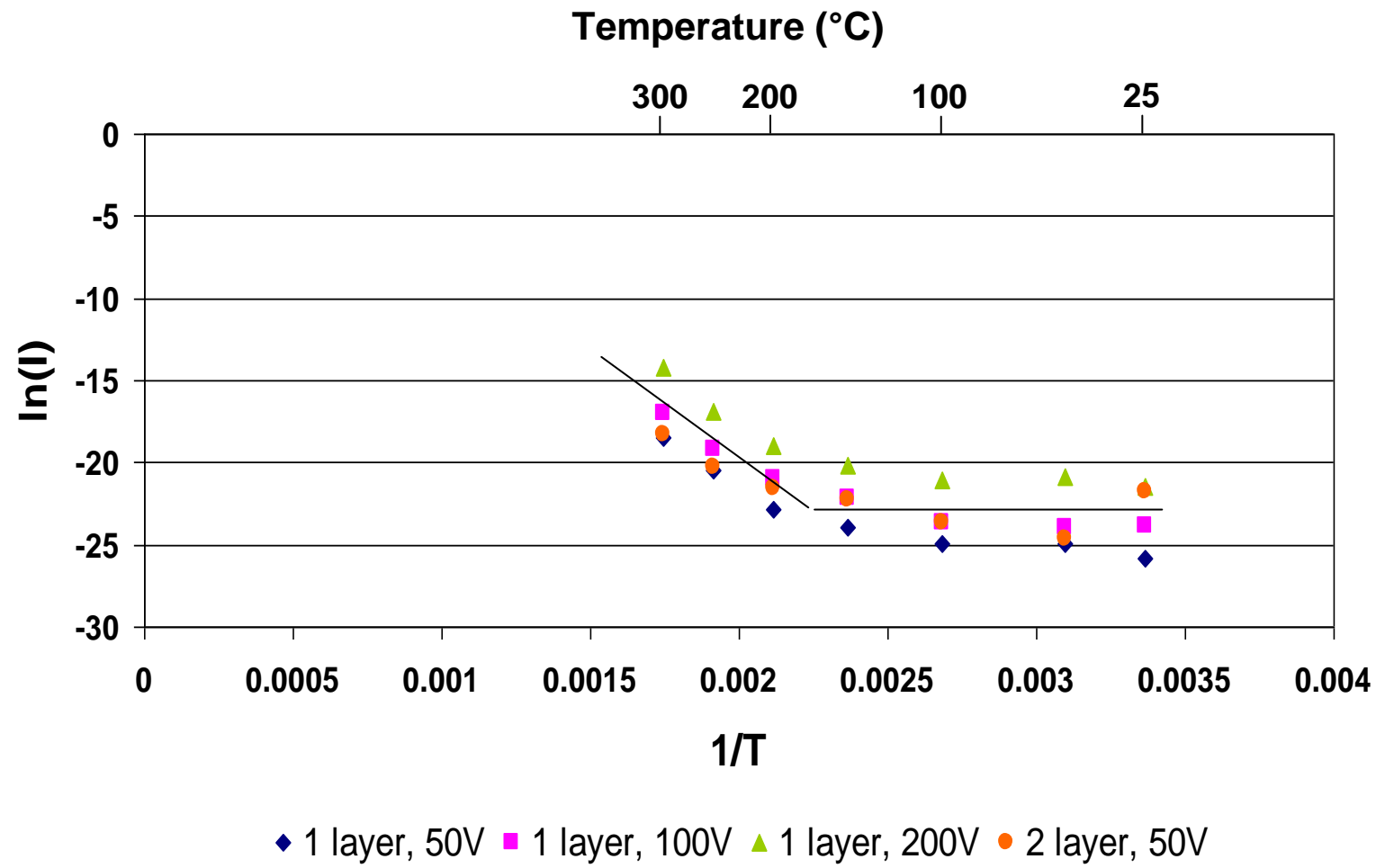


Figure 67. Arrhenius Plot of Leakage Current Data

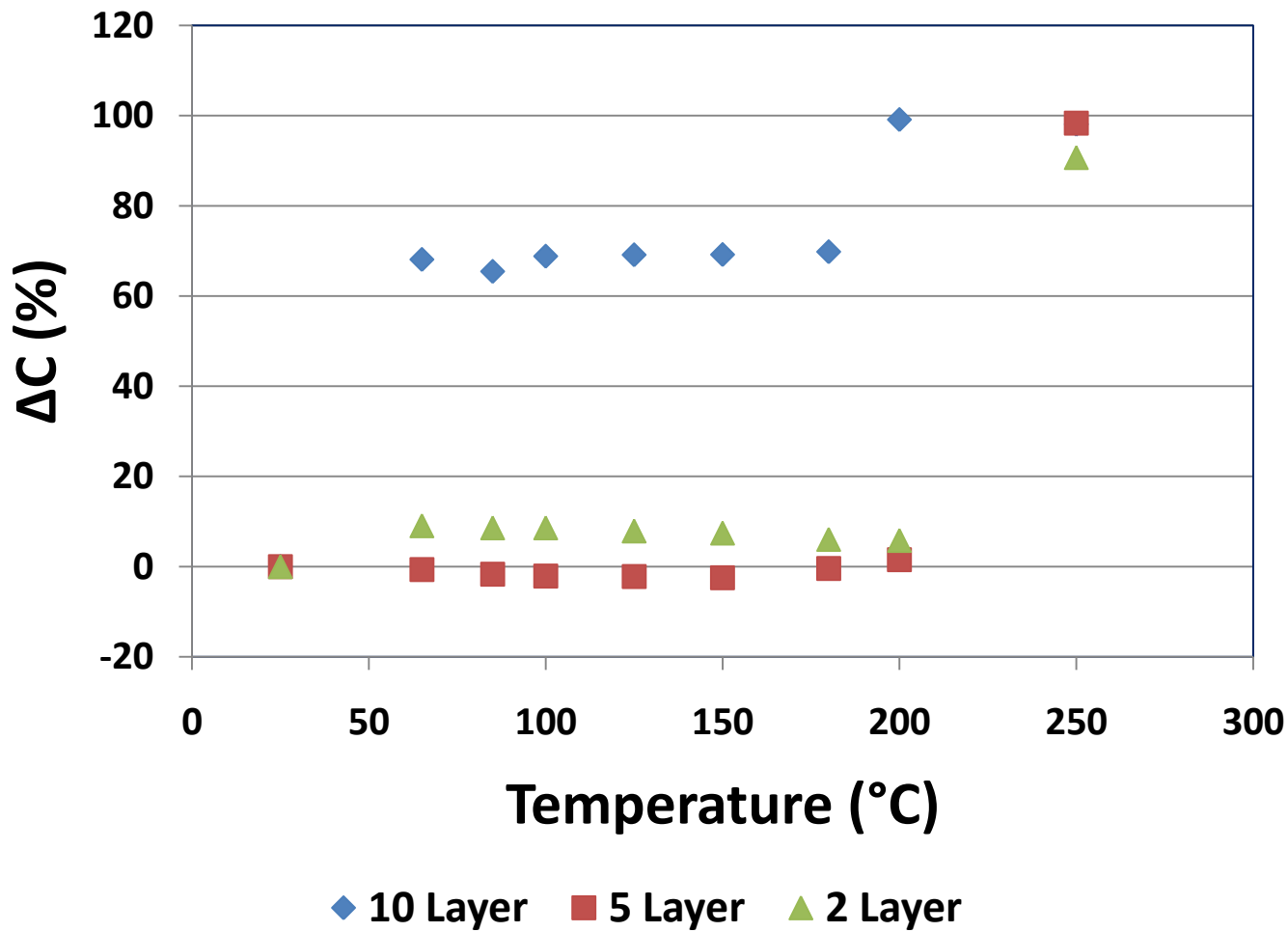


Figure 68. Temperature Stability of Packaged Capacitors

## **7. Discussion**

The objective of this project was to develop high energy density aluminum nitride capacitors. The material was characterized in terms of its dielectric breakdown strength and dissipation factor. Aluminum nitride and aluminum oxynitride dielectric films were studied. The dielectric properties of the oxynitride material were superior to the nitride films. A dielectric constant of ~9 was achieved, with a dissipation factor ~0.005 and a breakdown voltage >600 V/ $\mu$ m. These values result in a material energy density ~15 J/cc. The films also exhibit excellent thermal stability from -200 °C to 400 °C. The films remained amorphous and were free of pin-hole defects and were successfully deposited onto thin metal and polymer materials.

Another goal of the project was to simultaneously coat two sides of foil or polymer utilizing our custom designed web handling scanner system. We experienced difficulty in attaining this accomplishment. The high intensity plasma sputtering beam caused the aluminum foil to break under the tension of rolling. The foil did not maintain close contact with the scanner back plate, which allowed the plasma to overheat the foil. Better contact would transfer the heat away from the foil and reduce the stress during deposition. A set of process conditions was identified using lower DC power and tension where deposition was successful on foil, but it was not at the optimal conditions for dielectric performance. Several polymers were also examined. The majority could not withstand the plasma and melted. A high temperature polymer, FPE, was able to withstand the beam, but was not available in sufficient quantity to attempt deposition utilizing the web handler. Thin titanium and stainless steel foils were also investigated. Both showed superior strength than aluminum foil, but again we could not attempt to roll these foils.

In order to improve the rolled foils, we initiated an AF/OSD SBIR Phase II Enhancement program with the goal of modifying the scanner. The enhancement also examined techniques to improve the deposition rate, making the AlON deposition more economical. We also investigate a new stacked multilayer capacitor design to improve the volumetric energy density of our capacitors.

The deposition rate for AlON sputtering was improved by replacing the nitrogen/oxygen reactive gas mixture with nitrous oxide. Nitrous oxide bond strength is not as high as nitrogen and oxygen, resulting in a larger dissociation fraction in the plasma. Similar dielectric constant, dissipation factor and breakdown strength are obtained with N<sub>2</sub>O as with N<sub>2</sub>/O<sub>2</sub>.

Multilayer capacitor devices have been deposited using the sample manipulator to align the dielectric and metal layers. The capacitance increases linearly with increasing layers. In-situ processing allowed both the metal and dielectric layers to be processed without exposing the sample to atmospheric contamination. Packaged multilayer devices have been operated up to 250 °C. Minimal change in capacitance is observed in packaged multilayer capacitors at high temperatures. The bond material to connect the electrodes to the package leads is critical for high temperature performance.

## **8. Conclusions**

High quality aluminum oxynitride dielectric films for high energy density capacitor applications have been developed. The deposition rate for reactive sputtering AlON films has been increased 2x by switching from a N<sub>2</sub>/O<sub>2</sub> chemistry to an N<sub>2</sub>O chemistry. Capacitors with up to ten layers have been constructed and packaged. The capacitance increases linearly with increasing stacked layers. Films have been tested up to 400 °C. Aluminum oxynitride appears an excellent potential for high temperature, high capacitance devices, but processing and packaging challenges still exist to produce commercially viable AlON capacitors.

## **9. Deliverables**

- (1) Two (2) -10 feet Length of AlON coated aluminum foil/metalized polymer.
- (2) Two (2) -Three-layer AlON stacked capacitors.
- (3) Six (6) packaged capacitor devices

Two (2) Stacked AlON capacitors with two (2) dielectric layers (0.04  $\mu$ F, 200 V)

Two (2) Stacked AlON capacitors with five (5) dielectric layers (0.075  $\mu$ F, 100 V)

Two (2) Stacked AlON capacitors with ten (10) dielectric layers (0.195  $\mu$ F, 80 V)

- (4) Quarterly progress reports covering the period 17 February, 2004 to 31 August 2008
- (5) A final report detailing the work performed.

## **10. Technical Publications and Presentations**

### **10.1 Publications**

- (1) "Aluminum Nitride Dielectrics for High Energy Density Capacitors", R.L.C. Wu, J. Lawson, M. Samiee, P.B. Kosel, S.F. Adams, S. Fries-Carr and J. Weimer, Proceedings of 2004 National Space & Missile Materials Symposium, Seattle, Washington, (2004).
- (2) "Advanced Dielectrics for Pulsed Power Capacitor Devices", S. Fries-Carr, S. Adams, J. Weimer, R.L.C. Wu, H. Kosai, K. Bray, T. Furmaniak, E. Barshaw, S. Scozzie, R. Jow, R. Garrison, F. Warnock, Proceeding of 2004 SAE International Conference on Power & Thermal Technologies for Directed Energy Applications 2004-01, 3216, (2004).
- (3) "Aluminum Nitride Dielectrics for High Energy Density Capacitors", K.R. Bray, R.L.C. Wu, S. Fries-Carr, and J. Weimer, Advances in Electronic and Electrochemical Ceramics, Ceramic Transactions 179, F. Dogan and P. Kumta, editors, 45-55, (2006).
- (4) "Aluminum Oxynitride Dielectrics for High Power, Wide Temperature Capacitor Applications", K.R. Bray, R.L.C. Wu, S. Fries-Carr and J. Weimer, CARTS USA 2006, Proceedings of the 26<sup>th</sup> Symposium for Passive Components, 161-170, (2006).
- (5) "Aluminum Oxynitride Dielectrics for High Energy Density Capacitor Applications", K.R. Bray, R.L.C. Wu, S. Fries-Carr and J. Weimer, "Proceedings of the International Symposium on Advanced Dielectrics and Electronic Devices, Materials Science and Technology 2006, 647-656, (2006).
- (6) "Multilayer Aluminum Oxynitride Capacitors for Higher Energy Density, Wide Temperature Applications" K.R. Bray, R.L.C. Wu, S. Fries-Carr, J. Weimer, CARTS USA 2007, Proceeding of the 27<sup>th</sup> Symposium for Passive Components, 371-379 (2007).
- (7) "Aluminum Oxynitride Capacitors for Multilayer Devices with Higher Energy Density and Wide Temperature Properties", K.R. Bray, R.L.C. Wu, S. Fries-Carr, J. Weimer, CARTS USA 2008, Proceeding of the 28<sup>th</sup> Symposium for Passive Components, 51-61 (2008).

### **10.2 Presentations**

- (1) "Advanced Dielectrics for Pulsed Power Capacitor Device", S. Fries-Carr, S. Adams, J. Weimer, R.L.C. Wu, H. Kosai, K. Bray, T. Furmaniak, E. Barshaw, S. Scozzie, R. Jow, R. Garrison, F. Warnock, was presented at the 2004 SAE International Conference on Power & Thermal Technologies for Directed Energy Applications, Reno, Nevada, Nov. 2-4, (2004).
- (2) "Aluminum Nitride Dielectrics for High Energy Density Capacitors", R.L.C. Wu, J. Lawson, M. Samiee, P.B. Kosel, S.F. Adams, S. Fries-Carr and J. Weimer was presented

at the 2004 National Space & Missile Materials Symposium, Seattle, Washington, (2004).

- (3) "Aluminum Nitride Dielectrics for High Energy Density Capacitors", K.R. Bray, R.L.C. Wu, S. Fries-Carr, J. Weimer, was presented at 30<sup>th</sup> Dayton-Cincinnati Aerospace Sciences Symposium of the American Institute of Aeronautics and Astronautics, Dayton, OH, March 8 (2005).
- (4) "Aluminum Nitride Dielectrics for High Energy Density Capacitors", K.R. Bray, R.L.C. Wu, S. Fries-Carr, J. Weimer, was presented at the 107<sup>th</sup> Annual Meeting & Exposition of The American Ceramic Society, Baltimore, Maryland, April 10-13, (2005).
- (5) "Aluminum Oxynitride Dielectrics for High Power, Wide Temperature Capacitor Applications", K.R. Bray, R.L.C. Wu, S. Fries-Carr, J. Weimer, was presented at the 31<sup>st</sup> Dayton-Cincinnati Aerospace Sciences Symposium of the American Institute of Aeronautics and Astronautics, Dayton, OH, March 7, (2006).
- (6) "Aluminum Oxynitride Dielectrics for High Power, Wide Temperature Capacitor Applications", K.R. Bray, R.L.C. Wu, S. Fries-Carr, J. Weimer, was presented at CARTS USA 2006, the 26th Symposium for Passive Components, Orlando, FL, April 3-6, (2006).
- (7) "Aluminum Oxynitride Dielectrics for High Energy Density Capacitor Applications", K.R. Bray, R.L.C. Wu, S. Fries-Carr, J. Weimer, was presented at the Materials Science and Technology 2006 Conference and Exhibition, Cincinnati, OH, October 15-19, (2006).
- (8) "Multilayer Aluminum Oxynitride Capacitors for Higher Energy Density, Wide Temperature Applications" K.R. Bray, R.L.C. Wu, S. Fries-Carr, and J. Weimer, was presented at the 32nd Dayton-Cincinnati Aerospace Sciences Symposium, Dayton, OH, March 6, (2007).
- (9) "Multilayer Aluminum Oxynitride Capacitors for Higher Energy Density, Wide Temperature Applications" K.R. Bray, R.L.C. Wu, S. Fries-Carr, and J. Weimer, was presented at CARTS USA 2007, Albuquerque, NM, March 26-29, (2007).
- (10) "Aluminum Oxynitride Capacitors for Multilayer Devices with Higher Energy Density and Wide Temperature Properties" K.R. Bray, R.L.C. Wu, S. Fries-Carr, and J. Weimer, was presented at the 33rd Dayton-Cincinnati Aerospace Sciences Symposium, Dayton, OH, March 4, (2008).
- (11) "Aluminum Oxynitride Capacitors for Multilayer Devices with Higher Energy Density and Wide Temperature Properties" K.R. Bray, R.L.C. Wu, S. Fries-Carr, and J. Weimer, was presented at CARTS USA 2008, Newport Beach, CA, March 17-20, (2008).

## 11. References

- 1 M. Rabuffi and G. Picci. "Status quo and future prospects for metallized polypropylene energy storage capacitors," *IEEE Trans. Plasma Sci.*, **30**, (2002), 1939-1942.
- 2 W.M. Yim, E.J. Stofko, P.J. Zanzucchi, J.I. Pankove, M. Ettenberg, and S.L. Gilbert. "Epitaxial grown AlN and its optical band gap," *J. Appl. Phys.*, **44**, (1973), 292-296.
- 3 R.D. Vispute, J. Narayan, and J.D. Budai. "High quality optoelectronic grade epitaxial AlN films on  $\alpha$ -Al<sub>2</sub>O<sub>3</sub>, Si, and 6H-SiC by pulsed laser deposition," *Thin Solid Films*, **299**, (1997), 94-103.
- 4 F. Martin, P. Muralt, M.-A. Dubois, and A. Pezous. "Thickness dependence of the properties of highly c-axis textured AlN thin films," *J. Vac. Sci. Technol. A*, **22**, (2004), 361-365.
- 5 C.L Aardahl, J.W. Rogers Jr., H.K Yun, Y. Ono, D.J. Tweet, S.-T. Hsu. "Electrical properties of AlN thin films deposited at low temperature on Si(100)," *Thin Solid Films*, **146**, (1999), 174-180.
- 6 K.K. Harris, B.P. Gila, J. Deroaches, K.N. Lee, J.D. MacKenzie, C.R. Abernathy, F. Ren, and S.J. Pearton. "Microstructure and thermal stability of aluminum nitride thin films deposited at low temperature on silicon," *J. Electrochem. Soc.*, **149**, (2002), G128-G130.
- 7 V. Dimitrova, D. Manova, and E. Valcheva. "Optical and dielectric properties of dc magnetron sputtered AlN thin films correlated with deposition conditions," *Mater. Sci. Eng. B* **68**, (1999), 1-4.
- 8 J. Schulte and G. Sobe. "Magnetron sputtering of aluminum using oxygen or nitrogen as reactive gas," *Thin Solid Films*, **324**, (1998), 19-24.
- 9 J.-W Lee and S.C.N. Cheng. "Development of SiN<sub>x</sub> and AlN<sub>x</sub> passivation layers," *Thin Solid Films*, **358**, (2000), 215-222.
- 10 K. Jagannadham, K. Sharma, Q. Wei, R. Kalyanraman, and J. Narayan. "Structural characteristics of AlN films deposited by pulsed laser deposition and reactive magnetron sputtering: A comparative study," *J. Vac. Sci. Technol. A* **16**, (1998), 2804-2815.
- 11 T.T. Leung and C.W. Ong. "Nearly amorphous to epitaxial growth of aluminum nitride films," *Diamond Rel. Mater.* **13**, (2004), 1603-1608.
- 12 J. Kolodzey, E.A. Chowdhury, T.N. Adam, G. Qui, I. Rau, J.O. Olowolafe, J.S. Suehle, and Y. Chen. "Electrical conduction and dielectric breakdown in aluminum oxide insulators on silicon," *IEEE Trans. Electr. Dev.*, **47**, (2000), 121-128.
- 13 X-L Guo, H. Tabata, and T. Kawai, *Optical Materials*, **19**, (2002) 229.

14 F. Zhuge, L.P. Zhu, Z.Z. Ye, J.G. Lu, B.H. Zhao, J.Y. Huang, L. Wang, Z.H. Zhang, and Z.G. Ji, *Thin Solid Films*, **476**, (2005), 272.

15 W.S. Lau, M.T.C. Perera, P. Babu, A.K. Ow, T. Han, N.P. Sandler, C.H. Tung, T.T. Sheng, P.K. Chu, *Japanese Journal of Applied Physics, Part 2*, **37**, (1998), L435.

## APPENDIX A

Table A-1. AlN Deposition Conditions

<u>Sample#</u>	<u>DepTemp (C)</u>	<u>DepPress (mTorr)</u>	<u>DepTime (hr)</u>	<u>Gas ambient N<sub>2</sub>:O<sub>2</sub>:Ar</u>	<u>DC power (W)</u>	<u>Frequency (kHz)</u>	<u>Distance (inch)</u>
AIN003	25-75	7.5	1.50	1:0:0	500	0	3
AIN004	25-75	11.0	1.00	1:0:0	900	250	3
AIN006	25-75	3.7	0.50	1:0:0	900	250	3
AIN007	25-75	5.5	0.50	1:0:0	600	250	3
AIN008	25-75	9.0	0.42	1:0:0	900	250	3
AIN009	25-75	9.0	0.5	1:0:0	700	250	3
AIN010	25-75	5.0	0.50	1:0:0	900	250	4
AIN011	25-75	3.0	0.50	1:0:0	800	250	4
AIN012	25-147	10.0	0.67	1:0:0	900	150	4
AIN013	25-87	10.0	0.67	1:0:0	500	250	4
AIN014	25-87	7.0	0.75	1:0:0	900	50	4
AIN015	10-92	7.0	1.00	1:0:0	500	150	4
AIN016	13-105	7.0	1.00	1:0:0	700	250	4
AIN017	9-126	7.0	0.67	1:0:0	1000	250	4
AIN018	13-52	7.0	0.67	1:0:0	500	250	4
AIN019	40-131	4.5	0.75	1:0:0	1000	50	4
AIN020	40-94	4.5	0.75	1:0:0	700	150	4
AIN021	10-108	15.0	0.58	1:0:0	1000	250	4
AIN022	8-64	15.0	0.58	1:0:0	1000	50	4
AIN023	29-144	10.0	0.75	1:0:0	900	50	4
AIN024	26-79	10.0	0.75	1:0:0	700	150	4
AIN025	25-74	7.0	0.75	1:0:0	1000	150	4
AIN026	25-114	7.0	0.75	1:0:0	900	250	4
AIN027	24-82	15.0	0.67	1:0:0	700	250	4
AIN028	26-88	15.0	0.67	1:0:0	900	150	4
AIN029	24-106	10.0	0.67	1:0:0	1000	250	4
AIN030	28-84	10.0	0.67	1:0:0	700	150	4
AIN031	28-84	7.0	0.83	1:0:0	1000	150	4
AIN032	28-84	7.0	0.83	1:0:0	700	50	4

Table A-1. AlN Deposition Conditions (continued)

<u>Sample#</u>	<u>DepTemp (C)</u>	<u>DepPress (mTorr)</u>	<u>DepTime (hr)</u>	<u>Gas ambient N<sub>2</sub>:O<sub>2</sub>:Ar</u>	<u>DC power (W)</u>	<u>Frequency (kHz)</u>	<u>Distance (inch)</u>
AIN033	28-84	10.0	0.75	1:0:0	1000	250	4
AIN034	28-84	10.0	0.75	1:0:0	700	150	4
AIN035	24-80	10.0	0.58	1:0:0	1000	250	4
AIN036	24-72	10.0	0.58	1:0:0	700	150	4
AIN037	24-75	10.0	0.50	1:0:0	2000	250	5
AIN038	24-49	10.0	0.50	1:0:0	1000	150	5
AIN039		7.0		1:0:0	2000	150	5
AIN040		7.0	0.50	1:0:0	1500	250	5
AIN041		7.0	0.50	1:0:0	2000	150	5
AIN042		7.0	0.33	1:0:0	1500	250	5
AIN043	16-20	7.0	0.17	1:0:0	1500	250	6
AIN044	18-24	10.0	0.33	1:0:0	1500	250	6
AIN045	16-	15.0	0.17	1:0:0	2000	50	6
AIN046	16-19	10.0	0.17	1:0:0	1000	150	6
AIN047	11-54	15.0	0.17	1:0:0	2000	50	6
AIN048	18	10.0	0.58	1:0:0	1000	150	6
AIN049	17-34	15.0	0.33	1:0:0	2000	50	6
AIN050	19-28	15.0	0.67	1:0:0	2000	50	6
AIN051	19-28	16.0	0.50	3:0:1	2000	50	6
AIN052	24-70	12.5	0.67	1:0:0	1500	250	6
AIN053	24-66	10.0	0.50	1:0:0	2000	250	6
AIN054	22-56	15.0	0.67	1:0:0	1500	50	6
AIN055	22-28	12.5	0.67	1:0:0	1000	150	6
AIN056	24-58	15.0	0.50	1:0:0	2000	150	6
AIN057	24-84	15.0	0.67	1:0:0	1000	250	6
AIN058	24-84	12.5	0.50	1:0:0	2000	50	6
AIN059	24-84	12.5	0.50	1:0:0	2000	50	6
AIN060	24-84	10.0	0.75	1:0:0	1000	50	6
AIN061	24-84	10.0	0.50	1:0:0	1500	150	6
AIN062							
AIN063	20-22	20.0	0.67	1:0:0	700	25	6
AIN064	20-40	20.0	0.67	1:0:0	1000	50	6
AIN065	30-35	20.0	0.67	1:0:0	1000	50	6
AIN066	30-35	20.0	0.67	1:0:0	850	5	6
AIN067	10-20	25.0	0.50	1:0:0	850	25	6
AIN068	10-50	25.0	0.67	1:0:0	2000	25	6
AIN069	20-24	15.0	0.67	1:0:0	850	50	6
AIN070	20-30	15.0	0.67	1:0:0	1500	50	6

Table A-1. AlN Deposition Conditions (continued)

<u>Sample#</u>	<u>DepTemp (C)</u>	<u>DepPress (mTorr)</u>	<u>DepTime (hr)</u>	<u>Gas ambient N<sub>2</sub>:O<sub>2</sub>:Ar</u>	<u>DC power (W)</u>	<u>Frequency (kHz)</u>	<u>Distance (inch)</u>
AIN071	28-32	15.0	0.67	1:0:0	1000	25	6
AIN072	30-56	15.0	0.04	1:0:0	2500	50	6
AIN073	12-16	15.0	0.75	1:0:0	700	5	6
AIN074	18-20	15.0	0.75	1:0:0	700	5	6
AIN075	11-36	15.0	0.75	1:0:0	1000	50	6
AIN076	18-21	15.0	0.75	1:0:0	1000	50	6
AIN077		25.0	0.75	1:0:0	1000	5	6
AIN078		25.0	0.75	1:0:0	1000	5	6
AIN079		15.0	0.50	1:0:0	2000	50	6
AIN080		15.0	0.75	1:0:0	1000	250	6
AIN081	5-44	15.0	0.75	1:0:0	1000	50	6
AIN082	4-61	15.0	0.75	1:0:0	850	25	6
AIN083	2-38	20.0	0.75	1:0:0	850	5	6
AIN084	2-44	20.0	0.75	1:0:0	1000	50	6
AIN085	3-47	15.0	0.42	1:0:2	1500	50	6
AIN086	3-38	20.0	0.33	1:0:1	1000	150	6
AIN087	22-82	20.0	0.50	1:0:0	850	25	6
AIN088	22-129	20.0	0.50	1:0:0	1500	150	6
AIN089	22-98	25.0	0.75	1:0:0	1000	50	6
AIN093	24-147	15.0	0.50	1:0:0	2000	50	5
AIN094	22-106	15.0	0.75	1:0:0	850	25	5
AIN095	24-122	20.0	0.75	1:0:0	850	25	4
AIN096	24-100	20.0	0.75	1:0:0	850	25	5
AIN097	40-120	10.0	0.67	1:0:0	900	50	4
AIN098	38-120	10.0	0.67	1:0:0	900	50	5
AIN099	26-82	7.0	0.75	1:0:0	700	250	4
AIN100	26-68	7.0	0.75	1:0:0	700	250	5
AIN101	29-114	3.0	1.00	1:0:0	800	250	4
AIN102	29-113	3.0	1.00	1:0:0	800	250	5
AIN103	30-116	5.0	0.75	1:0:0	850	150	4
AIN104	30-88	5.0	0.75	1:0:0	850	150	5
AIN105	30-94	7.5	0.75	1:0:0	900	300	5
AIN106	29-69	5.0	0.75	1:0:0	600	25	5
AIN107	26-90	10.0	1.00	1:0:0	750	150	5
AIN108	28-86	10.0	1.00	1:0:0	750	150	5
AIN109	26-100	21.0	0.75	2:1:0	1000	25	5
AIN110	25-92	12.0	1.00	5:1:0	850	25	5
AIN111	25-92	16.5	1.00	10:1:0	700	25	5
AIN112	25-92	16.5	1.00	10:1:0	1000	25	5

Table A-1. AlN Deposition Conditions (continued)

<u>Sample#</u>	<u>DepTemp (C)</u>	<u>DepPress (mTorr)</u>	<u>DepTime (hr)</u>	<u>Gas ambient N<sub>2</sub>:O<sub>2</sub>:Ar</u>	<u>DC power (W)</u>	<u>Frequency (kHz)</u>	<u>Distance (inch)</u>
AIN113	28-155	12.0	1.00	23:1:0	2000	50	5
AIN114	30-102	12.0	0.83	23:1:0	850	50	5
AIN115	36-116	5.0	0.50	0:1:0	850	50	5
AIN116	35-108	3.0	1.25	0:1:0	500	150	5
AIN117	35-110	3.0	1.25	0:1:0	700	250	5
AIN118	32-133	11.0	1.50	10:1:0	850	25	5
AIN119	32-138	11.0	1.50	10:1:0	1500	150	5
AIN120	26-104	10.0	0.80	1:(10:1:0)	850	50	5
AIN121	26-96	10.0	0.80	1:(10:1:0)	1000	25	5
AIN122	26-96	10.0	0.80	1:(10:1:0)	1000	50	5
AIN123	26-96	10.0	0.80	1:(10:1:0)	850	50	5
AIN124	26-96	10.5	1.00	20:1:0	850	25	5
AIN125	26-96	10.5	1.00	20:1:0	1000	50	5
AIN126	32-118	10.0	1.00	1(10:1:0)	850	50	5
AIN127	34-88	10.0	1.00	1(10:1:0)	850	250	5
AIN128	36-130	11.5	1.50	7:1:0	850	50	5
AIN129	36-110	11.5	1.50	7:1:0	850	50	5
AIN130	34-127	11.5	2.00	7:1:0	850	50	5
AIN131	35-100	11.5	2.00	7:1:0	850	50	5
AIN132	29-112	11.5	2.00	7:1:0	700	50	5
AIN133	29-77	11.5	2.00	7:1:0	500	50	5
AIN134	37-113	13.0	1.50	12:1:0	850	50	5
AIN135	38-95	13.0	1.50	12:1:0	850	25	5
AIN136	37-120	21.0	1.50	20:1:0	850	25	5
AIN137	36-92	21.0	1.50	20:1:0	700	25	5
AIN138	33-135	16.5	1.75	10:1:0	1000	50	5
AIN139	33-124	16.5	1.75	10:1:0	1200	50	5
AIN140	34-133	11.5	1.75	7:1:0	1000	50	5
AIN141	36-98	11.5	1.75	7:1:0	850	50	5
AIN142	34-122	16.5	2.00	10:1:0	1000	50	5
AIN143	29-101	16.5	2.00	10:1:0	1000	25	5
AIN146	35-137	11.5	1.75	7:1:0	900	50	5
AIN147	36-102	11.5	1.75	7:1:0	850	50	5
AIN148	36-135	11.5	1.75	7:1:0	900	50	5
AIN149	36-98	11.5	1.75	7:1:0	900	50	5
AIN150	28-114	11.5	1.75	7:1:0	900	50	5
AIN151	28-114	11.5	1.75	7:1:0	900	50	5
AIN152	35-103	11.5	0.67	7:1:0	850	50	5
AIN153	35-103	11.5	0.67	7:1:0	850	50	5
AIN154	18-110	11.5	1.00	7:1:0	850	50	5

Table A-1. AlN Deposition Conditions (continued)

<u>Sample#</u>	<u>DepTemp (C)</u>	<u>DepPress (mTorr)</u>	<u>DepTime (hr)</u>	<u>Gas ambient N<sub>2</sub>:O<sub>2</sub>:Ar</u>	<u>DC power (W)</u>	<u>Frequency (kHz)</u>	<u>Distance (inch)</u>
AIN155	18-110	11.5	1.00	7:1:0	850	50	5
AIN156	32-55	11.5	0.17	7:1:0	850	50	5
AIN157	32-55	11.5	0.17	7:1:0	850	50	5
AIN158	33-97	11.5	0.58	7:1:0	850	50	5
AIN159	33-97	11.5	0.58	7:1:0	850	50	5
AIN160	32-102	11.5	2.17	7:1:0	850	50	6
AIN161	32-102	11.5	2.17	7:1:0	850	50	6
AIN162	29-113	11.5	2.50	7:1:0	1000	50	5
AIN163	29-113	11.5	2.50	7:1:0	1000	50	5
AIN164		11.5	2.17	7:1:0	850	50	5
AIN165		11.5	2.17	7:1:0	850	50	5
AIN166	29-108	11.5	1.75	7:1:0	850	50	5
AIN167	29-108	11.5	1.75	7:1:0	850	50	5
AIN168	29-106	11.5	1.42	7:1:0	850	50	5
AIN169	29-106	11.5	1.42	7:1:0	850	50	5
AIN174	30-160	10.0	2.00	0:3:2	1500	50	5
AIN175	30-100	11.5	1.67	7:1:0	850	50	5
AIN176	30-100	11.5	1.67	7:1:0	850	50	5
AIN177	34-118	11.5	1.25	7:1:0	850	50	5
AIN178	34-118	11.5	1.25	7:1:0	850	50	5
AIN179	34-122	11.5	1.67	7:1:0	850	50	5
AIN180	34-122	11.5	1.67	7:1:0	850	50	5
AIN181	30-120	11.5	1.67	7:1:0	850	50	5
AIN182	30-120	11.5	1.67	7:1:0	850	50	5
AIN196	30-120	15.5	1.00	7:1:3	850	50	5
AIN197	30-120	19.5	1.00	7:1:5	850	50	5
AIN198	30-120	11.5	1.67	7:1:0	850	50	5
AIN199	30-120	5.5	1.67	7:1:0	850	50	5
AIN200	30-120	11.5	1.67	7:1:0	850	50	5
AIN201	30-120	11.5	1.67	7:1:0	850	50	5
AIN202	30-120	11.5	1.67	7:1:0	850	50	5
AIN203	30-120	11.5	1.67	7:1:0	850	50	5
AIN204	30-120	9.0	1.67	7:1:7	850	50	5
AIN205	30-120	7.0	1.67	7:1:3.5	850	50	5
AIN206	30-120	11.5	1.00	7:1:0	1000	50	5
AIN207	30-120	11.5	1.00	7:1:0	1000	50	5

Table A-1. AlN Deposition Conditions (continued)

<u>Sample#</u>	<u>DepTemp (C)</u>	<u>DepPress (mTorr)</u>	<u>DepTime (hr)</u>	<u>Gas ambient N<sub>2</sub>:O<sub>2</sub>:Ar</u>	<u>DC power (W)</u>	<u>Frequency (kHz)</u>	<u>Distance (inch)</u>
AIN208	30-120	11.5	1.67	7:1:0	850	50	5
AIN209	30-120	6.0	1.67	7:1:7	850	50	5
AIN210	30-120	9.0	1.92	7:1:7	850	50	5
AIN211	30-120	13.0	1.75	7:1:14	850	50	5
AIN214	30-120	11.5	1.67	7:1:0	850	50	5
AIN215	30-120	9.0	1.42	7:1:7	850	50	5
AIN216	30-120	11.5	1.67	7:1:0	850	50	5
AIN217	30-120	9.0	1.33	7:1:7	850	50	5
AIN218	30-120	11.5	1.67	7:1:0	850	50	5
AIN219	30-120	11.5	1.67	7:1:0	850	50	5
AIN220	30-120	11.5	1.50	7:1:0	850	50	5
AIN222	30-120	11.5	1.67	7:1:0	850	50	5
AIN223	30-120	11.5	1.67	7:1:0	850	50	5
AIN224	30-120	11.5	1.50	7:1:0	850	50	5
AIN225	30-120	11.5	1.50	7:1:0	850	50	5
AIN226	30-120	11.5	1.50	7:1:0	850	50	5
AIN227	30-120	11.5	1.50	7:1:0	850	50	5
AIN228	30-120	11.5	1.67	7:1:0	850	50	5
AIN229	30-120	11.5	1.67	7:1:0	850	50	5
AIN230	30-120	11.5	1.67	7:1:0	850	50	5
AIN231	30-120	11.5	1.67	7:1:0	850	50	5
AIN232	30-120	11.5	1.67	7:1:0	850	50	5
AIN233	30-120	11.5	1.67	7:1:0	850	50	5
AIN234	30-120	11.5	1.67	7:1:0	850	50	5
AIN235	30-120	11.5	1.67	7:1:0	850	50	5
AIN236	30-120	11.5	1.67	7:1:0	850	50	5
AIN237	30-120	11.5	1.67	7:1:0	850	50	5
AIN238	30-120	11.5	1.67	7:1:0	850	50	5
AIN239	30-120	11.5	1.67	7:1:0	850	50	5
AIN240	30-120	11.5	1.67	7:1:0	850	50	5
AIN241	30-120	11.5	1.67	7:1:0	850	50	5

## APPENDIX B

Table B-1. Dielectric Properties of AlN Films

<u>Sample#</u>	<u>Substrate</u>	<u>Film (Å)</u>	<u>Df</u>	<u>Cap (nF)</u>	<u>R<sub>p</sub> (MΩ)</u>	<u>R<sub>d</sub> (MΩ)</u>	<u>IR (MΩ)</u>	<u>HV</u>	<u>k</u>	<u>ρ (Ω-cm)</u>	<u>V/μ</u>	<u>DepRate (Å/s)</u>
AIN003	Si	10513	0.02449	0.47	29.12	13.89	0.00	279	7.86	6.72E+02	265.39	1.95
AIN004	Si	11067	0.01048	0.46	38.44	33.17	2740000.00	480	8.10	1.75E+15	433.73	3.07
AIN006	Si	5840	0.01753	1.26	10.35	7.21			11.76	1.21E+03		3.24
AIN007	Si	4967	0.01339	1.32	9.47	8.97			10.52	1.42E+03		2.76
AIN008	Si	2859	0.02283	1.68	4.13	4.15			7.67	2.47E+03		1.91
AIN009	Si	2937	0.01202	1.70	7.82	7.78			7.99	2.41E+03		1.63
AIN010	Si	3672	0.00951	1.47	11.69	11.41			8.61	1.93E+03		2.04
AIN011	Si	3623	0.00839	1.84	10.33	10.32			10.65	1.95E+03		2.01
AIN012	Si	5294	0.00580	0.99	27.70	27.66	445000.00	180	8.39	5.94E+14	340.04	2.21
AIN013	Si	3380	0.01889	1.59	8.44	5.29	2232.00	125	8.60	4.67E+12	369.79	1.41
AIN014	Si	5235	36.76350	1.82	0.00	0.00			15.23	1.35E+03		1.94
AIN015	Si	4861	0.01103	1.16	13.10	12.40			9.04	5.80E+09		1.35
AIN016	Si	7504	0.00552	0.73	33.06	39.73	4350.00	185	8.71	4.10E+12	246.54	2.08
AIN017	Si	5534	0.01936	1.10	8.95	7.46	38.80		9.75	4.96E+10		2.31
AIN018	Si	3329	0.03129	1.82	5.63	2.80	41600.00	20	9.68	8.83E+13	60.08	1.39
AIN021	Si	4716	0.05958	1.06	0.26	2.52			8.01	1.50E+03		2.25
AIN022	Si	6709	0.01359	0.71	16.71	16.41	64500.00	257.5	7.66	6.80E+13	383.83	3.19
AIN023	Si	4599	0.01677	1.10	8.83	8.59	77600.00	105	8.12	1.19E+14	228.29	1.70
AIN024	Si	4750	0.17573	1.26	1.26	0.72	8980.00		9.59	1.34E+13		1.76
AIN025	Si	5709		1.04	0.13	0.00			9.54	1.24E+03		2.11
AIN026	Si	5950	0.03129	1.82	5.63	2.80			17.30	1.19E+03		2.20
AIN027	Si	3158	-	-	-	-	-	-	-	-	-	1.32
AIN027	Foil	3158	-	-	-	-	-	-	-	-	-	1.32
AIN028	Si	6986	0.05825	1.60	1.73	1.71	9980.00	141.667	17.83	1.01E+13	202.79	2.91

Table B-1. Dielectric Properties of AlN Films (continued)

<u>Sample#</u>	<u>Substrate</u>	<u>Film (Å)</u>	<u>Df</u>	<u>Cap (nF)</u>	<u>R<sub>p</sub> (MΩ)</u>	<u>R<sub>p</sub> (MΩ)</u>	<u>IR (MΩ)</u>	<u>HV</u>	<u>k</u>	<u>ρ (Ω-cm)</u>	<u>V/μ</u>	<u>DepRate (Å/s)</u>
AIN028	Foil	6986	-	-	-	-	-	-	-	-	-	2.91
AIN029	Si	4337	-	-	-	-	-	-	-	-	-	1.81
AIN029	Foil	4337	-	-	-	-	-	-	-	-	-	1.81
AIN030	Si	4167	-	-	-	-	-	-	-	-	-	1.74
AIN030	Foil	4167	-	-	-	-	-	-	-	-	-	1.74
AIN031	Si	-	-	-	-	-	-	-	-	-	-	-
AIN032	Si	-	-	-	-	-	-	-	-	-	-	-
AIN033	Si	5663	-	-	-	-	-	-	-	-	-	2.10
AIN034	Si	3800	-	-	-	-	-	-	-	-	-	1.41
AIN037	Si	7207	0.01776	0.73	13.36	12.20	2340.00	271	8.46	2.30E+12	376.02	4.00
AIN037	Foil	7207	0.01099	0.78	17.46	18.58	68000.00	127.667	8.98	6.67E+13	177.14	4.00
AIN038	Si	2932	0.0157	1.542	6.64	6.572			7.23			1.63
AIN039	Foil											
AIN040	Foil											
AIN041	Foil											
AIN042	Foil											
AIN043	Foil											
AIN044	Foil											
AIN045	Foil											
AIN046	Foil											
AIN047	Foil											
AIN048	Foil	2803	0.0351	1.725	2.68	2.633	16350	90.00	7.73	4.12E+13	321.11	1.33
AIN049	Foil	4783	0.0424	1.555	2.49	2.413	5000	140.00	11.89	7.39E+12	292.73	3.99
AIN050	Foil	7522	0.0675	0.804	3.39	2.932	13550	375.00	9.67	1.27E+13	498.57	3.13

Table B-1. Dielectric Properties of AlN Films (continued)

<u>Sample#</u>	<u>Substrate</u>	<u>Film (Å)</u>	<u>Df</u>	<u>Cap (nF)</u>	<u>R<sub>p</sub> (MΩ)</u>	<u>R<sub>b</sub> (MΩ)</u>	<u>IR (MΩ)</u>	<u>HV</u>	<u>k</u>	<u>ρ (Ω-cm)</u>	<u>V/μ</u>	<u>DepRate (Å/s)</u>
AIN051	Foil	8504	0.0297	0.752	7.24	7.140	67166.67	333.33	10.22	5.58E+13	391.99	4.72
AIN052	Foil	6544	0.0217	0.806	9.91	9.100	32400	176.67	8.43	3.50E+13	269.96	2.73
AIN052	Si	6544	0.0305	0.832	6.27	6.265	18550	277.50	8.70	2.00E+13	424.04	2.73
AIN053	Foil	6323	0.0159	0.967	11.60	10.332	59266.67	126.25	9.77	6.63E+13	199.67	3.51
AIN054	Foil	5882	0.0543	1.102	2.76	2.659	12182.75	301.67	10.36	1.46E+13	512.89	2.45
AIN055	Foil	3609	0.0318	1.438	3.89	3.480	17793.33	145.00	8.30	3.49E+13	401.77	1.50
AIN056	Foil	4219	0.0319	1.027	4.99	4.852	15800	178.75	6.93	2.65E+13	423.68	2.34
AIN057	Foil	4017	0.0363	1.166	3.78	3.759	12833.33	211.67	7.48	2.26E+13	526.96	1.67
AIN058	Foil	5416	0.0178	0.930	9.71	9.606	13766.67	189.00	8.05	1.80E+13	349.00	3.01
AIN059	Foil	5459	0.0198	0.936	8.73	8.579	35175	162.50	8.17	4.55E+13	297.67	3.03
AIN060	Foil	3681	0.0241	1.210	5.62	5.466	8069.25	163.75	7.12	1.55E+13	444.82	1.36
AIN061	Foil	4231	0.0313	1.504	3.42	3.386	17750	166.25	10.17	2.97E+13	392.91	2.35
AIN062	Aborted											
AIN063	Foil	2304	0.2844	3.503	0.16	0.160			12.90			0.96
AIN063-2	Foil	2304	0.0600	1.958	1.39	1.354			7.21			0.96
AIN064	Foil	4029	0.1577	1.551	0.66	0.651	534.6667	21.67	9.99	9.38E+11	53.78	1.68
AIN064-2	Foil	4029	0.0794	1.177	1.71	1.702	534.6667	21.67	7.58	9.38E+11	53.78	1.68
AIN065	Foil	3017	0.3423	6.038	0.08	0.077	11.5	15.00	29.12	2.69E+10	49.72	1.26
AIN065-2	Foil	3017	0.1766	1.968	0.46	0.458	11.5	15.00	9.49	2.69E+10	49.72	1.26
AIN067	Foil	2533	0.3163	11.978	0.04	0.042	263.5	52.50	48.51	7.35E+11	207.24	1.41
AIN067-2	Foil	2533	0.2619	3.754	0.16	0.162	263.5	52.50	15.20	7.35E+11	207.24	1.41
AIN068	Foil	6387	0.2092	1.919	0.41	0.397	13200	267.50	19.59	1.46E+13	418.82	2.66
AIN068-2	Foil	6387	0.0767	1.095	2.89	1.896	13200	267.50	11.18	1.46E+13	418.82	2.66
AIN069	Foil	2878	0.1559	1.957	0.53	0.521	9003.333	166.67	9.00	2.21E+13	579.16	1.20

Table B-1. Dielectric Properties of AlN Films (continued)

<u>Sample#</u>	<u>Substrate</u>	<u>Film (Å)</u>	<u>Df</u>	<u>Cap (nF)</u>	<u>R<sub>p</sub> (MΩ)</u>	<u>R<sub>p</sub> (MΩ)</u>	<u>IR (MΩ)</u>	<u>HV</u>	<u>k</u>	<u>ρ (Ω-cm)</u>	<u>V/μ</u>	<u>DepRate (Å/s)</u>
AIN069-2	Foil	2878	0.0401	1.377	2.94	2.886	9003.333	166.67	6.33	2.21E+13	579.16	1.20
AIN070	Foil	6012	0.0842	0.895	2.27	2.112	14466.67	338.75	8.60	1.70E+13	563.49	2.50
AIN070-2	Foil	6012	0.0422	0.803	4.94	4.700	14466.67	338.75	7.72	1.70E+13	563.49	2.50
AIN071	Foil	3479	0.3115	5.065	0.11	0.101	980.5	62.50	28.17	1.99E+12	179.67	1.45
AIN071-2	Foil	3479	0.1393	2.470	0.50	0.462	980.5	62.50	13.74	1.99E+12	179.67	1.45
AIN072	Foil											
AIN073	Foil	2993	0.3053	8.720	0.06	0.060	541	107.50	41.72	1.28E+12	359.17	1.11
AIN073-2	Foil	2993	0.1359	3.732	0.35	0.314	541	107.50	17.86	1.28E+12	359.17	1.11
AIN073	Si	2993	0.1891	2.718	0.31	0.310			13.01	2.36E+03		1.11
AIN074	Foil	2822	0.0499	1.799	1.81	1.772	13133.33	55.00	8.12	3.29E+13	194.93	1.05
AIN074-2	Foil	2822	0.0476	1.767	1.95	1.892	13133.33	55.00	7.97	3.29E+13	194.93	1.05
AIN074	Si	2822	0.1559	2.622	0.46	0.389			11.83	2.51E+03		1.05
AIN075	Foil	4666	0.1117	1.707	0.84	0.834	2783.333	200.00	12.74	4.22E+12	428.63	1.73
AIN075-2	Foil	4666	0.0624	1.484	1.73	1.720	2783.333	200.00	11.07	4.22E+12	428.63	1.73
AIN076	Foil	4693	0.1204	1.504	0.93	0.878	2250	171.67	11.29	3.39E+12	365.77	1.74
AIN077	Foil	5270										1.95
AIN078	Foil	4387										1.62
AIN079		4285		Sent to NASA							2.38	
AIN080		2696		Sent to NASA							1.00	
AIN081	Si	4258	0.0762	1.273	1.64	1.641			8.67			1.58
AIN081	Glass	4534	0.2247	1.853	0.39	0.382	1350	90.00	13.43	2.10E+12	198.50	1.68
AIN082	Glass	3479	0.2383	2.563	0.27	0.261	1282.667	81.67	14.25	2.61E+12	234.72	1.29
AIN083	Glass, Si	3671										1.36
AIN084	Glass, Si	4114										1.52
AIN085	Foil	1743	0.1157	1.436	0.98	0.958	910.4	68.33	4.00	3.69E+12	392.12	1.16
AIN085	Si	1743	0.3288	2.446	0.21	0.198	4739.5	85.00	6.81	1.92E+13	487.76	1.16

Table B-1. Dielectric Properties of AlN Films (continued)

<u>Sample#</u>	<u>Substrate</u>	<u>Film (Å)</u>	<u>Df</u>	<u>Cap (nF)</u>	<u>R<sub>p</sub> (MΩ)</u>	<u>R<sub>p</sub> (MΩ)</u>	<u>IR (MΩ)</u>	<u>HV</u>	<u>k</u>	<u>ρ (Ω-cm)</u>	<u>V/μ</u>	<u>DepRate (Å/s)</u>
AIN086	Foil	1645	0.2351	3.351	0.23	0.202			8.81	4.30E+03		1.37
AIN086	Glass	1867	0.1207	1.950	0.68	0.676			5.82	3.79E+03		1.56
AIN086	Si	1645	0.2383	2.563	0.27	0.261			6.74	4.30E+03		1.37
AIN087	Foil	2127	0.0623	2.542	1.05	1.005			8.64	3.32E+03		1.18
AIN087	Glass	1874	0.1327	3.153	0.39	0.380			9.45	3.77E+03		1.04
AIN087	Si	2127	0.1293	3.258	0.60	0.378			11.08	3.32E+03		1.18
AIN088	Foil	3417	0.0604	1.213	2.24	2.174	15000	123.33	6.62	3.10E+13	360.94	1.90
AIN088	Glass	4444	0.3315	2.089	0.23	0.230	2720	172.50	14.84	4.33E+12	388.13	2.47
AIN088	Si	3417	0.6772	7.100	0.03	0.033	1310	190.00	38.78	2.71E+12	556.04	1.90
AIN089	Glass	4559	0.6344	3.686	0.07	0.068	179.6667	192.50	26.86	2.79E+11	422.21	1.69
AIN089	Si	3609	0.9365	12.897	0.01	0.013			74.41	1.96E+03	0.00	1.34
AIN093	Foil	5576	0.0343	0.860	5.73	5.396	19296.67	198.33	7.66	2.45E+13	355.71	3.10
AIN093	Glass	6386	0.0179	0.787	11.57	11.321	274780	279.00	8.04	3.04E+14	436.87	3.55
AIN093	Si	5576	0.0737	0.935	3.50	2.310	2720	265.00	8.33	3.45E+12	475.27	3.10
AIN094	Foil	3849	0.0303	1.026	5.64	5.120	58566.67	190.00	6.31	1.08E+14	493.67	1.43
AIN094	Glass	4175	0.0602	1.219	2.20	2.170	15233.33	120.00	8.14	2.58E+13	287.41	1.55
AIN094	Si	3849	0.0644	1.267	2.05	1.949	8043.333	233.33	7.80	1.48E+13	606.26	1.43
AIN095	Glass	5858	0.2040	1.120	0.74	0.697	7537.6	216.67	10.48	9.10E+12	369.89	2.17
AIN095	Si	5212	0.1376	1.141	1.02	1.014	20275	245.00	9.50	2.75E+13	470.04	1.93
AIN096	Foil	3837	0.2976	0.934	0.61	0.573	9100	85.00	5.73	1.68E+13	221.51	1.42
AIN096	Glass	4189	0.4314	3.502	0.11	0.105	2061	96.67	23.45	3.48E+12	230.74	1.55
AIN096	Si	3837	0.8998	10.520	0.02	0.017	1310	170.50	64.53	2.41E+12	444.32	1.42
AIN097	Foil	5051	0.0427	0.809	4.69	4.613	58550	54.00	6.53	8.19E+13	106.92	2.10
AIN097	Si	5051	0.2221	1.420	0.52	0.505	4103.333	66.00	11.46	5.74E+12	130.68	2.10
AIN098	Foil	3113	0.0726	1.272	1.73	1.724	33300	75.00	6.33	7.56E+13	240.90	1.30
AIN098	Si	3113	0.4824	4.580	0.07	0.072	6263.333	40.00	22.79	1.42E+13	128.48	1.30

Table B-1. Dielectric Properties of AlN Films (continued)

<u>Sample#</u>	<u>Substrate</u>	<u>Film (Å)</u>	<u>Df</u>	<u>Cap (nF)</u>	<u>R<sub>p</sub> (MΩ)</u>	<u>R<sub>p</sub> (MΩ)</u>	<u>IR (MΩ)</u>	<u>HV</u>	<u>k</u>	<u>ρ (Ω-cm)</u>	<u>V/μ</u>	<u>DepRate (Å/s)</u>
AIN099	Glass	4963	0.0489	1.060	3.17	3.075	2746677	100.00	8.41	3.91E+15	201.48	1.84
AIN099	Si	5320	0.0170	0.979	9.61	9.592	4675000	0.00	8.32	6.21E+15	0.00	1.97
AIN100	Glass	4417	0.0265	1.231	4.99	4.877	2275000	252.50	8.69	3.64E+15	571.62	1.64
AIN100	Si	4091	0.0186	1.019	8.73	8.376	7110710	288.33	6.66	1.23E+16	704.80	1.52
AIN101	Glass	8023	0.0250	0.659	9.70	9.668	2259500	421.25	8.45	1.99E+15	525.09	2.23
AIN101	Si	9081	0.0501	0.610	5.40	5.203	956250	441.25	8.86	7.44E+14	485.92	2.52
AIN102	Glass	5227	0.0256	0.823	7.77	7.555	901666.7	323.33	6.88	1.22E+15	618.58	1.45
AIN102	Si	6939	0.0563	0.710	4.80	3.986	5010000	326.67	7.87	5.10E+15	470.79	1.93
AIN103	Foil	4181	0.0305	1.181	4.59	4.416			7.89			1.55
AIN103	Si	4181	0.0303	1.278	4.18	4.104			8.54			1.55
AIN104	Foil	4456	0.0321	1.408	4.44	3.519			10.03			1.65
AIN104	Si	4456	0.0351	1.436	3.39	3.159	4365000	167.50	10.23	6.92E+15	375.90	1.65
AIN105	Glass	4598	0.0097	1.359	12.26	12.124	28809.33	48.33	9.99	4.43E+13	105.13	1.70
AIN105	Si	4289	0.0105	1.400	10.85	10.819	2442588	46.25	9.60	4.03E+15	107.83	1.59
AIN106	Glass	3138	0.0104	2.336	6.55	6.531	233963.3	17.50	11.72	5.27E+14	55.78	1.16
AIN106-A	Glass	2237	0.0140	2.227	5.15	5.108	806133.3	36.67	7.96	2.55E+15	163.91	0.83
AIN106	Si	3075	0.0107	2.500	5.08	5.927	15.915	12.50	12.29	3.66E+10	40.65	1.14
AIN107	Glass	5025	0.0375	1.300	3.39	3.264	18822.25	92.50	10.45	2.65E+13	184.08	1.40
AIN107	Si	4287	0.0131	1.290	9.81	9.424	301166.7	70.00	8.84	4.97E+14	163.30	1.19
AIN108	Glass	5010	0.0177	1.130	7.98	7.935	51875	158.33	9.05	7.32E+13	316.02	1.39
AIN109	Foil	2042	0.0641	3.573	0.74	0.695			11.66			0.76
AIN109-A	Foil	2042	0.0114	2.927	5.16	4.779	166000	25.00	9.55	5.75E+14	122.46	0.76
AIN109	Si	2042	0.1071	3.910	0.39	0.380	169333.3	55.00	12.76	5.86E+14	269.41	0.76
AIN110	Foil	1713	0.0078	2.466	8.33	8.310	860000.6	60.00	6.75	3.55E+15	350.22	0.48
AIN110-A	Foil	1713	0.0064	2.532	9.90	9.875			6.94			0.48
AIN110	Si	1713	0.0113	2.804	5.11	5.022	701.25	80.00	7.68	2.89E+12	466.96	0.48
AIN111	Glass	3420	0.0108	1.274	15.91	11.564	177148	180.00	6.96	3.66E+14	526.39	0.95

Table B-1. Dielectric Properties of AlN Films (continued)

<u>Sample#</u>	<u>Substrate</u>	<u>Film (Å)</u>	<u>Df</u>	<u>Cap (nF)</u>	<u>R<sub>p</sub> (MΩ)</u>	<u>R<sub>b</sub> (MΩ)</u>	<u>IR (MΩ)</u>	<u>HV</u>	<u>k</u>	<u>ρ (Ω-cm)</u>	<u>V/μ</u>	<u>DepRate (Å/s)</u>
AIN112	Glass	5094	0.0042	0.715	54.62	53.442	382670	304.00	5.82	5.31E+14	596.78	1.42
AIN112-A	Glass	5132	0.0055	0.849	37.72	34.352	3793333	310.00	6.97	5.22E+15	604.03	1.43
AIN113	Glass	13436	0.0072	0.356	59.88	61.978	392833.3	330.00	7.66	2.07E+14	245.61	3.73
AIN113-A	Glass	13316	0.0054	0.326	91.82	89.955	10654750	540.00	6.94	5.66E+15	405.53	3.70
AIN114	Glass	3867	0.0082	1.354	12.26	14.361	1607667	170.00	8.37	2.94E+15	439.65	1.29
AIN114	Mylar	3867	0.0060	1.323	21.49	20.132	3462325	176.00	8.18	6.33E+15	455.16	1.29
AIN115	Glass	1485										0.82
AIN116	Glass	1141										0.25
AIN117	Glass	980										0.22
AIN118	Glass	3497	0.0062	1.384	25.05	18.574	2.61E+05	166.67	7.73	5.28E+14	476.63	0.65
AIN119	Glass	7410	0.0038	0.609	63.78	69.021	4.52E+06	338.00	7.22	4.31E+15	456.14	1.37
AIN120	Glass	3111	0.0105	1.416	10.99	10.675	7.40E+04	180.00	7.04	1.68E+14	578.67	1.08
AIN121	Glass	5359	0.0135	1.220	10.26	9.659	3.20E+05	202.50	10.45	4.22E+14	377.90	1.86
AIN122	Glass	4901	0.0090	1.228	14.96	14.356	1.30E+05	167.50	9.62	1.88E+14	341.77	1.70
AIN123	Glass	4459	0.0109	1.460	10.12	10.020	2.54E+05	152.86	10.41	4.03E+14	342.81	1.55
AIN124	Glass	5754	0.0062	1.011	25.70	25.415	1.72E+06	162.00	9.30	2.11E+15	281.53	1.60
AIN125	Glass	6304	0.0076	0.822	25.59	25.334	2.30E+05	110.00	8.29	2.58E+14	174.50	1.75
AIN126	Glass	4463	0.0205	1.470	6.20	5.283	8.67E+05	230.00	10.48	1.37E+15	515.38	1.24
AIN127	Glass	3724	0.0161	1.438	7.02	6.871	3.75E+05	140.00	8.56	7.11E+14	375.92	1.03
AIN128	Glass	2561	0.0040	2.082	19.71	19.149	5.43E+05	155.00	8.52	1.50E+15	605.35	0.47
AIN129	Glass	2704	0.0072	2.090	10.73	10.644	1.06E+06	141.67	9.03	2.78E+15	523.95	0.50
AIN130	Glass	2672	0.0040	1.361	29.56	29.257	1.68E+06	142.14	5.81	4.45E+15	531.93	0.37
AIN131	Glass	3281	0.0052	1.432	22.78	21.424	1.12E+06	194.38	7.51	2.41E+15	592.46	0.46
AIN132	Glass	2533	0.0039	1.941	19.23	20.858	1.82E+05	146.67	7.86	5.08E+14	579.02	0.35
AIN133	Glass	1882	0.0087	3.011	6.46	6.080	2.35E+05	93.57	9.06	8.83E+14	497.24	0.26
AIN134	Glass	2950	0.0042	1.321	30.49	28.878	1.27E+06	170.00	6.23	3.04E+15	576.22	0.55

Table B-1. Dielectric Properties of AlN Films (continued)

<u>Sample#</u>	<u>Substrate</u>	<u>Film (Å)</u>	<u>Df</u>	<u>Cap (nF)</u>	<u>R<sub>p</sub> (MΩ)</u>	<u>R<sub>p</sub> (MΩ)</u>	<u>IR (MΩ)</u>	<u>HV</u>	<u>k</u>	<u>ρ (Ω-cm)</u>	<u>V/μ</u>	<u>DepRate (Å/s)</u>
AIN135	Glass	2612	0.0154	1.533	9.31	6.755	1.34E+05	90.00	6.40	3.63E+14	344.63	0.48
AIN136	Glass	4576	0.0176	0.997	14.11	9.078	1.20E+06	192.00	7.29	1.85E+15	419.63	0.85
AIN137	Glass	4313	0.0635	1.680	1.92	1.492	4.42E+01	193.33	11.58	7.24E+10	448.26	0.80
AIN138	Glass	3981	0.0047	1.191	28.82	28.325	1.17E+06	206.67	7.58	2.07E+15	519.13	0.63
AIN139	Glass	4487	0.0100	0.957	40.27	16.606	3.94E+05	216.67	6.86	6.20E+14	482.85	0.71
AIN140	Glass	3389	0.0051	1.256	44.41	24.965	2.91E+06	160.00	6.81	6.06E+15	472.12	0.54
AIN141	Glass	2928	0.0106	1.541	10.28	9.753	1.45E+06		7.21	3.50E+15		0.46
AIN142	Glass	6527	0.0080	0.692	29.92	28.906	3.67E+05	156.67	7.22	3.97E+14	240.01	0.91
AIN143	Glass	5933	0.0210	0.760	11.78	9.952	3.91E+05	180.00	7.21	4.66E+14	303.38	0.82
AIN146	Glass	5198	0.0048	1.185	28.92	27.756	1.48E+06	218.33	9.85	2.01E+15	420.07	0.83
AIN147	Glass	3629	0.0101	1.252	16.23	12.631	2.02E+06	166.00	7.26	3.94E+15	457.46	0.58
AIN148	Glass	5142	0.0036	1.081	41.85	41.220	6.08E+05	291.00	8.89	8.36E+14	565.91	0.82
AIN149	Glass	5103	0.0037	1.017	41.82	42.133	9.78E+05	294.00	8.29	1.35E+15	576.11	0.81
AIN150	Polyester	Mylar burned										
AIN151	Foil	5125	0.0043	1.257	29.19	29.206	1.00E-06	1.00	10.30	1.38E+03	1.95	0.81
AIN152	Polyester											
AIN153	Glass	1986	0.0153	4.004	2.67	2.606	9.75E+04	60.00	12.71	3.47E+14	302.14	0.83
AIN154	Glass	3330	0.0075	2.082	10.43	10.195	9.89E+03	114.17	11.08	2.10E+13	342.88	0.92
AIN155	Polyester											
AIN156	Polyester											
AIN157	Glass	732	0.0855	12.525	0.17	0.149	3.34E+01	23.71	14.66	3.22E+11	323.86	1.22
AIN158	Polyester											
AIN159	Polyester											
AIN160	Polyester											
AIN161	Glass	3499	0.0053	1.347	22.37	22.299	1.64E+06	190.00	7.53	3.31E+15	543.08	0.45
AIN162	Polyester	4686	0.0026	1.003	62.13	60.166	9.98E+05	170.00	7.51	1.50E+15	362.76	0.52
AIN163	Glass	4686	0.0061	0.853								
AIN164	Foil	6396	0.0293	1.338								
AIN165	Foil	6396	0.0137	1.604	7.53	7.261	6.91E+04	76.67	16.39	7.64E+13	119.87	0.82

Table B-1. Dielectric Properties of AlN Films (continued)

<u>Sample#</u>	<u>Substrate</u>	<u>Film (Å)</u>	<u>Df</u>	<u>Cap (nF)</u>	<u>R<sub>p</sub> (MΩ)</u>	<u>R<sub>p</sub> (MΩ)</u>	<u>IR (MΩ)</u>	<u>HV</u>	<u>k</u>	<u>ρ (Ω·cm)</u>	<u>V/μ</u>	<u>DepRate (Å/s)</u>
AIN166	Polyester	5166										
AIN167	Polyester											
AIN168	Polyester	4182	0.0354	1.500	5.04	3.000	6.01E+02	10.00	10.03	1.02E+12	23.91	0.82
AIN169	Polyester	4182										0.82
AIN174	Glass	10000	0.0766	1.652	1.99	1.258			26.42			1.39
AIN175	FPE	4920	0.0134	1.494	8.28	7.973			11.75			0.82
AIN176	FPE	4920	0.0131	1.331	8.97	9.111	1.88E+06	10.00	10.47	2.70E+15	20.33	0.82
AIN177	FPE	3474	0.0126	1.404	9.34	8.999	0.00E+00	0.00	7.79	0.00E+00	0.00	0.77
AIN177	Glass	3474	0.0149	1.434	7.49	7.467	1.14E+05	110.00	7.97	2.31E+14	316.62	0.77
AIN178	FPE	3474	0.0138	1.449	8.32	7.984	1.07E+06	101.67	8.05	2.18E+15	292.63	0.77
AIN178	Glass	3474	0.0066	1.527	16.93	15.744	7.65E+04	80.00	8.48	1.56E+14	230.27	0.77
AIN179	FPE	5320	0.0069	1.277	14.93	18.029	5.92E+05	228.33	10.86	7.86E+14	429.20	0.89
AIN179	Glass	5320	0.0276	1.397	4.59	4.136	4.94E+03	203.75	11.88	6.56E+12	383.01	0.89
AIN180	FPE	4612	0.0079	1.397	11.10	14.451	9.27E+04	140.00	10.30	1.42E+14	303.56	0.77
AIN180	Glass	4612	0.0080	1.438	13.97	13.828	2.57E+05	165.00	10.60	3.93E+14	357.76	0.77
AIN181	FPE	4920	0.0074	1.397	16.35	15.383	2.12E+05	145.00	10.99	3.04E+14	294.72	0.82
AIN181	Foil	4920	0.0060	1.309	20.45	20.176	4.42E+05	181.67	10.30	6.35E+14	369.24	0.82
AIN182	FPE	4920	0.0125	1.329	9.82	9.611	1.15E+06	156.67	10.45	1.65E+15	318.43	0.82
AIN182	Foil	4920	0.0114	1.341	10.69	10.434	1.01E+05	186.67	10.55	1.45E+14	379.40	0.82
AIN196	Glass	2330	0.0569	3.288	0.88	0.851			12.25			0.65
AIN197	Glass	2205	0.0318	2.879	1.77	1.737			10.15			0.61
AIN198	Glass	4011	0.0042	1.605	23.44	23.389			10.29			0.67
AIN199	Glass	3766	0.0040	1.421	28.07	27.937			8.55			0.63
AIN200	S.S.	4000										0.67
AIN201	Ti	4000										0.67
AIN202	S.S.	3698	0.0054	1.253	24.65	23.382			7.41			0.62
AIN203	Ti	3698	0.0040	1.279	32.54	31.096			7.56			0.62
AIN204	Glass	5033	0.0054	1.147	27.70	25.600	1.01E+05	130.00	9.23	1.42E+14	258.30	0.84

Table B-1. Dielectric Properties of AlN Films (continued)

<u>Sample#</u>	<u>Substrate</u>	<u>Film (Å)</u>	<u>Df</u>	<u>Cap (nF)</u>	<u>R<sub>p</sub> (MΩ)</u>	<u>R<sub>e</sub> (MΩ)</u>	<u>IR (MΩ)</u>	<u>HV</u>	<u>k</u>	<u>ρ (Ω-cm)</u>	<u>V/μ</u>	<u>DepRate (Å/s)</u>
AIN205	Glass	4737	0.0059	1.098	24.71	24.403	2.19E+05	213.33	8.32	3.27E+14	450.38	0.79
AIN206	S.S.	3698	0.0054	1.668	17.76	17.606	1.87E+07	40.00	9.00	3.57E+16	118.53	1.03
AIN207	Ti	3401	0.0062	1.655	15.63	15.596	short		9.00	short		0.94
AIN208	Glass	3471	0.0053	1.683	18.06	17.919	2.39E+05	133.33	9.34	4.86E+14	384.14	0.58
AIN209	Glass	6162	0.0097	0.818	20.76	20.093	1.44E+06	252.00	8.06	1.65E+15	408.99	1.03
AIN210	Glass	6318	0.0063	0.881	28.93	28.663	2.44E+05	133.33	8.90	2.73E+14	211.03	0.92
AIN211	Glass	6710	0.0657	0.858	2.98	2.823	1.79E+03	180.00	9.20	1.88E+12	268.25	1.07
AIN214	Glass	5249	0.0131	1.370	9.89	8.857	9.43E+02	86.67	11.49	1.27E+12	165.12	0.87
AIN215	Glass	6471	0.0371	1.060	4.09	4.047	2.07E+03	80.00	10.97	2.26E+12	123.62	1.27
AIN216	Glass	3426	0.0052	1.525	20.10	19.892	4.59E+04	155.71	8.35	9.48E+13	454.57	0.57
AIN217	Glass	5764	0.0246	1.041	6.29	6.201	2.81E+04	160.00	9.60	3.45E+13	277.57	1.20
AIN218	Glass	5532	0.0034	1.048	44.25	44.177	2.24E+05	132.50	9.27	2.86E+14	239.54	0.92
AIN219	SS	5532										0.92
AIN220	Glass	4182	0.0043	1.285	29.42	28.967	4.71E+04	210.00	8.59	7.96E+13	502.15	0.77
AIN222	Glass	6017	0.1454	0.986	1.71	1.110			9.49			1.00
AIN223	Glass	3947										0.66
AIN224	Ti	4055	0.0048	1.311	26.32	25.346	3.77E+06	140.00	8.50	6.57E+15	345.23	0.75
AIN225	S.S.	3647	0.0048	1.458	22.82	22.580	2.14E+06	202.00	8.50	4.15E+15	553.90	0.68
AIN226	Glass	4183	0.0075	1.299	16.47	16.304	1.46E+03	162.50	8.68	2.47E+12	388.51	0.77
AIN227	Glass	3768	0.0047	1.305	26.48	26.158			7.86			0.70
AIN228	Glass	5384	0.0051	0.957	34.22	32.343	5.70E+04	185.00	8.23	7.48E+13	343.63	0.90
AIN229	Glass	4532	0.0067	1.140	22.38	20.832	5.98E+03	156.67	8.26	9.32E+12	345.67	0.76
AIN230	S.S.	4157	0.0057	1.279	22.30	21.944	1.67E+06	186.00	8.50	2.84E+15	447.45	0.69
AIN231	S.S.	3816	0.0056	1.394	20.91	20.309	6.58E+05	170.00	8.50	1.22E+15	445.55	0.64
AIN232	Glass	4709	0.0053	1.121	27.04	26.875	1.43E+05	130.00	8.44	2.15E+14	276.07	0.78
AIN233	Glass	4555	0.0058	1.206	23.13	22.942	2.67E+04	158.00	8.78	4.14E+13	346.87	0.76

Table B-1. Dielectric Properties of AlN Films (continued)

<u>Sample#</u>	<u>Substrate</u>	<u>Film (Å)</u>	<u>Df</u>	<u>Cap (nF)</u>	<u>R<sub>p</sub> (MΩ)</u>	<u>R<sub>e</sub> (MΩ)</u>	<u>IR (MΩ)</u>	<u>HV</u>	<u>k</u>	<u>ρ (Ω-cm)</u>	<u>V/μ</u>	<u>DepRate (Å/s)</u>
AIN234	S.S	4834										
AIN235	S.S	4496										
AIN236	FPE	5209	0.0061	1.081	24.41	24.035	2.22E+06	235.00	9.00	3.01E+15	451.16	0.87
AIN237	FPE	4847	0.0058	1.162	23.72	23.559	4.33E+05	250.00	9.00	6.32E+14	515.82	0.81
AIN238	Glass	4386	0.0052	1.231	24.68	24.786	7.86E+05	238.00	8.63	1.27E+15	542.68	0.73
AIN239	Glass	4268	0.0048	1.327	26.55	24.837	2.59E+06	267.50	9.05	4.29E+15	626.83	0.71

## APPENDIX C

Table C-1. AlON Deposition Conditions Using N<sub>2</sub>/O<sub>2</sub>

Sample#	DepTemp (°C)	DepPress (mTorr)	DepTime (hr)	Layers	Metal	HE	Gas ambient N <sub>2</sub> :O <sub>2</sub> :Ar	DC power (W)	Frequency (kHz)	Distance (inch)
AIN245	30-120	11.5	1.50	2	Al	N	7:1:0	850	50	5
AIN246	30-120	11.5	2.00	1	Al	N	7:1:0	850	50	5
AIN247	30-120	11.5	2.00	2	Al	N	7:1:0	850	50	5
AIN248	30-120	11.5	2.00	2	Al	N	7:1:0	850	50	5
AIN249	30-120	11.5	2.00	1	Al	N	7:1:0	850	50	5
AIN250	30-120	11.5	2.00	2	Al	N	7:1:0	850	50	5
AIN251	30-120	11.5	2.00	3	Al	N	7:1:0	850	50	5
AIN252	30-120	11.5	2.00	3	Al	N	7:1:0	850	50	5
AIN254	30-120	11.5	1.50		Al	N	7:1:0	850	50	5
AIN255	30-120	11.5	1.00	1	Al	N	7:1:0	850	50	5
AIN256	30-120	11.5	1.00	3	Al	N	7:1:0	850	50	5
AIN257	30-120	11.5	2.00	4	Al	N	7:1:0	850	50	5
AIN258	30-120	11.5	2.00	2	Al	N	7:1:0	850	50	5
AIN259	30-120	11.5	2.00	1	Al	N	7:1:0	850	50	5
AIN260	30-120	11.5	2.00	2	Al	N	7:1:0	850	50	5
AIN261	30-120	11.5	2.00	6	Al	N	7:1:0	850	50	5
AIN262	30-120	11.5	2.00	8	Al	N	7:1:0	850	50	5
AIN263	30-120	11.5	2.00	4	Al	N	7:1:0	850	50	5
AIN264	30-120	11.5	2.00	7	Al	N	7:1:0	850	50	5
AIN265	30-120	11.5	2.00	8	Al	N	7:1:0	850	50	5
AIN266	30-120	11.5	2.00	3	Al	N	7:1:0	850	50	5
AIN267	30-120	11.5	2.00	4	Al	N	7:1:0	850	50	5
AIN268	30-120	11.5	2.00	8	Al	N	7:1:0	850	50	5

Table C-2. AlON Deposition Conditions Using N<sub>2</sub>O

Sample#	DepTemp (°C)	DepPress (mTorr)	DepTime (hr)	Layers	Metal	HE	Gas ambient N <sub>2</sub> :N <sub>2</sub> O	DC power (W)	Frequency (kHz)	Distance (inch)
AIN270	30-120	10.0	1.50	1	Al	N	9:1	500	50	5
AIN271	30-120	5.0	1.50	1	Al	N	9:1	1000	150	5
AIN272	30-120	15.0	1.50	1	Al	N	1:1	1000	50	5
AIN273	30-120	10.0	1.50	1	Al	N	0:1	1000	250	5
AIN274	30-120	15.0	1.00	1	Al	N	9:1	1500	250	5
AIN275	30-120	15.0	1.25	1	Al	N	0:1	500	150	5
AIN276	30-120	5.0	1.67	1	Al	N	1:1	500	250	5
AIN277	30-120	5.0	1.25	1	Al	N	0:1	1500	50	5
AIN278	30-120	10.0	1.25	1	Al	N	1:1	1500	150	5
AIN279	30-120	15.0	1.50	1	Al	N	1:1	1000	50	5
AIN280	30-120	10.0	1.50	1	Al	N	0:1	1000	250	5
AIN281	30-120	5.0	2.33	1	Al	N	1:1	500	250	5
AIN282	30-120	5.0	1.00	1	Al	N	0:1	1500	50	5
AIN285	30-120	5.0	0.83	1	Al	N	0:1	1500	50	5
AIN286	30-120	5.0	0.83	1	Al	N	0:1	1500	50	5
AIN287	30-120	5.0	0.83	1	Al	N	0:1	1500	50	5
AIN288	30-120	5.0	0.83	1	Al	N	0:1	1500	50	5
AIN289	30-120	5.0	0.83	1	Al	N	0:1	1500	50	5
AIN290	30-120	5.0	1.00	1	Al	N	0:1	1000	50	5
AIN291	30-120	5.0	1.00	1	Al	N	0:1	1000	50	5
AIN293	30-120	5.0	0.83	1	Al	N	0:1	1500	50	5
AIN294	30-120	5.0	0.80	1	Al	N	0:1	1500	50	5
AIN295	30-120	5.0	0.80	1	Al	N	0:1	1500	50	5
AIN296	30-120	5.0	0.80	1	Al	N	0:1	1500	50	5
AIN297	30-120	5.0	0.80	1	Al	N	0:1	1500	50	5
AIN298	30-120	5.0	1.00	1	Al	N	0:1	1500	50	5
AIN299	30-120	5.0	1.00	1	Al	N	0:1	1500	50	5
AIN300	30-120	5.0	1.00	1	Al	N	0:1	1500	50	5

Table C-2. AlON Deposition Conditions Using N<sub>2</sub>O (continued)

Sample#	DepTemp (°C)	DepPress (mTorr)	DepTime (hr)	Layers	Metal	HE	Gas ambient N <sub>2</sub> :N <sub>2</sub> O	DC power (W)	Frequency (kHz)	Distance (inch)
AIN301	30-120	5.0	1.00	1	Al	N	0:1	1500	50	5
AIN302	30-120	5.0	0.92	1	Al	N	0:1	1500	50	5
AIN303	30-120	5.0	0.92	1	Al	N	0:1	1500	50	5
AIN304	30-120	10.0	0.58	1	Al	N	1:1	1500	50	5
AIN305	30-120	10.0	0.58	1	Al	N	1:1	1500	50	5
AIN306	30-120	10.0	0.58	1	Al	N	1:1	1500	50	5
AIN307	30-120	10.0	0.58	1	Al	N	1:1	1500	50	5
AIN308	30-120	10.0	0.67	1	Al	N	1:1	1500	50	5
AIN309A	30-120	5.0	0.83	1	Al	N	0:1	1500	50	5
AIN309B	30-120	5.0	0.83	1	Al	N	0:1	1500	50	5
AIN310	30-120	5.0	0.83	1	Al	N	0:1	1500	50	5
AIN311	30-120	5.0	0.83	1	Al	N	0:1	1500	50	5
AIN314	30-120	5.0	0.75	1	Al	N	0:1	1500	50	5
AIN315	30-120	5.0	0.75	2	Al	N	0:1	1500	50	5
AIN316	30-120	5.0	0.75	1	Al	N	0:1	1500	50	5
AIN317	30-120	5.0	0.75	2	Al	N	0:1	1500	50	5
AIN318	30-120	5.0	0.67	1	Al	N	0:1	1500	50	3
AIN319	30-120	5.0	0.75	1	Al	N	0:1	1500	50	3
AIN320	30-120	5.0	0.75	1	Al	N	0:1	1500	50	3
AIN321	30-120	5.0	0.75	1	Al	N	0:1	1500	50	3
AIN322	30-120	5.0	0.75	3	Al	N	0:1	1500	50	3
AIN323	30-120	5.0	0.75	1	Al	N	0:1	1500	50	3
AIN324	30-120	5.0	0.75	3	Al	N	0:1	1500	50	4
AIN325	30-120	5.0	0.75	3	Al	N	0:1	1500	50	4
AIN326	30-120	5.0	0.75	1	Al	N	0:1	1500	50	4

Table C-2. AlON Deposition Conditions Using N<sub>2</sub>O (continued)

Sample#	DepTemp (°C)	DepPress (mTorr)	DepTime (hr)	Layers	Metal	HE	Gas ambient N <sub>2</sub> :N <sub>2</sub> O	DC power (W)	Frequency (kHz)	Distance (inch)
AIN327	30-120	5.0	0.83	1	Al	N	0:1	1500	50	4
AIN328	30-120	5.0	0.92	3	Al	N	0:1	1500	50	4
AIN329	30-120	5.0	0.92	3	Al	N	0:1	1500	50	4
AIN330	30-120	5.0	0.92	4	Al	N	0:1	1500	50	4
AIN331	30-120	5.0	0.92	2	Al	N	0:1	1500	50	4
AIN332	30-120	5.0	0.92	2	Al	N	0:1	1500	50	4
AIN333	30-120	5.0	0.92	1	Al	N	0:1	1500	50	4
AIN334	30-120	5.0	0.92	1	Al	N	0:1	1500	50	4
AIN335	30-120	5.0	0.92	1	Al	N	0:1	1500	50	4
AIN336	30-120	5.0	0.92	3	Al	N	0:1	1500	50	4
AIN337	30-120	5.0	0.92	1	Al	N	0:1	1500	50	4
AIN338	30-120	5.0	0.92	2	Al	N	0:1	1500	50	4
AIN339	30-120	5.0	0.92	1	Al	N	0:1	1500	50	4
AIN340	30-120	5.0	0.92	2	Al	N	0:1	1500	50	4
AIN341	30-120	5.0	0.92	2	Al	Y	0:1	1500	50	4
AIN342	30-120	5.0	0.95	2	Al	Y	0:1	1500	50	4
AIN343	30-120	5.0	0.92	3	Al	Y	0:1	1500	50	4
AIN344	30-120	5.0	0.92	3	Al	Y	0:1	1500	50	4
AIN345	30-120	5.0	0.92	1	AL	Y	0:1	1500	50	4
AIN346	30-120	5.0	0.92	2	Al	Y	0:1	1500	50	4
AIN347	30-120	5.0	0.92	2	Ti	Y	0:1	1500	50	4
AIN348	30-120	5.0	0.92	2	Ti	Y	0:1	1500	50	4
AIN349	30-120	5.0	1.50	2	Ti	Y	0:1	1500	50	4
AIN350	30-120	5.0	0.92	2	Ti	Y	0:1	1500	50	4
AIN351	30-120	5.0	0.92	2	Ti	Y	0:1	1500	50	4
AIN353	30-120	5.0	0.92	1	Ti	Y	0:1	1500	50	4
AIN354	30-120	5.0	0.92	2	Ti	N	0:1	1500	50	4
AIN355	30-120	5.0	0.92	1	Al	Y	0:1	1500	50	4

Table C-2. AlON Deposition Conditions Using N<sub>2</sub>O (continued)

Sample#	DepTemp (°C)	DepPress (mTorr)	DepTime (hr)	Layers	Metal	HE	Gas ambient N <sub>2</sub> :N <sub>2</sub> O	DC power (W)	Frequency (kHz)	Distance (inch)
AlN356	30-120	5.0	0.92	1	Al	Y	0:1	1500	50	4
AlN357	30-120	5.0	0.92	1	Al	Y	0:1	1500	50	4
AlN358	30-120	5.0	0.92	1	Al	Y	0:1	1500	50	4
AlN359	30-120	5.0	0.92	1	Al	Y	0:1	1500	50	4
AlN360	30-120	5.0	0.92	1	Al	Y	0:1	1500	50	4
AlN361	30-120	5.0	0.45	1	Al	Y	0:1	1500	50	4
AlN362	30-120	5.0	0.45	1	Al	Y	0:1	1500	50	4
AlN363	30-120	5.0	0.45	1	Al	Y	0:1	1500	50	4
AlN364	30-120	5.0	1.83	1	Al	Y	0:1	1500	50	4
AlN365	30-120	5.0	1.83	1	Al	Y	0:1	1500	50	4
AlN366	30-120	5.0	1.83	1	Al	Y	0:1	1500	50	4
AlN367	30-120	5.0	0.92	1	Al	Y	0:1	1500	50	4
AlN368	30-120	5.0	1.83	1	Al	Y	0:1	1500	50	4
AlN369	30-120	5.0	1.83	1	Al	Y	0:1	1500	50	4
AlN370	30-120	5.0	0.92	1	Al	Y	0:1	1500	50	4
AlN371	30-120	5.0	0.92	1	Al	N	0:1	1500	50	4
AlN372	30-120	5.0	1.83	1	Al	Y	0:1	1500	50	4
AlN373	30-120	5.0	1.33	1	Al	Y	0:1	1500	50	4
AlN374	30-120	5.0	0.67	1	Al	Y	0:1	1500	50	4
AlN375	30-120	5.0	1.33	1	Al	N	0:1	1500	50	4
AlN376	30-120	5.0	1.33	1	Al	N	0:1	1500	50	4
AlN377	30-120	5.0	1.33	1	Al	N	0:1	1500	50	4
AlN378	30-120	5.0	1.33	1	Al	N	0:1	1500	50	4
AlN379	30-120	5.0	1.00	1	Al	N	0:1	1500	50	3
AlN380	30-120	5.0	0.67	1	Al	N	0:1	1500	50	3
AlN381	30-120	5.0	0.67	1	Al	N	0:1	1500	50	3
AlN382	30-120	5.0	0.67	1	Al	N	0:1	1500	50	3
AlN383	30-120	5.0	0.67	1	Al	N	0:1	1500	50	3
AlN384	30-120	5.0	0.67	1	Al	N	0:1	1500	50	3
AlN385	30-120	5.0	0.67	1	Al	N	0:1	1500	50	3

Table C-2. AION Deposition Conditions Using N<sub>2</sub>O (continued)

Sample#	DepTemp (°C)	DepPress (mTorr)	DepTime (hr)	Layers	Metal	HE	Gas ambient N <sub>2</sub> :N <sub>2</sub> O	DC power (W)	Frequency (kHz)	Distance (inch)
AIN386	30-120	5.0	0.50	1	Al	N	0:1	1500	50	3
AIN387	30-120	5.0	0.67	1	Al	N	0:1	1500	50	3
AIN388	30-120	5.0	0.67	1	Al	N	0:1	1500	50	3
AIN389	30-120	5.0	0.67	2	Al	N	0:1	1500	50	3
AIN390	30-120	5.0	0.67	1	Al	N	0:1	1500	50	3
AIN391	30-120	5.0	0.67	1	Al	N	0:1	1500	50	3
AIN392	30-120	5.0	0.67	1	Al	N	0:1	1500	50	3
AIN393	30-120	5.0	0.67	1	Al	N	0:1	1500	50	3
AIN394	30-120	5.0	0.50	1	Al	N	0:1	1500	50	3
AIN395	30-120	5.0	0.55	1	Al	N	0:1	1500	50	3
AIN396	30-120	5.0	0.55	1	Al	N	0:1	1500	50	3
AIN397	30-120	5.0	0.55	1	Al	N	0:1	1500	50	3
AIN398	30-120	5.0	0.55	1	Al	N	0:1	1500	50	3
AIN399	30-120	5.0	0.55	1	Al	N	0:1	1500	50	3
AIN400	30-120	5.0	0.55	1	Al	N	0:1	1500	50	3
AIN401	30-120	5.0	0.55	1	Al	N	0:1	1500	50	3
AIN405	30-120	5.0	0.55	1	Al	N	0:1	1500	50	3
AIN406	30-120	5.0	0.50	1	Al	N	0:1	1500	50	1.75
AIN407	30-120	5.0	0.67	1	Al	N	0:1	1500	50	4
AIN408	30-120	5.0	0.92	2	Al	N	0:1	1500	50	4
AIN409	30-120	5.0	0.92	1	Al	N	0:1	1500	50	4
AIN410	30-120	5.0	0.92	1	Al	N	0:1	1500	50	4
AIN411	30-120	5.0	0.92	1	Al	N	0:1	1500	50	4
AIN412	30-120	5.0	0.92	1	Al	N	0:1	1500	50	4
AIN413	30-120	5.0	0.92	1	Al	N	0:1	1500	50	4

Table C-2. AlON Deposition Conditions Using N<sub>2</sub>O (continued)

Sample#	DepTemp (°C)	DepPress (mTorr)	DepTime (hr)	Layers	Metal	HE	Gas ambient N <sub>2</sub> :N <sub>2</sub> O	DC power (W)	Frequency (kHz)	Distance (inch)
AIN414	30-120	5.0	0.92	1	Al	N	0:1	1500	50	4
AIN415	30-120	5.0	0.92	1	Al	N	0:1	1500	50	4
AIN416	30-120	5.0	0.92	1	Al	N	0:1	1500	50	4
AIN417	30-120	5.0	0.92	2	Al	N	0:1	1500	50	4
AIN418	30-120	5.0	0.92	3	Al	N	0:1	1500	50	4
AIN419	30-120	5.0	0.92	2	Al	N	0:1	1500	50	4
AIN421	30-120	5.0	0.92	2	Al	N	0:1	1500	50	3
AIN422	30-120	5.0	0.92	1	Al	N	0:1	1500	50	3
AIN423	30-120	5.0	0.92	5	Al	N	0:1	1500	50	3
AIN424	30-120	5.0	0.92	4	Al	N	0:1	1500	50	4
AIN425	30-120	5.0	0.92	2	Al	N	0:1	1500	50	4
AIN426	30-120	5.0	0.92	5	Al	N	0:1	1500	50	4
AIN427	30-120	5.0	0.92	5	Al	N	0:1	1500	50	4
AIN428	30-120	5.0	0.92	10	Al	N	0:1	1500	50	4
AIN429	30-120	5.0	0.92	5	Al	N	0:1	1500	50	4
AIN430	30-120	5.0	0.92	5	Al	N	0:1	1500	50	4
AIN431	30-120	5.0	0.92	2	Al	N	0:1	1500	50	4
AIN432	30-120	5.0	0.92	1	Al	N	0:1	1500	50	4
AIN433	30-120	5.0	0.92	1	Al	N	0:1	1500	50	4
AIN434	30-120	5.0	0.92	2	Al	N	0:1	1500	50	4
AIN435	30-120	5.0	0.92	5	Al	N	0:1	1500	50	4
AIN436	30-120	5.0	0.92	10	Al	N	0:1	1500	50	4
AIN442	30-120	5.0	0.92	2	Al	N	0:1	1500	50	4
AIN443	30-120	5.0	0.92	3	Al	N	0:1	1500	50	4
AIN444	30-120	5.0	0.92	10	Al	N	0:1	1500	50	4
AIN445	30-120	5.0	0.92	10	Al	N	0:1	1500	50	4

## APPENDIX D

Table D-1. Dielectric and Electrical Properties

Sample#	Substrate	Film (Å)	Layers	Df	Cap (nF)	R <sub>p</sub> (MΩ)	R <sub>p</sub> (MΩ)	IR (MΩ)	HV	k	ρ(Ω-cm <sup>□</sup> )	V/μm	DepRate (Å/s)	
AIN245	Glass	4320	2											0.80
AIN246	Glass	5760	1	0.0138	2.994	3.85	3.848	1.17E+06	355.00	10.82	3.66E+15	616.32		0.80
AIN247	Glass	5760	2	0.0546	8.486	0.34	0.344			10.23				0.80
AIN248	Glass	5760	2	0.0557	7.068	0.40	0.404			8.52				0.80
AIN249	Glass	5760	1											0.80
AIN250	Glass	5760	2	0.0689	8.627	0.27	0.268			10.03				0.80
AIN251	Glass	5760	3	0.0127	7.788	1.59	1.609			10.76				0.80
AIN252	Glass	5760	3	0.0083	14.326	1.34	1.335			11.95				0.80
AIN254	Glass	4556							276.67				607.26	0.84
AIN255	Glass	2880	1											0.80
AIN256	Glass	2880	3											0.80
AIN257	Glass	5760	4	0.0591	14.322	0.19	0.188			11.10				0.80
AIN258	Glass	5760	2	0.0433	14.461	0.26	0.254			13.45				0.80
AIN259	Glass	5760	1	0.0124	1.753	7.35	7.344			12.54				0.80
AIN260	Glass	5760	2	0.0110	3.985	3.62	3.623			8.64				0.80
AIN261	Glass	5760	6	0.0188	23.831	0.36	0.356			11.75				0.80
AIN262	Glass	5760	8											0.80
AIN263	Glass	5760	4	0.0294	8.563	0.63	0.633			9.95				0.80
AIN264	Glass	5760	7	0.0473	26.233	0.14	0.128			11.61				0.80
AIN265	Glass	5760	8	0.1478	39.095	0.03	0.028			12.23				0.80
AIN266	Glass	5760	3	0.1478	39.095	0.03	0.028			12.23				0.80
AIN267	Glass	5760	4	0.0000	0.000	0.00				0.00				0.80
AIN268	Glass	5760	8	0.0271	24.358	0.24	0.241	2.17E+05	270.00	11.32	5.28E+15	468.75		0.80
AIN270	Glass	5760	1	0.0902	91.921	0.24	0.019			16.62				0.80
AIN271	Glass	7009	1	0.0121	0.823	16.10	15.924	2.57E+04	80.00	9.23	2.59E+13	114.15		1.30
AIN272	Glass	5409	1	0.0077	0.977	21.46	21.189	1.99E+05	215.00	8.45	2.59E+14	397.52		1.00
AIN273	Glass		1											
AIN274	Glass		1											
AIN275	Glass	4181	1	0.0073	1.157	18.95	18.785	1.38E+05	175.00	7.73	2.34E+14	418.60		1.16
AIN276	Glass	1500	1	0.0091	4.106	4.25	4.243	2.68E+04	10.00	9.85	1.26E+14	66.67		0.33

Table D-1. Dielectric and Electrical Properties (continued)

Sample#	Substrate	Film (Å)	Layers	Df	Cap (nF)	R <sub>p</sub> (MΩ)	R <sub>p</sub> (MΩ)	IR (MΩ)	HV	k	ρ(Ω·cm□)	V/μm	DepRate (Å/s)
AIN277	Glass	1762	1	0.0641	3.272	0.76	0.759	0.00E+00	0.00	9.21	0.00E+00	0.00	0.29
AIN278	Glass	8278	1	0.0267	0.574	10.53	10.401	0.00E+00	0.00	7.59	0.00E+00	0.00	1.84
AIN279	Si	10853	1	0.0038	0.411	103.09	102.571	5.89E+05	437.50	7.12	3.83E+14	403.11	2.41
AIN280	Si	4932	1										0.91
AIN281	Si	4104	1	0.0134	1.333	8.99	8.910	1.53E+06	143.33	8.75	2.64E+15	349.25	0.76
AIN282	Si	2180	1	0.0115	2.673	5.27	5.198	2.04E+05	100.00	9.31	6.62E+14	458.77	0.26
AIN285	Glass	6027	1	0.0032	0.755	65.55	65.426	9.65E+05	375.00	7.27	1.13E+15	622.17	1.67
AIN286	Glass	2672	1	0.0056	1.924	14.84	14.802	2.29E+06	77.50	8.22	6.04E+15	290.02	0.89
AIN287	Glass	7708	1	0.0042	0.601	65.53	63.427	3.53E+05	353.33	7.40	3.24E+14	458.40	2.57
AIN288	Glass	2416	1	0.0077	2.551	7.80	8.061			9.85			0.81
AIN289	Glass	2315	1	0.0065	2.154	11.53	11.456	6.16E+03	50.00	7.97	1.88E+13	215.95	0.77
AIN290	Glass		1										
AIN291	Glass	1818	1										0.50
AIN293	Glass	5492	1										1.53
AIN294	Glass	3840	1										1.28
AIN295	Glass	3113	1										1.08
AIN296	Glass,Si	2802	1										0.97
AIN297	Glass,Si	3993	1										1.39
AIN298	Oxide	3094	1	0.0067	1.717	13.88	13.748	1.33E+06	110.00	8.49	3.04E+15	355.53	0.86
AIN299	Oxide	5154	1	0.0058	1.053	26.53	26.155	1.98E+06	270.00	8.68	2.72E+15	523.84	1.43
AIN300	Oxide	3734	1	0.0069	1.628	14.20	14.141			9.72			1.04
AIN301	Oxide	5979	1	0.0063	1.004	25.46	25.284	1.43E+06	184.00	9.59	1.69E+15	307.73	1.66
AIN302	Oxide	3504	1										1.06
AIN303	Oxide	5519	1	0.0062	1.034	24.79	24.746	5.25E+06	147.50	9.12	6.72E+15	267.26	1.67
AIN304	Si	4085	1	0.0030	1.287	41.39	41.281	2.34E+06	160.00	8.41	4.04E+15	391.69	1.95
AIN305	Si		1										
AIN306	Si	4313	1	0.0070	1.192	19.32	19.150	3.08E+06	160.00	8.22	5.05E+15	370.99	2.05
AIN307	Si		1										
AIN308	Si	4483	1	0.0086	1.288	14.59	14.397	2.18E+06	160.00	9.23	3.43E+15	356.89	1.87
AIN309A	Oxide	4880	1	0.0034	1.074	43.30	43.236	3.61E+06	150.00	8.38	5.22E+15	307.38	1.63
AIN309B	Oxide	4902	1	0.0068	1.247	18.89	18.825	4.84E+06	160.00	9.77	6.98E+15	326.37	1.63
AIN310	Oxide	2767	1										0.92

Table D-1. Dielectric and Electrical Properties (continued)

Sample#	Substrate	Film (Å)	Layers	Df	Cap (nF)	R <sub>p</sub> (MΩ)	R <sub>p</sub> (MΩ)	IR (MΩ)	HV	k	ρ(Ω·cm□)	V/μm	DepRate (Å/s)
AIN311	Oxide	3197	1										1.07
AIN314	Oxide	5000	1	0.0155	25.705	0.41	0.400	1.02E+06		9.00	3.29E+16		1.85
AIN315	Oxide	5000	2	0.0105	36.983	0.45	0.408	2.26E+06		6.48	1.46E+17		1.85
AIN316	Oxide	5000	1	0.0115	25.669	0.55	0.539	9.03E+05		8.99	2.91E+16		1.85
AIN317	Oxide	5000	2	0.0169	43.091	0.23	0.219			7.55	6.45E+04		1.85
AIN318	Oxide	5000	1										2.08
AIN319	Oxide	5000	1	0.0145	26.022	0.43	0.423			9.12			1.85
AIN320	Oxide	5000	1										1.85
AIN321	Oxide	5000	1										1.85
AIN322	Oxide	5000	3	0.0203	75.355	0.11	0.104	2.44E+06		8.80	2.36E+17		1.85
AIN323	Oxide	5000	1	0.0117	22.142	0.63	0.615	2.93E+03		7.76	9.44E+13		1.85
AIN324	Oxide	5000	3										1.85
AIN325	Oxide	5000	3	0.0244	124.758	0.05	0.052	7.88E+02		14.57	7.63E+13		1.85
AIN326	Oxide	4300	1	0.0141	54.974	0.23	0.205	1.00E-06		16.56	3.75E+04		1.59
AIN327	Oxide	5000	1	0.0127	42.861	0.30	0.293			15.01			1.67
AIN328	Oxide	5000	3	0.0550	98.043	0.03	0.030			11.45			1.52
AIN329	Oxide	5000	3	0.0131	132.908	0.09	0.091			15.52			1.52
AIN330	Oxide	5000	4	0.1422	165.202	0.01	0.007			14.47			1.52
AIN331	Oxide	5000	2										1.52
AIN332	Oxide	5000	2	0.0123	66.209	0.20	0.196			11.60			1.52
AIN333	Oxide	5000	1										1.52
AIN334	Oxide	5000	1										1.52
AIN335	Oxide	5000	1	0.0744	37.568	0.06	0.057			13.16			1.52
AIN336	Oxide	5000	3		38.000					4.44			1.52
AIN337	Oxide	5000	1							0.00			1.52
AIN338	Oxide	5000	2							0.00			1.52
AIN339	Oxide	5000	1		33.000					11.56			1.52
AIN340	Oxide	5000	2		33.000					5.78			1.52
AIN341	Oxide	5000	2							0.00			1.52
AIN342	Oxide	5000	2	0.0100	92.000	0.00	0.173			16.11			1.46

Table D-1. Dielectric and Electrical Properties (continued)

Sample#	Substrate	Film (Å)	Layers	Df	Cap (nF)	R <sub>p</sub> (MΩ)	R <sub>p</sub> (MΩ)	IR (MΩ)	HV	k	ρ(Ω·cm <sup>□</sup> )	V/μm	DepRate (Å/s)
AIN343	Oxide	5000	3	0.0100	115.000		0.138			13.43			1.52
AIN344	Oxide	5000	3										1.52
AIN345	Oxide	5000	1										1.52
AIN346	Oxide	5000	2										1.52
AIN347	Oxide	5000	2										1.52
AIN348	Oxide	5000	2										1.52
AIN349	Oxide	7500	2										1.39
AIN350	Oxide	5000	2										1.52
AIN351	Oxide	5000	2										1.52
AIN353	Oxide	5000	1										1.52
AIN354	Oxide	5000	2										1.52
AIN355	Oxide	5000	1	0.0242	16.293	0.41	0.404	1.21E+05		14.27	1.56E+15		1.52
AIN356	Oxide	5000	1	0.0139	33.002	0.35	0.346	2.51E+04		28.90	3.24E+14		1.52
AIN357	Oxide	5000	1	0.0153	15.819	0.66	0.656	3.29E+04		13.85	4.25E+14		1.52
AIN358	Oxide	5134	1	0.0075	7.913	2.69	2.687	7.35E+05		7.12	9.24E+15		1.56
AIN359	Glass	5000	1	0.0335	4.811	0.99	0.988	5.03E+05		4.21	6.49E+15		1.52
AIN360	SiO <sub>2</sub>	5000	1		24.000					21.02			1.52
AIN361	Glass	2500	1										1.54
AIN362	Glass	2500	1										1.54
AIN363	Glass	2500	1										1.54
AIN364	Glass	10000	1	0.0088	2.084	8.76	8.636	2.37E+04		4.09	1.36E+14		1.52
AIN365	Glass	10000	1	0.0000									1.52
AIN366	Glass	10000	1	0.0124	2.901	4.41	4.414	2.24E+02		5.70	1.29E+12		1.52
AIN367	Glass	5000	1	0.0093	5.139	3.36	3.314	1.30E+03		5.05	1.49E+13		1.52
AIN368	Glass	10000	1	0.0080	5.578	3.57	3.577			10.96			1.52
AIN369	Glass	10000	1	0.0190	7.770	1.07	1.076			15.27			1.52
AIN370	Glass	5000	1	0.0098	12.283	1.35	1.327			12.07			1.52
AIN371	Glass	5000	1										1.52
AIN372	Glass	14550	1	0.0669	3.554	0.98	0.669	5.77E+02		10.16	2.28E+12		2.20

Table D-1. Dielectric and Electrical Properties (continued)

Sample#	Substrate	Film (Å)	Layers	Df	Cap (nF)	R <sub>p</sub> (MΩ)	R <sub>p</sub> (MΩ)	IR (MΩ)	HV	k	ρ(Ω·cm <sup>□</sup> )	V/μm	DepRate (Å/s)
AIN373	Glass	10000	1	0.0314	11.578	0.46	0.437	6.82E+01		22.75	3.92E+11		2.08
AIN374	Glass	5000	1							11.30	4.58E+12		2.08
AIN375	Glass	10000	1										2.08
AIN376	Glass	10000	1										2.08
AIN377	Oxide	5000	1										1.04
AIN378	Oxide	5000	1										1.04
AIN379	Oxide	9000	1	0.0084	8.383	2.25	2.249	1.08E+05		8.20	1.24E+15		2.50
AIN380	Oxide	6000	1	0.0075	10.420	2.04	2.024	1.14E+05	440.00	7.76	1.73E+15	733.33	2.50
AIN381	Oxide	6000	1	0.0123	13.845	0.94	0.932	1.01E+05	350.00	9.03	1.75E+15	583.33	2.50
AIN382	Oxide	6067	1	0.0147	13.833	0.80	0.785			9.12			2.53
AIN383	Oxide	6067	1										2.53
AIN384	Oxide	6067	1										2.53
AIN385	Oxide	6067	1	0.0191	14.239	0.59	0.584			9.39			2.53
AIN386	Oxide	4538	1	0.0390	17.268	0.24	0.236			8.51			2.52
AIN387	Oxide	6067	1	0.0199	12.266	0.66	0.651			8.09			2.53
AIN388	Oxide	6067	1	0.0182	16.209	0.55	0.539			10.68			2.53
AIN389	Oxide	6067	2	0.0341	30.338	0.16	0.154			10.00			2.53
AIN390	Oxide	6067	1										2.53
AIN391	Oxide	6067	1										2.53
AIN392	Oxide	6067	1	0.0310	14.043	0.38	0.366			9.26			2.53
AIN393	Oxide	6067	1	0.0292	15.766	0.35	0.345			10.39			2.53
AIN394	Oxide	4538	1	0.0688	23.077	0.10	0.100			11.38			2.52
AIN395	Oxide	5000	1										2.53
AIN396	Oxide	5000	1	0.0723	10.843	0.20	0.203			6.73			2.53
AIN397	Oxide	5000	1	0.0130	25.545	0.48	0.481			8.75			2.53
AIN398	Oxide	5000	1	0.0282	13.645	0.43	0.414			8.47			2.53
AIN399	Oxide	5000	1										2.53
AIN400	Oxide	5000	1	0.0109	41.419	0.35	0.352			22.50			2.53
AIN401	Oxide	5000	1	0.0369	10.907	0.43	0.395			5.93			2.53

Table D-1. Dielectric and Electrical Properties (continued)

Sample#	Substrate	Film (Å)	Layers	Df	Cap (nF)	R <sub>p</sub> (MΩ)	R <sub>p</sub> (MΩ)	IR (MΩ)	HV	k	ρ(Ω·cm <sup>□</sup> )	V/μm	DepRate (Å/s)	
AIN405	Oxide	5000	1											2.53
AIN406	Oxide	6000	1	0.0298	10.619	0.56	0.503	8.59E+04	250.00	6.00	1.72E+15	416.67	3.33	
AIN407	Oxide	3600	1	0.0413	24.132	0.17	0.160	1.00E+05	220.00	8.18	3.34E+15	611.11	1.50	
AIN408	Oxide	4950	2	0.0500	30.400	0.18	0.105			7.08			1.50	
AIN409	Oxide	4868	1	0.0470	21.000		0.161	9.46E+04	200.00	9.63	2.33E+15	410.85	1.48	
AIN410	Oxide	4868	1	0.0189	14.943	0.58	0.565	8.72E+04		6.85	2.49E+16		1.48	
AIN411	Oxide	4950	1	0.0621	9.727	0.27	0.264	0.00E+00		6.80	0.00E+00		1.50	
AIN412	Oxide	4950	1	0.0311	18.438	0.29	0.278	8.72E+04		8.59	2.11E+15		1.50	
AIN413	Oxide	4950	1	0.0459	19.277	0.18	0.180	6.97E+05		8.98	1.69E+16		1.50	
AIN414	Oxide	4950	1	0.0229	15.387	0.45	0.452	0.00E+00		7.17			1.50	
AIN415	Oxide	4950	1											1.50
AIN416	Oxide	5700	1	0.0407	15.863	0.25	0.246			8.51				1.73
AIN417	Oxide	4950	2	0.0358	41.538	0.12	0.107	1.14E+06	170.00	9.68	5.53E+16	343.43	1.50	
AIN418	Oxide	4950	3	0.2345	53.439	0.02	0.013			8.30				1.50
AIN419	Oxide	4950	2	0.0212	55.890	0.14	0.135			13.03				1.50
AIN421	Oxide	8250	2	1.3876	20.309	0.01	0.006			9.86				2.50
AIN422	Oxide	8250	1	0.0458	21.484									2.50
AIN423	Oxide	8250	5											2.50
AIN424	Oxide	4950	4											1.50
AIN425	Oxide	4950	2	0.0733	26.944	0.08	0.081			6.98				1.50
AIN426	Oxide	4950	5	0.0886	87.812	0.02	0.020			8.40				1.50
AIN427	Oxide	4950	5	0.0555	99.049	0.03	0.029	6.44E+05	80.00	9.47	7.61E+16	161.62	1.50	
AIN428	Oxide	4950	10	0.0863	202.287	0.01	0.009	2.90E+03		9.67	6.85E+14			1.50
AIN429	Oxide	4950	5	0.0424	81.319	0.05	0.046			8.42				1.50
AIN430	Oxide	4950	5	0.0522	75.832	0.04	0.040	9.86E+05	115.00	13.46	6.27E+16	232.32	1.50	
AIN431	Oxide	4950	2	0.0338	43.869	0.11	0.107	4.86E+05		19.47	1.24E+16			1.50
AIN432	Oxide	3650	1	0.0384	23.086	0.18	0.180			15.11				1.11
AIN433	Oxide	4443	1	0.0516	16.310	0.19	0.189	4.26E+05		13.00	6.04E+15			1.35
AIN434	Oxide	4620	2	0.0316	28.762	0.17	0.175	8.76E+05		11.92	2.39E+16			1.40
AIN435	Oxide	4620	5	0.0465	68.399	0.05	0.050	4.27E+05		11.34	2.91E+16			1.40
AIN436	Oxide	4620	10	0.0652	129.140	0.02	0.019	6.98E+05		10.70	9.52E+16			1.40

Table D-1. Dielectric and Electrical Properties (continued)

Sample#	Substrate	Film (Å)	Layers	Df	Cap (nF)	R <sub>p</sub> (MΩ)	R <sub>p</sub> (MΩ)	IR (MΩ)	HV	k	ρ(Ω-cm□ )	V/μm	DepRate (Å/s)
AIN442	Oxide	4620	2	0.0353	13.805	0.33	0.326			6.67			0.92
AIN443	Oxide	4620	3	0.2021	26.087	0.03	0.030			8.41			0.92
AIN444	Oxide	4620	10	0.2687	107.366	0.01	0.006			10.38			0.92
AIN445	Oxide	4620	10										0.92